united nations educational, scientific and cultural organization

international atomic energy agency

the
abdus salam
international centre for theoretical physics

SMR 1216 - 18

Joint INFM - the Abdus Salam ICTP School on "Magnetic Properties of Condensed Matter Investigated by Neutron Scattering and Synchrotron Radiation Techniques"

1 - 11 February 2000

Further Background Material

for

DICHROIC PHOTOEMISSION FOR PEDESTRIANS

Gerrit van der LAAN
Daresbury Laboratory
Warrington, WA4 4AD, U.K.

These are preliminary lecture notes, intended only for distribution to participants.

J. Synchrotron Rad. (1999). **6**, 694–695

Sum rule practice

Gerrit van der Laan*

Daresbury Laboratory, Warrington WA4 4AD, UK. E-mail: g.vanderlaan@dl.ac.uk

We discuss the theoretical limitations and experimental restrictions of the sum rules for x-ray magnetic dichroism, which relate the integrated signals of the spin-orbit split core levels to ground state properties, such as spin and orbital magnetic moments. A special choice of geometry, such as a transverse magnetic field, makes it possible to separate ground state moments which cannot be distinguished in a collinear geometry.

Keywords: magnetic circular dichroism; orbital magnetization; spin polarization; x-ray absorption spectroscopy.

1. Introduction

Thole *et al.* (1992) and Carra *et al.* (1993a) derived sum rules which relate the integrated signals over the spin-orbit split core edges of the x-ray magnetic circular dichroism (XMCD) to ground state orbital and spin magnetic moments. These rules were extended by Carra *et al.* (1993b) to include electric quadrupole transitions and magnetic linear dichroism. A generalization to x-ray magnetic scattering was given by Luo *et al.* (1993) and to photoemission by Thole and van der Laan (1993). Ankudinov and Rehr (1995) rederived the sum rules using the independent electron approximation. Ebert (1996) used first-principles spin-polarized relativistic multiple-scattering calculations for metallic magnets. Van der Laan (1998a) derived sum rules for jj-coupled operators by including cross terms between the $j = l \pm 1/2$ levels, so that these sum rules are no longer restricted to jj-coupling but valid in intermediate coupling.

2. Theoretical limitations

The derivation of the sum rules requires a separation of the transition probability into a physical and geometric part. To perform the angular momentum recoupling, it is assumed that the radial matrix elements are constant over the absorption edge. Although each j edge extends only over a narrow energy range of a few eV, transitions from different parts of the valence band can have different cross-sections. Wu *et al.* (1994) showed that the radial matrix integrals at the Ni $L_{2,3}$ in the metal vary linearly with photon energy from the bottom to the top of the band due to a change in spin-orbit interaction. Since this change is proportional to the expectation value of the orbital moment, L_z, the effect on the orbital sum rule is not dramatic, however, the effect on the spin sum rule can be larger. Such effects are usually absent in the strongly localized f shell of the rare earths, which have narrow band widths, but can be present in actinides.

The sum rules are based on the assumption that it is possible to integrate the signal of a core level assigned by a good quantum numbers, such as the total angular momentum j. However, core-valence interactions can induce a transfer of spectral weight between the j edges, invalidating both the spin-orbit sum rule (Thole & van der Laan, 1988; van der Laan, & Thole 1988a) and the spin sum rule. Alternatively, the sum rules can be used indirectly, by scaling the calculated absorption curve to the measured spectrum. For localized calculations this eliminates the effect of jj mixing. However, band structure calculations can display a different line shape when the core-valence interaction is not properly included. Band theory can also have difficulties to calculate the correct number of holes and branching ratio of the isotropic spectrum (Ebert, 1996). Anderson impurity model calculations give usually a good result for localized materials including transition metal oxides and rare earths (van der Laan & Thole, 1992).

To explain the x-ray absorption spectrum (XAS) it is often sufficient to consider only electric dipole transitions, certainly in the soft x-ray range. Carra and Altarelli (1990) pointed out the importance of the electric quadrupole transitions $2p \rightarrow 4f$ at the $L_{2,3}$ edges of the rare earths. These excitations can be strong due to the large magnetic moment of the $4f$ compared to the $5d$ shell. Electric dipole and quadrupole transitions have a different angular and temperature dependence, so they can be separated as demonstrated by Lang *et al.* (1995) and Giorgetti *et al.* (1995). It is more difficult to separate the $c + 1$ and $c - 1$ channels in the dipole excitation. Fortunately, for the $2p$ excitation in $3d$ transition metals the s channel can be neglected since its cross-section is less than 1 % of the total. Overall, the consensus seems to be that the uncertainty in the orbital and spin moment for $3d$ transition metals is within 10 %. For the L_z/S_z ratio the accuracy appears to be even better, around 5 %, mainly because the number of holes drops out.

3. Experimental complications

Saturation effects occur in both electron yield and fluorescence. The electron escape depth is of the order of tens of Å, which makes the electron yield signal extremely surface sensitive, necessitating surface science preparation. The orbital moment at the surface can be different from the bulk due to symmetry breaking. For thickness dependent studies the electron escape depth must be taken explicitly into account. The yield electrons can undergo spin dependent scattering, resulting in an imbalance between the spin majority and minority electrons. Evidence for this effect seems to come from spin scattering through thin ferromagnetic films (Oberli *et al.*, 1998).

Saturation effects occur because the electron escape depth cannot be neglected with respect to the x-ray attenuation length (van der Laan & Thole 1988b), especially at grazing incidence. Measurements in transmission are preferred, but unfortunately the x-ray attenuation length is very short; only a few hundreds Å. Chen *et al.* (1995) measured 50-70 Å thick films of Fe and Co on 1 mm thick parylene. However, strain deformation in thin films induced by the substrate can lead to changes in the crystalline structure, which changes the orbital moment.

The total electron yield sensitivity is dependent on the type of detector and its precise location with respect to the sample. Since electrons of lower kinetic energy originate on average from deeper in the sample, different detectors might probe different sample depths. This complicates the comparison between measurements carried out by various research groups.

To obtain absolute moments we need to know precisely the degree of circular polarization of the x-rays. Difficulties can arise when the polarization is different at each edge. For instance, the Pd $L_{2,3}$ edges are well separated (3173 and 3330 eV) so that the change in the degree of circular polarization can be large, especially when the monochromator crystals are operating near the Brewster angle ($\sim 45°$). Furthermore, it is often forgotten that the

measured intensity is given by the product of line strength and photon energy, while the sum rule applies to the line strength. This requires a correction, e. g. for Pd $L_{2,3}$ edges. A reliable I_0 monitor is essential, because the photon flux is not constant as a function energy. Undulator devices often show strong flux variations over a short energy range. When the I_0 normalization is incorrect, the two j edges are weighted with different factors resulting in wrong spin dependent moments.

Also the anisotropy of the crystal lattice can give variations in the observed spin to orbital moment ratio. For instance, when the magnetization is not along a high-symmetry direction, the orbital moment is no longer parallel to the spin direction. Since we measure only the projection of moments, a too small orbital moment is obtained when the light polarization is parallel to the magnetization direction (Dürr *et al.*, 1996).

The arbitrariness in the choice of the integration limits is another source of errors. In principle, the signal must be integrated over the entire absorption edge. This works often nicely for the dichroic signal which goes rapidly to zero above the edge where the continuum states are non-magnetic. However, to obtain moments *per hole* also the isotropic spectrum has to be integrated. The *background* below and above the edge has usually not the same height so that it is not straightforward to separate discrete and continuum states. Furthermore, the application of the spin sum rule requires the choice of a specific energy point to separate the two edges. Such a choice is ambiguous when the dichroic signal is not entirely zero in between the two edges, as is often the case in e. g. $3d$ transition metals.

The isotropic spectrum is rarely measured. Since the light can only be polarized transversally, three measurements with orthogonal linear polarization need to be added. Instead, the sum of the two spectra with opposite helicities is usually taken. However, this is only correct when the linear dichroism vanishes. Some research groups prefer to use, instead of XMCD, the asymmetry. However, the latter depends also on the linear dichroism, so that orbital and quadrupole moments are entangled.

The spin sum rule contains also the magnetic dipole term, T_z, which is usually small in $3d$ transition metal systems with cubic symmetry but which is large in actinides due to the strong $5f$ spin-orbit coupling (Collins *et al.*, 1995). Several ways have been proposed to separate S_z and T_z. Since in $3d$ transition metals, $T_z \approx S_z Q_{zz}$, where the quadrupole moment, Q, is a traceless tensor, Stöhr and König (1995) proposed to take the sum of three mutually orthogonal XMCD measurements, in which case T_z vanishes and only S_z remains. In practise, obscuration effects make it difficult to perform this procedure. Alternatively, one can measure the dichroism under different angles (Weller *et al.*, 1995). However, the magnetocrystalline anisotropy of the sample requires measurements along the principal axes of the crystal (Dürr *et al.*, 1996; Dürr & van der Laan, 1996). Alternatively, it is possible to measure the transverse x-ray magnetic circular dichroism (TXMCD), where one exploits the competition between the crystal field and spin-orbit interaction to measure the anisotropy in the moments (Dürr & van der Laan, 1996; van der Laan, 1998b). When the spins are forcefully aligned along a non-symmetry direction by a saturating external magnetic field, the spin-orbit coupling tries to align the orbital moment parallel to the spin moment, whereas the crystal field prefers an alignment of the orbital moment along the easy-direction of magnetization. Consequently, the orbital moment is no longer collinear with the spin moment, and has a component perpendicular to the spin moment which serves as a direct measure for the orbital anisotropy. This transverse orbital component is obtained by applying the sum rules to the TXMCD spectrum. Likewise, the transverse geometry enables us to separate the magnetic dipole term, describing the spin anisotropy, from the isotropic spin moment (van der Laan, 1998b).

Summarizing we can say that although it has become clear that there are many theoretical and experimental complications attached to the application of the sum rules, it provides still the only *direct* tool to separate the orbital and spin contribution to the total magnetic moments. This method is element specific, sensitive to submonolayer coverages and buried interfaces, non-destructive and generally applicable to all classes of magnetic materials, such $3d$, $4d$ and $5d$ transition metals, lanthanides and actinides.

References

Ankudinov, A. & Rehr, J. J. (1995). *Phys. Rev. B* **51**, 1282–1285.
Carra, P. & Altarelli, M. (1990). *Phys. Rev. Lett.* **64**, 1286–1289.
Carra, P., Thole, B. T., Altarelli, M. & Wang, X. (1993a). *Phys. Rev. Lett.* **70**, 694–697.
Carra, P., König, H., Thole, B. T. & Altarelli, M. (1993b). *Physica B* **192**, 182–190.
Chen, C. T., Idzerda, Y. U., Lin, H. J., Smith, N. V., Meigs, G., Chaban, E., Ho, G., Pellegrin, E. & Sette, F. (1995). *Phys. Rev. Lett.* **75**, 152–155.
Collins, S. P., Laundy, D., Tang, C. C. & van der Laan, G. (1995) *J. Phys. Condens. Matter* **7**, 9325–9341.
Dürr, H. A., van der Laan, G. & Thole, B. T. (1996). *Phys. Rev. Lett.* **76**, 3464–3464.
Dürr, H. A. & van der Laan, G. (1996). *Phys. Rev. B* **54**, R760–763.
Ebert, H. (1996). *Rep. Prog. Phys.* **59**, 1665–1735.
Giorgetti, Ch., Dartyge, E., Brouder, Ch., Baudelet, F., Meyer, C., Pizzini, S., Fontaine, A. & Galera, R.-M. (1995). *Phys. Rev. Lett.* **75**, 3186–3189.
Lang, J. C., Starjer, G., Detlefs, C., Goldman, A. I., König, H., Wang, X. D., Harmon, B. N. & McCallum, R. W. (1995). *Phys. Rev. Lett.* **74**, 4935–4938.
Luo, J., Trammell, G. T. & Hannon, J. P. (1993). *Phys. Rev. Lett.* **71**, 287–290.
Oberli, D., Burgermeister, R., Riesen, S., Weber, W. & Siegmann, H. C. (1998). *Phys. Rev. Lett.* **81**, 4228–4231.
Thole, B. T. & van der Laan, G. (1988). *Phys. Rev. B* **38**, 3158–3171; *Phys. Rev. A* **38**, 1943–1947.
Thole, B. T., Carra, P., Sette, F. & van der Laan, G. (1992). *Phys. Rev. Lett.* **68**, 1943–1946.
Thole, B. T. & van der Laan, G. (1993). *Phys. Rev. Lett.* **70**, 2499–2502.
van der Laan, G. & Thole, B. T. (1988a). *Phys. Rev. Lett.* **60**, 1977–1800.
van der Laan, G. & Thole, B. T. (1988b). *J. Electron Spectrosc. Relat. Phenomen.* **46**, 123–129.
van der Laan, G. & Thole, B. T. (1992). *J. Phys. Condens. Matter* **4**, 4181–4188.
van der Laan, G. (1998a). *Phys. Rev. B* **57**, 112–115.
van der Laan, G. (1998b). *Phys. Rev. B* **57**, 5250–5258.
Stöhr, J. & König, H. (1995). *Phys. Rev. Lett.* **75**, 3748–3751.
Weller, D. Stöhr, J., Nakajima, R., Carl, A., Samant, M.G., Chappert, C., Mégy, R., Beauvillain, P., Veillet, P. & Held, G. (1995). *Phys. Rev. Lett.* **75**, 3752–3755.
Wu, R.Q. & Freeman, A.J. (1994). *Phys. Rev. Lett.* **73**, 1994–1997.

(Received 10 August 1998; accepted 8 January 1999)

SR BASED TECHNIQUES

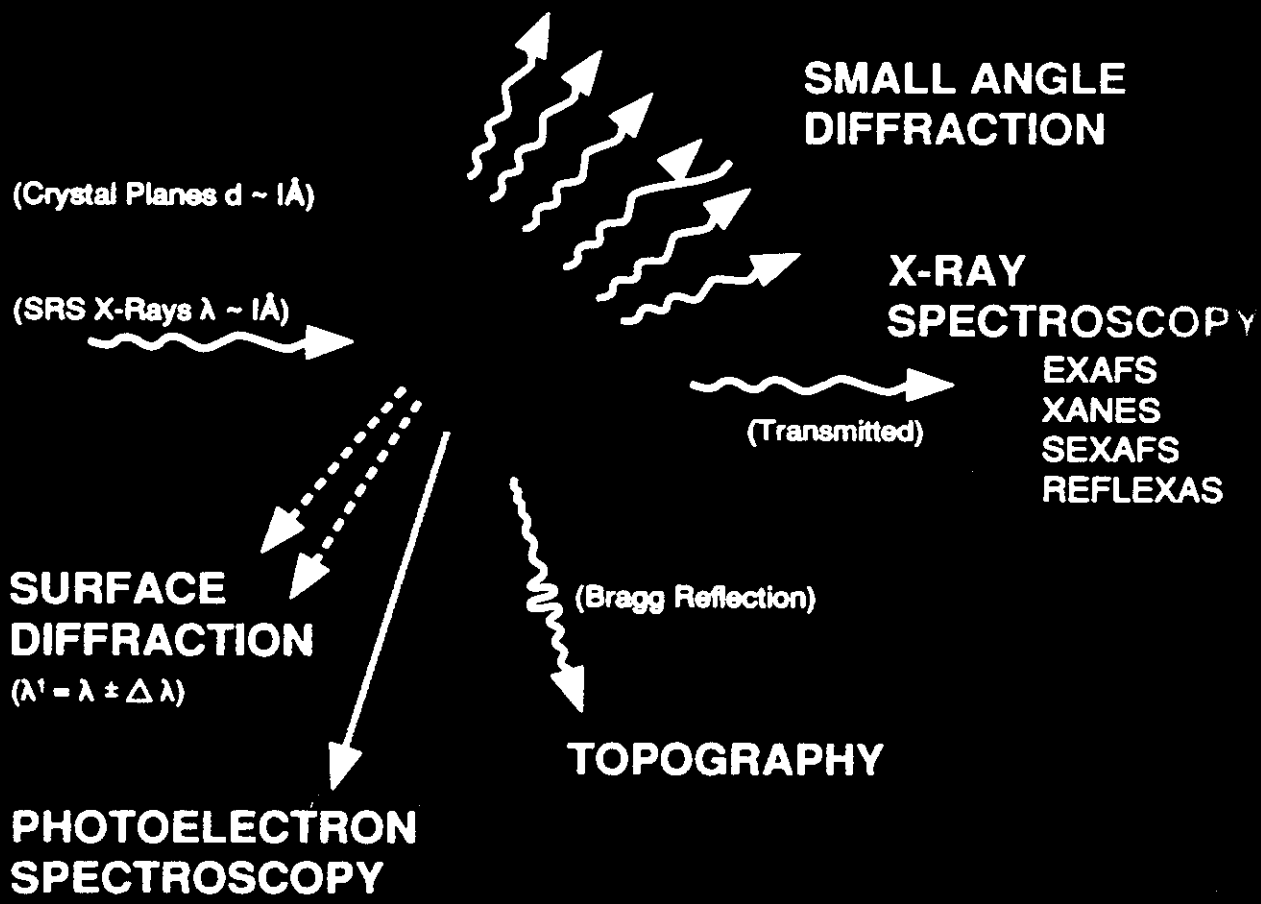

Most experiments are

Photon In ⟶ Photon Out
(Electron /Ion Out)

Determined by

$n\lambda_j = 2d_j \sin\theta_j$

The Faraday Effect

A term

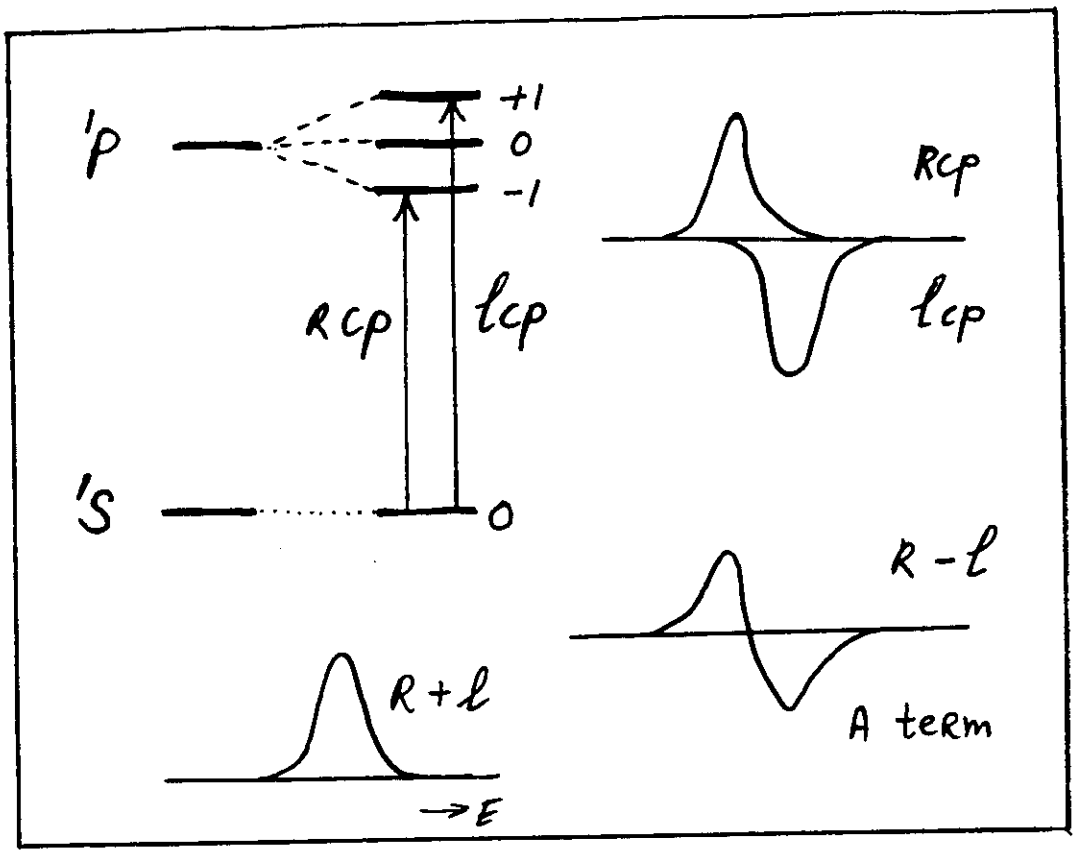

C term

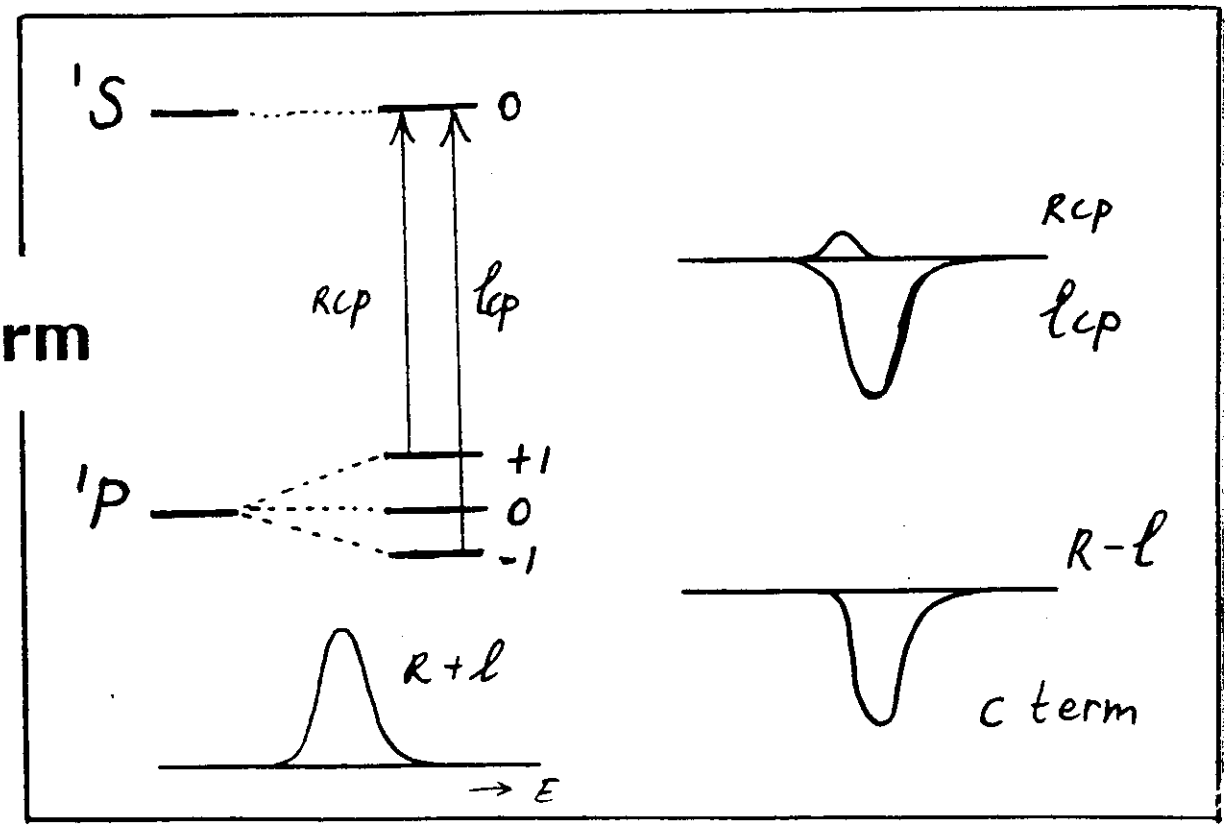

(a) Magneto-optical Kerr effect and Faraday effect

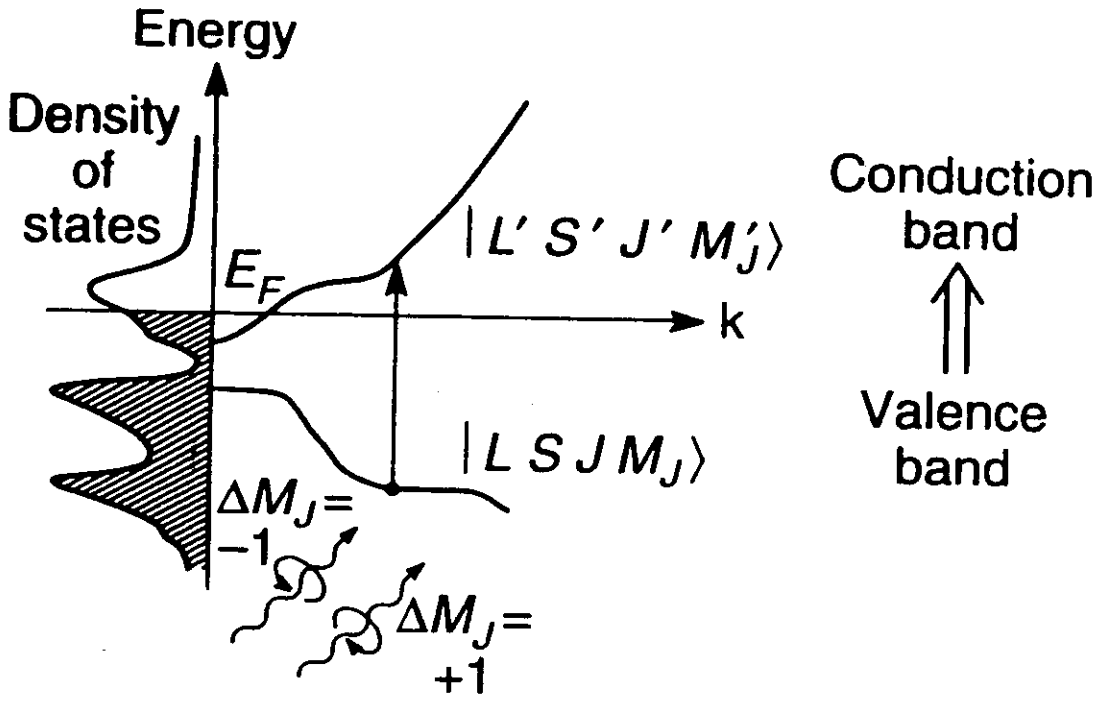

(b) X-ray magnetic circular dichroism

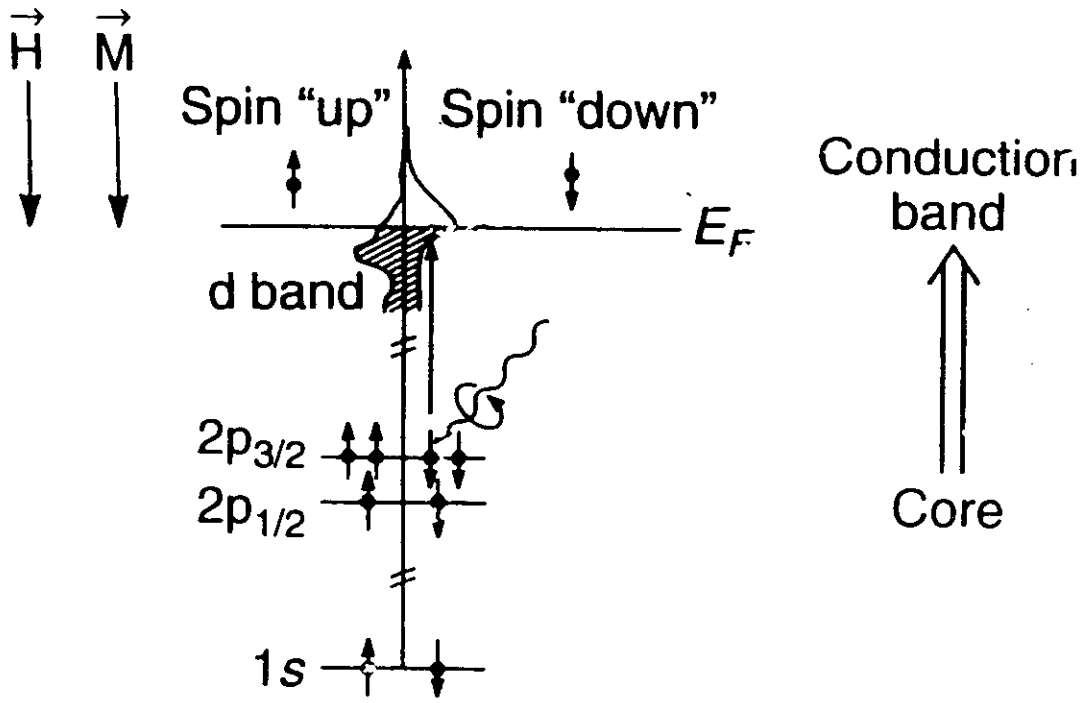

Observed magneto-optic effects in the x-ray region

1972 Magnetic diffraction

:

:

:

:

1985 Magnetic x-ray dichroism

:

1988 Magnetic resonance scattering

:

1990 Faraday rotation

Kerr effect in reflectivity

MCD in photoemission

1993 Magnetic imaging

Magnetic linear dichroism in photoemission

MCD in resonant photoemission

1995 Quadrupolar resonant photoemission

Magnetic photoelectron diffraction

Production of circularly polarized x-rays

Synchrotron radiation from a bending magnet

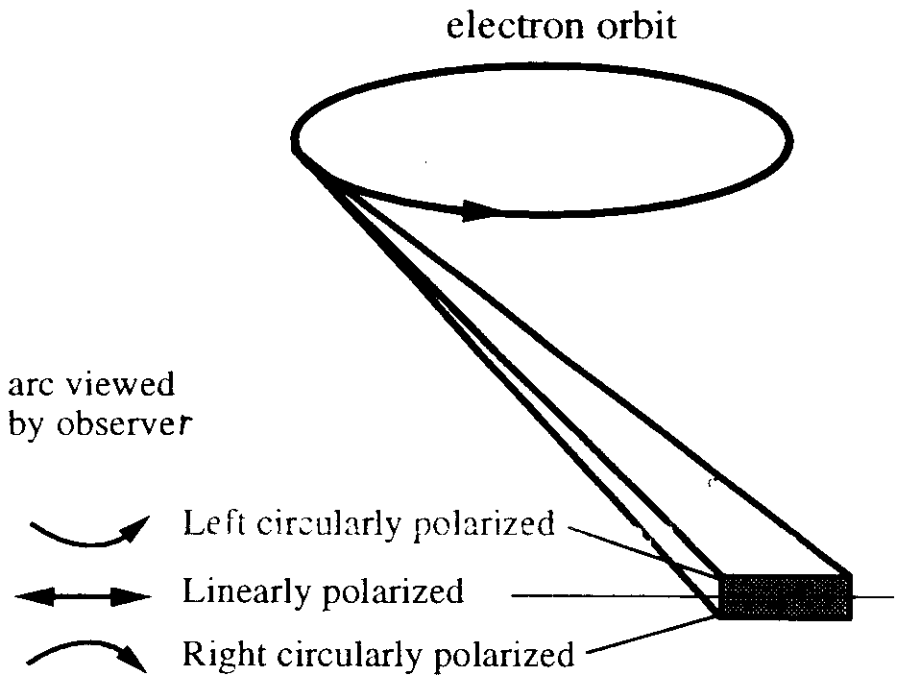

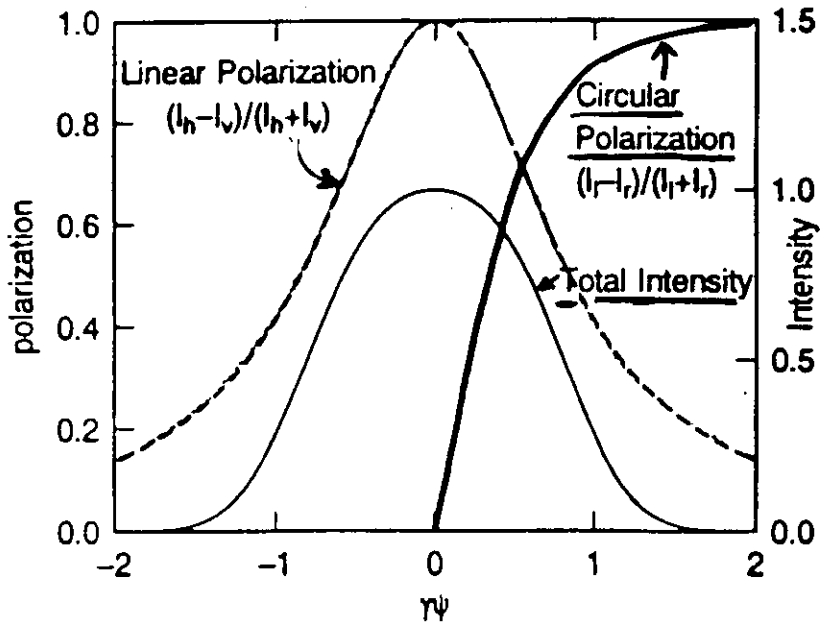

Circularly Polarized X-rays from the SGM beamline 8-2 at SSRL

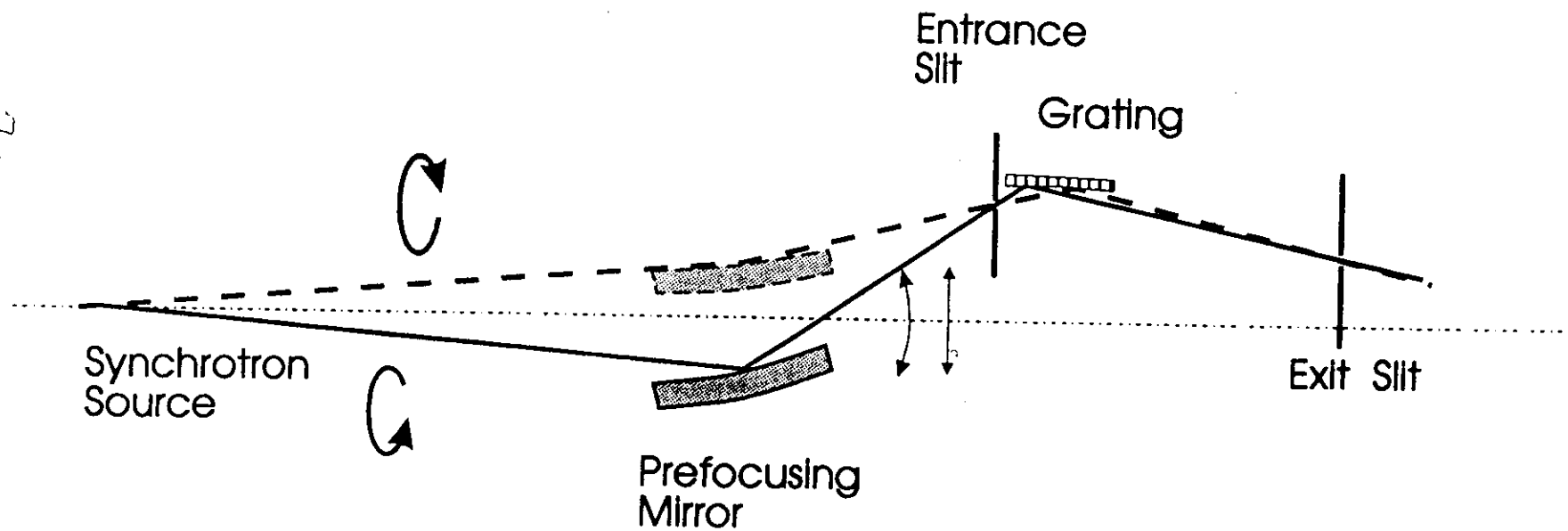

$100eV \lesssim h\nu \lesssim 1500eV$

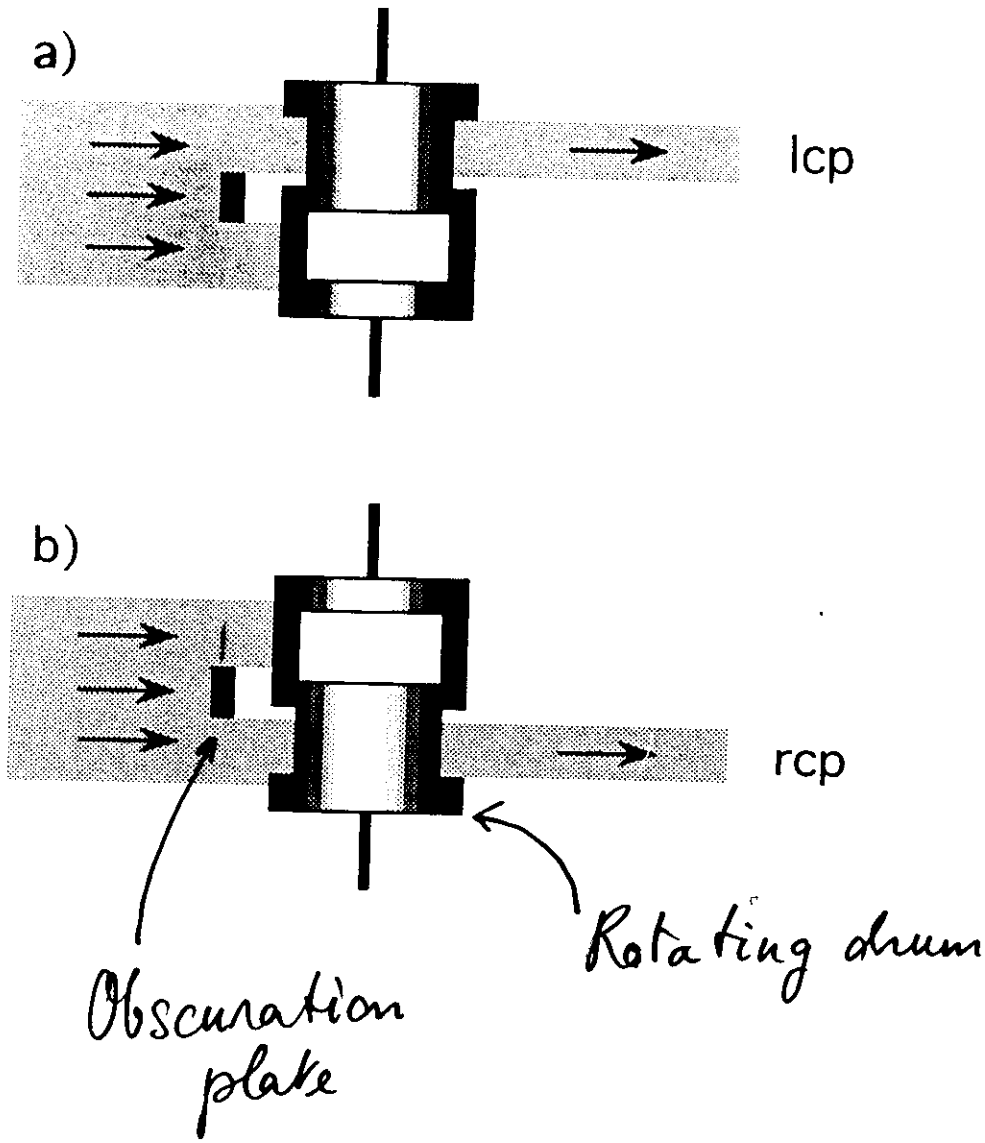

Polarization Chopper

SRS beamlines for MXD in soft x-ray region

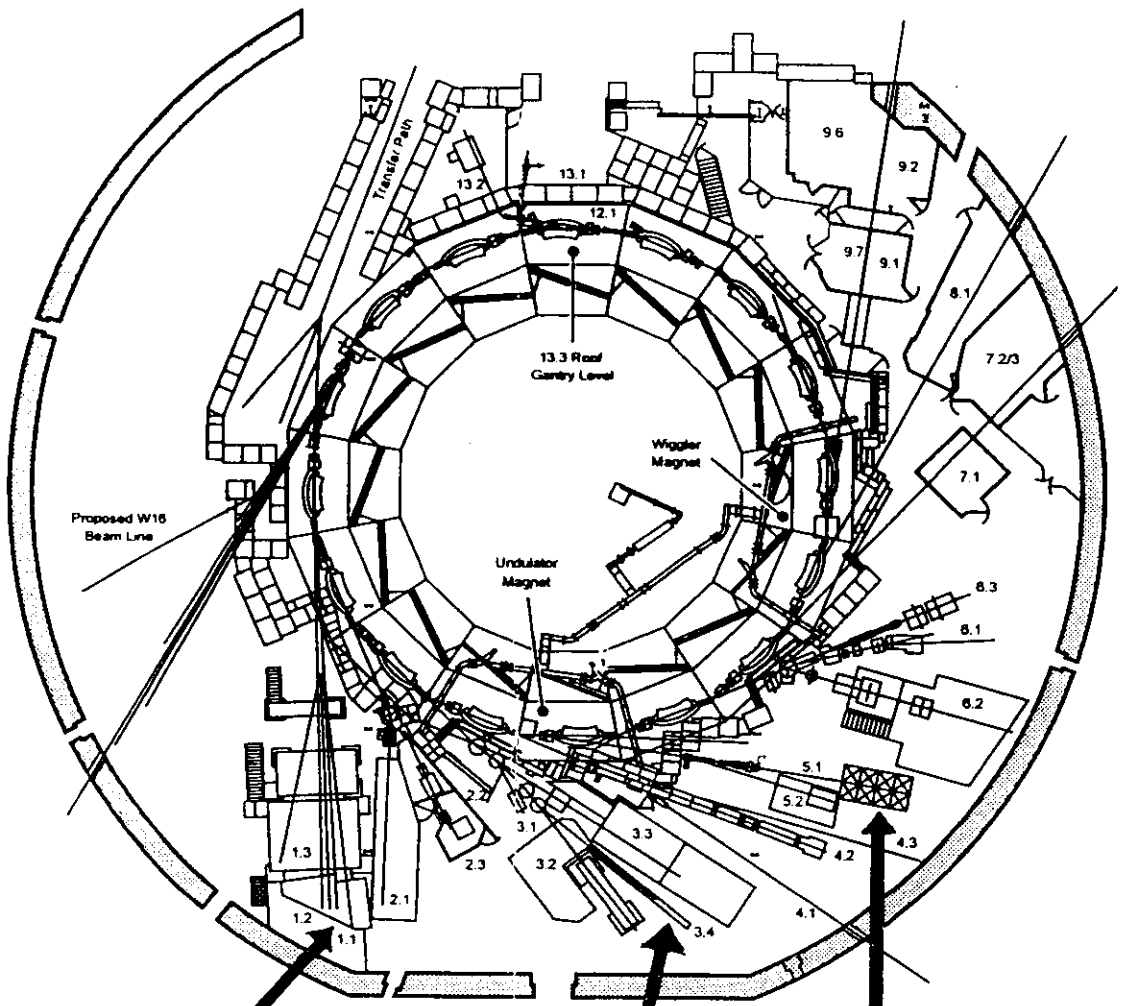

Beamline 1.1, HESGM
300 - 1000 eV
circular polarization

3d transition metal $L_{2,3}$ edges

Beamline 5.U1, SX700
150 - 1000 eV
linear polarization

3d transition metal $L_{2,3}$ edges

Beamline 3.4, DXM
800 - 4000 eV
circular polarization

4d transition metal $L_{2,3}$ edges
5d transition metal $M_{2,3}$ edges
rare earth $M_{4,5}$ edges

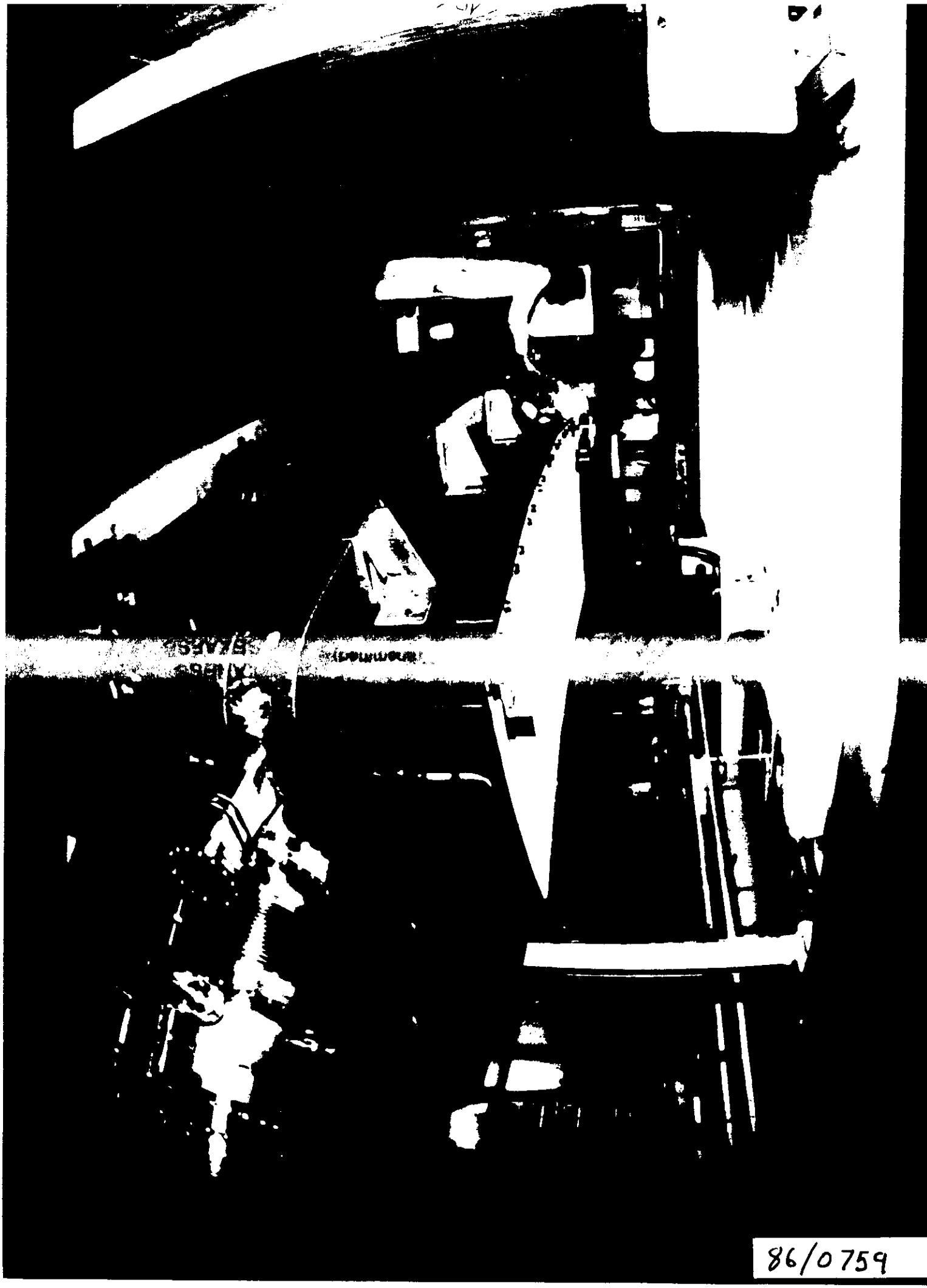

86/0759

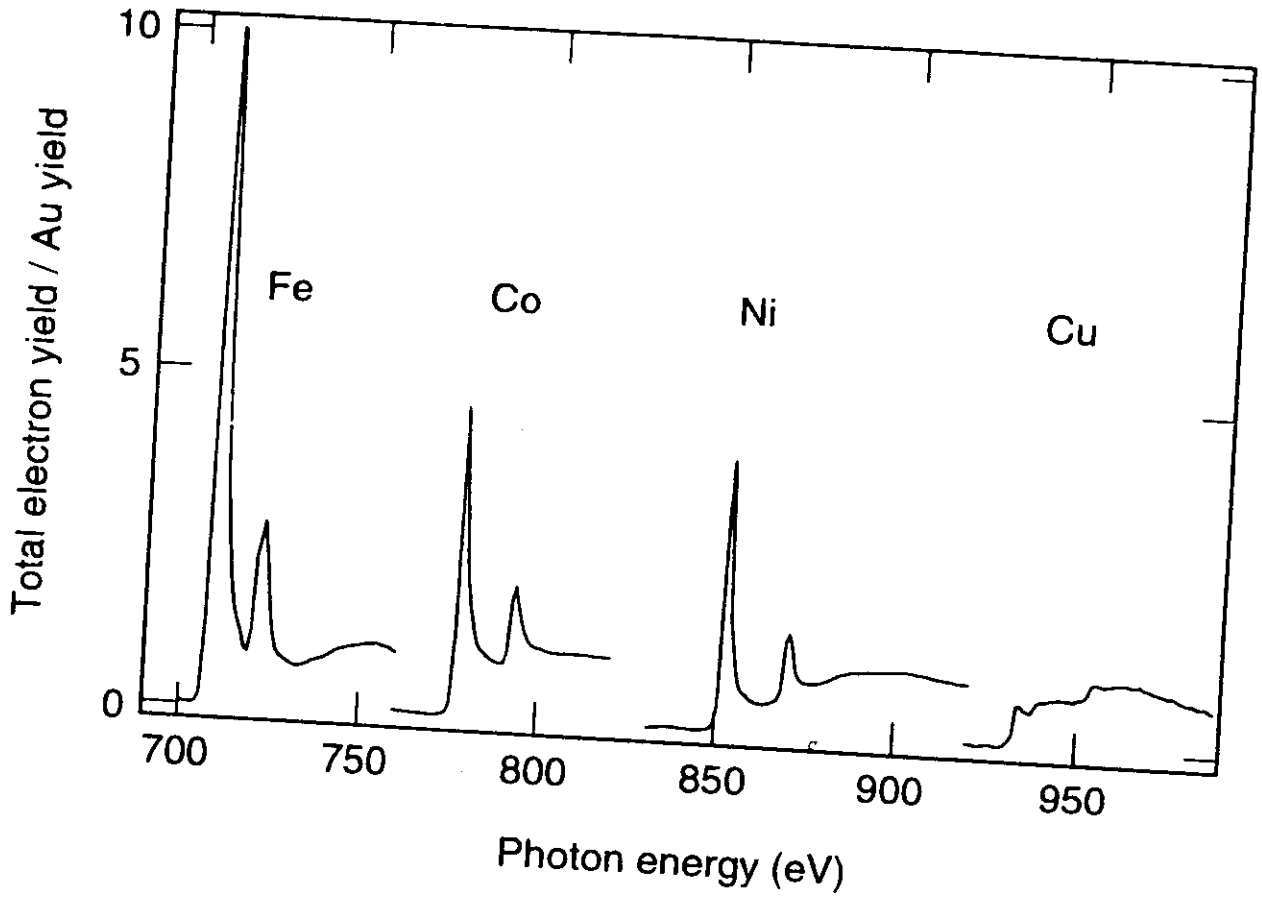

$L_{2,3}$ edge absorption spectra of $3d$ transition metals

- Element specific
- Intensity proportional to number of $3d$ holes

Magnetic Circular X-ray Dichroism

* Element specific local probe
* Surface sensitive
* Sum rules: Edge intensities give the spin and orbital contributions to the magnetic moment

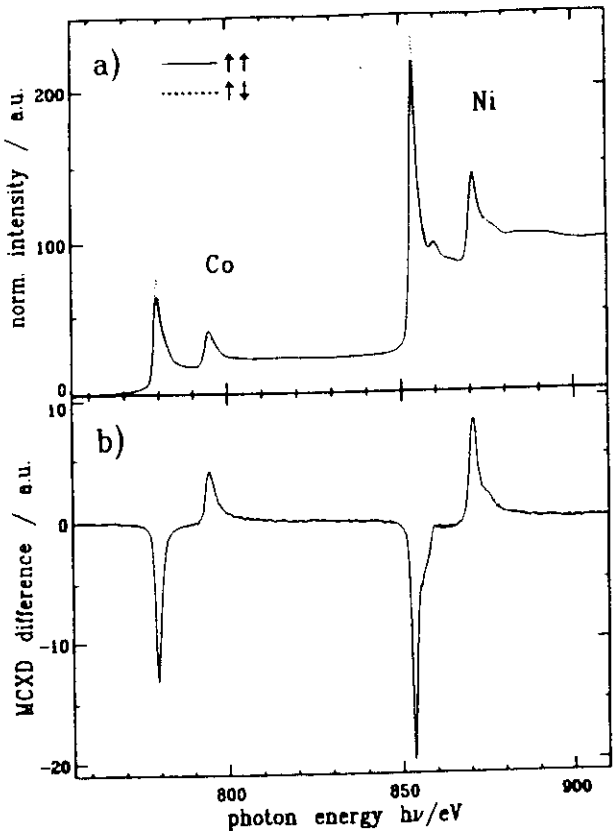

$L_{2,3}$ absorption edges of CoNi compound

Ideal to study magnetic metallic thin films and multilayers.
Applications: magneto-optic recording media.

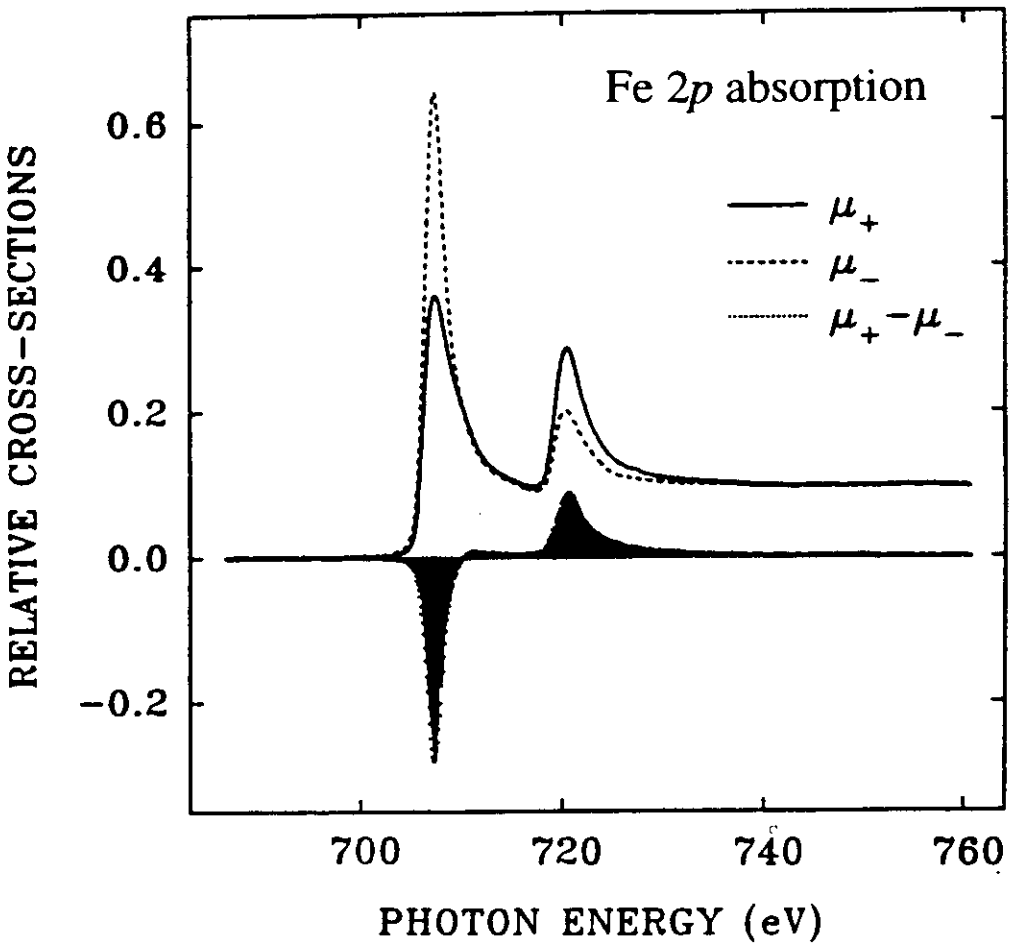

Orbital magnetization sumrule

Thole, Carra, Sette, van der Laan, Phys. Rev. Lett. **68**, 1943 (1992)

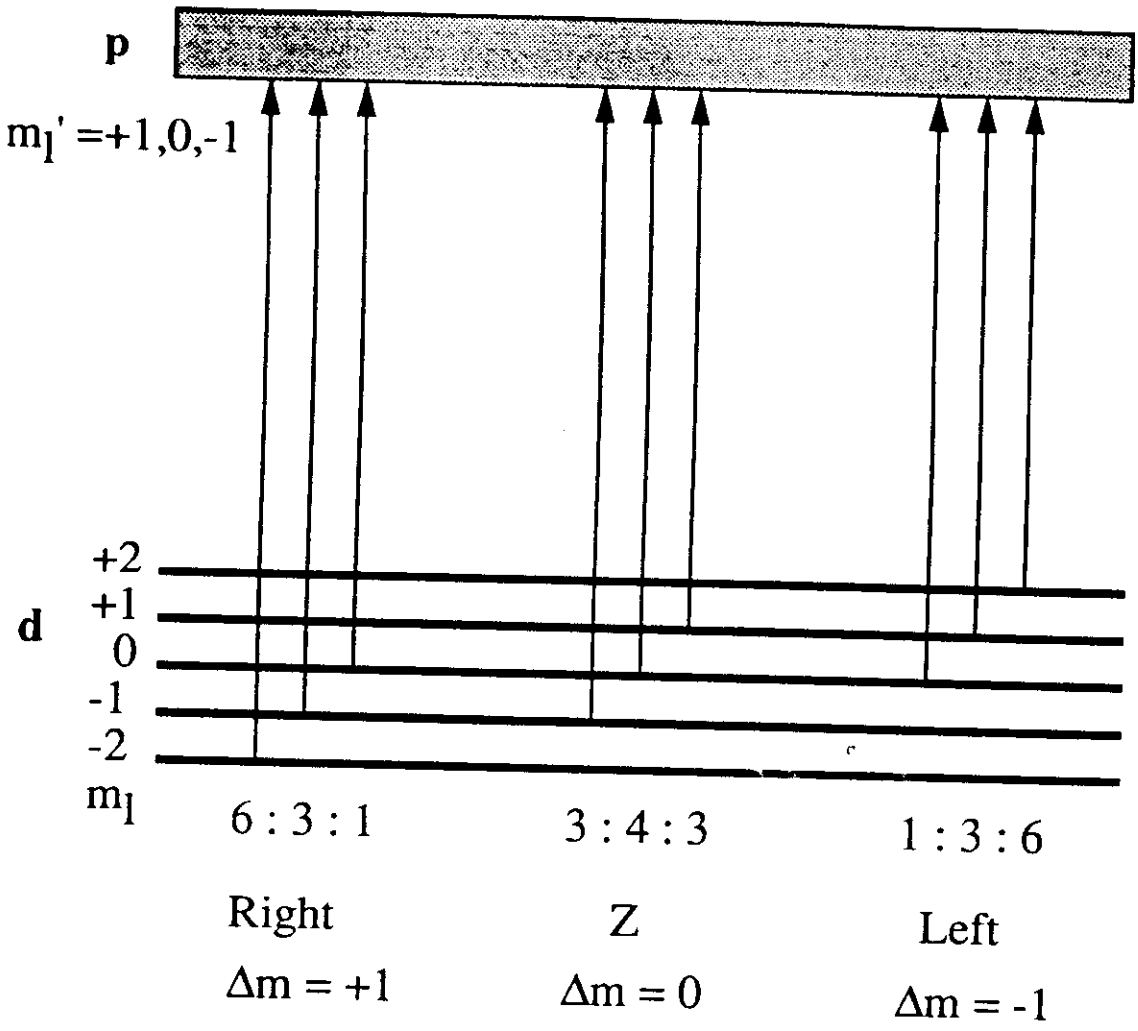

Sum Rules
Integrated intensities
(sum over final states)

Orbital Magnetic Moment:

$$L_z = \sum_{m\sigma} \langle n_{m\sigma} \rangle \, m$$

Spin Magnetic Moment:

$$S_z = \sum_{m\sigma} \langle n_{m\sigma} \rangle \, \sigma$$

Magnetic Dipole Term:

$$\mathbf{T} = \mathbf{S} - 3\hat{r}\,(\hat{r}\cdot\mathbf{S}) \cong \tfrac{1}{2}\, Q \cdot \hat{S}$$

Quadrupole Moment:

$$Q_{zz} = \sum_{m\sigma} \langle n_{m\sigma} \rangle \, [m^2 - \tfrac{1}{3}\, l(l+1)]$$

---

from XAS using SUMRULES

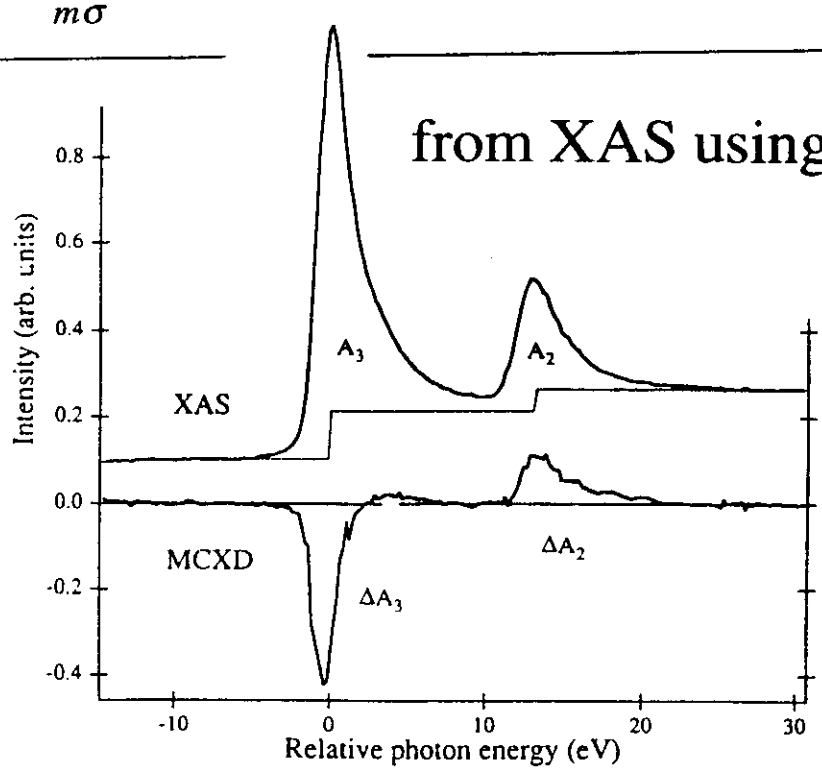

PRB 50, 11467 (1994)

SPECTRAL MOMENT ANALYSIS

"Beyond the Sum Rules"

$$I(\omega) = \sum_f \langle g | T | f \rangle \langle f | T | g \rangle \delta(E_f - E_g - \omega)$$

where T is the dipole operator

---

n-th moment:

$$I^{(n)} \equiv \int_0^\infty d\omega \; \omega^n I(\omega)$$

$$= \sum_f \langle g | T | f \rangle \langle f | T | g \rangle E_f^n$$

$$= \sum_f \langle g | T | f \rangle \langle f | H^n | f \rangle \langle f | T | g \rangle$$

$$= \sum_{ff'} \langle g | T | f \rangle \langle f | H^n | f' \rangle \langle f' | T | g \rangle$$

$|f\rangle$ are eigenstates of H and form a complete set: (closure)

$$I^{(n)} = \langle g | TH^nT | g \rangle$$

For n=0: $I^{(n)} = \langle T^2 \rangle$ -> "sum rules"

For n=1: $I^{(n)} = \langle THT \rangle$ -> effective operators.

Spectral Distributions (cont.)

$$I^{(n)} = \langle T^\dagger H^n T \rangle, \qquad H = \text{final state Ham.}$$

e.g. $n=0$: Integrated intensity.

$I^{(0)} = \langle T^2 \rangle \rightarrow$ sum rules

depends only on GS and T, not on details of $H_{f.s.}$

$n=1$ Line asymmetry.

$$I^{(1)} = \langle T^\dagger H T \rangle$$

e.g. <u>One-electron model.</u> H_s = effective field

$$H = H_s \delta_2 + \xi \, l \cdot s$$

$$\rightarrow E_{jm} = \frac{j(j+1) + s(s+1) - l(l+1)}{2j(j+1)} H_s^m$$

Contributions to the $2p$ MXD spectrum
for each ground state moment in a $3d$ metal

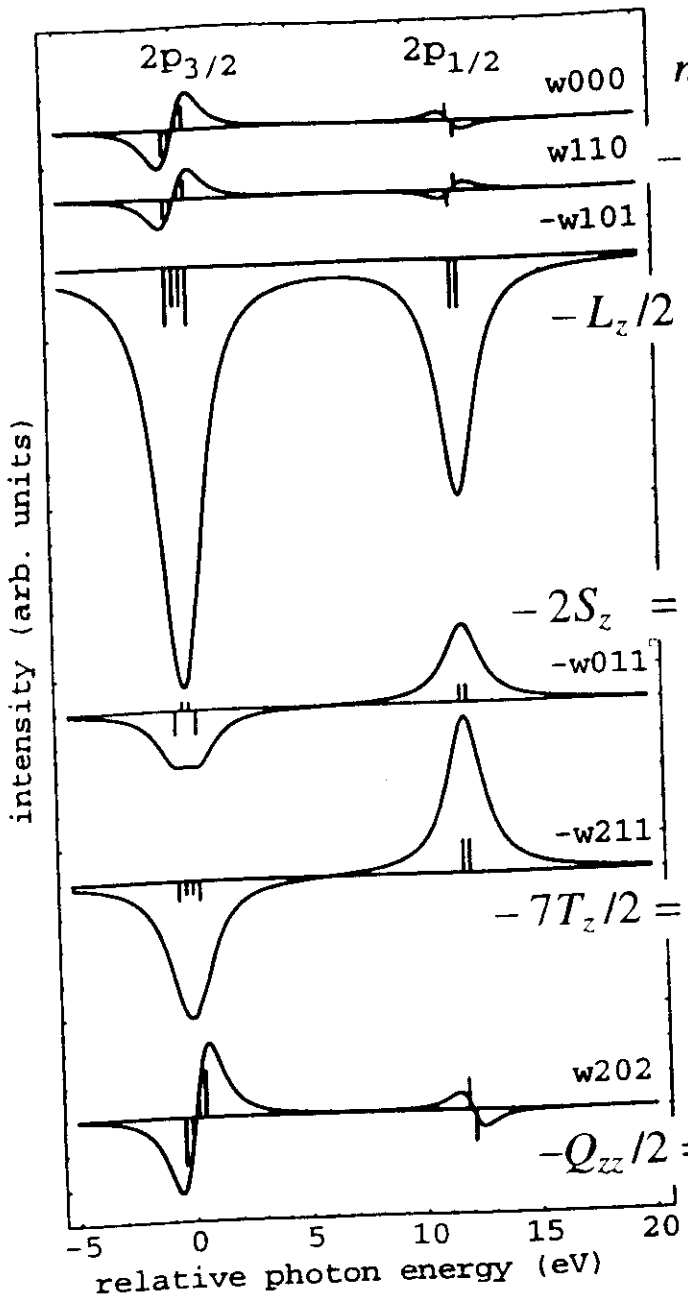

n_h = number of holes

$-\,l \cdot s$ = spin-orbit operator

$-\,L_z/2$ = orbital magnetic moment

$-\,2S_z$ = spin magnetic moment

$-\,7T_z/2$ = magnetic dipole term

$-Q_{zz}/2$ = quadrupole moment

0.2 ML Fe/Ni (110)

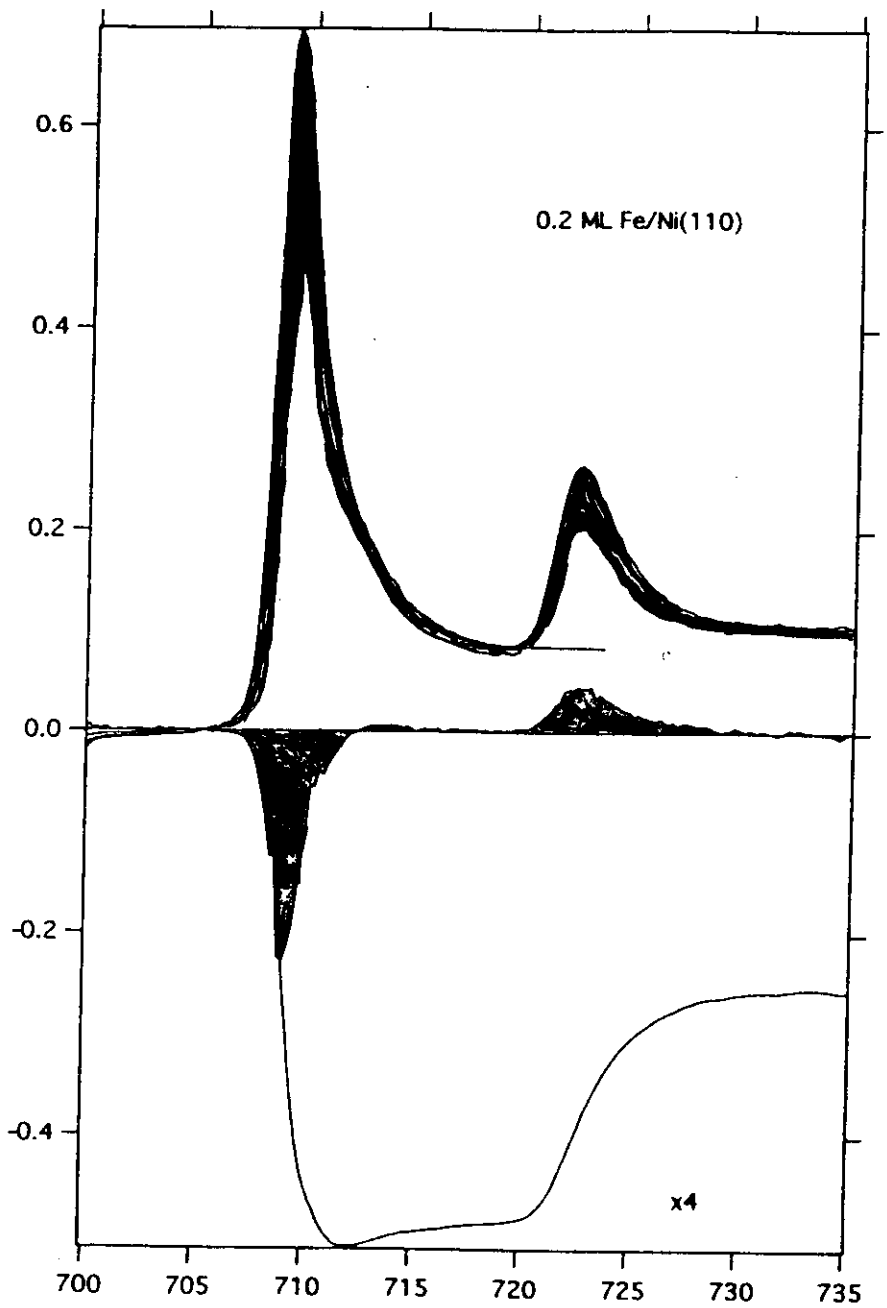

Dürr et al.

Role of the spin polarization in x-ray magnetic circular dichroism spectra of itinerant magnets

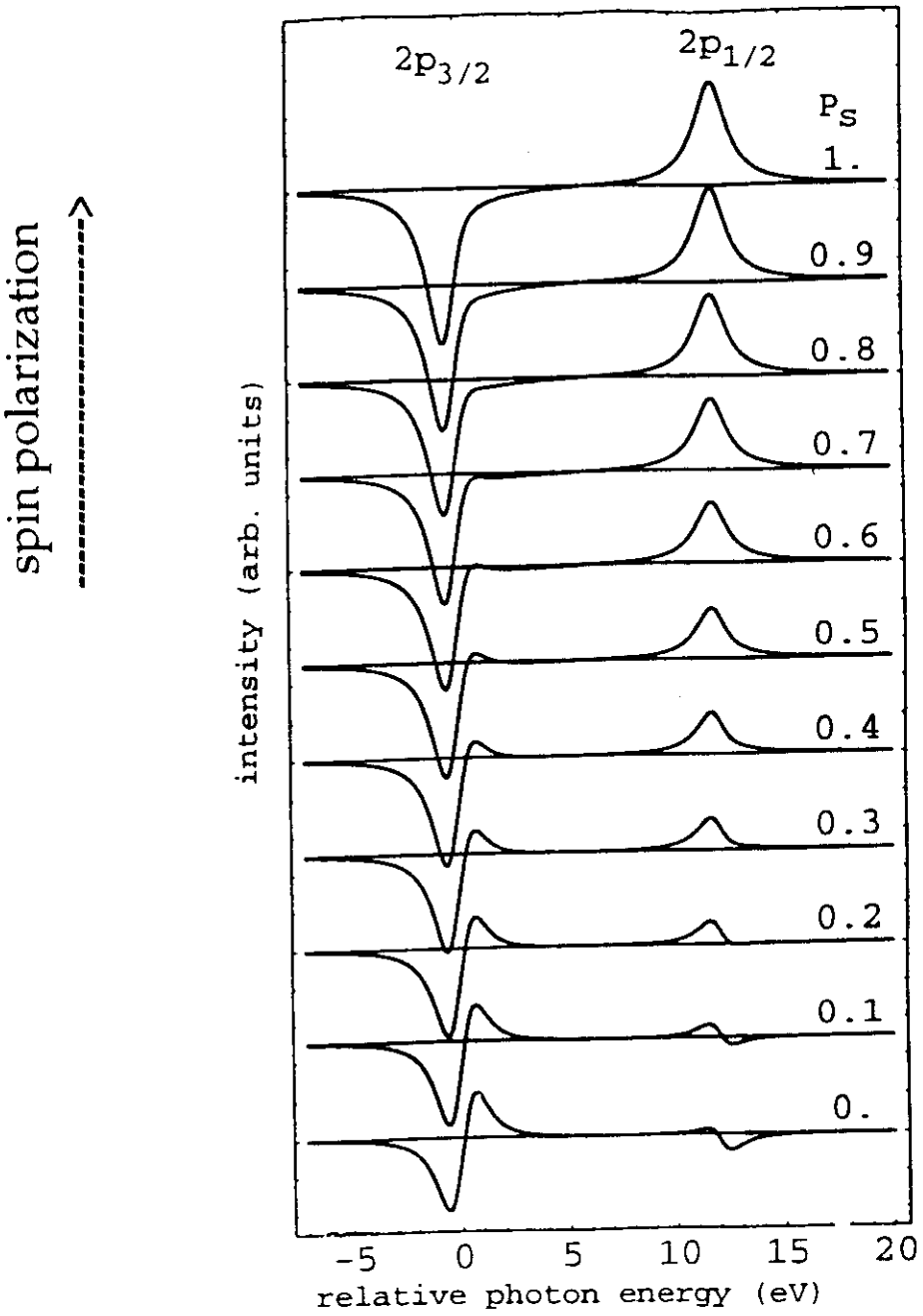

2*p* MXD in 3*d* metals

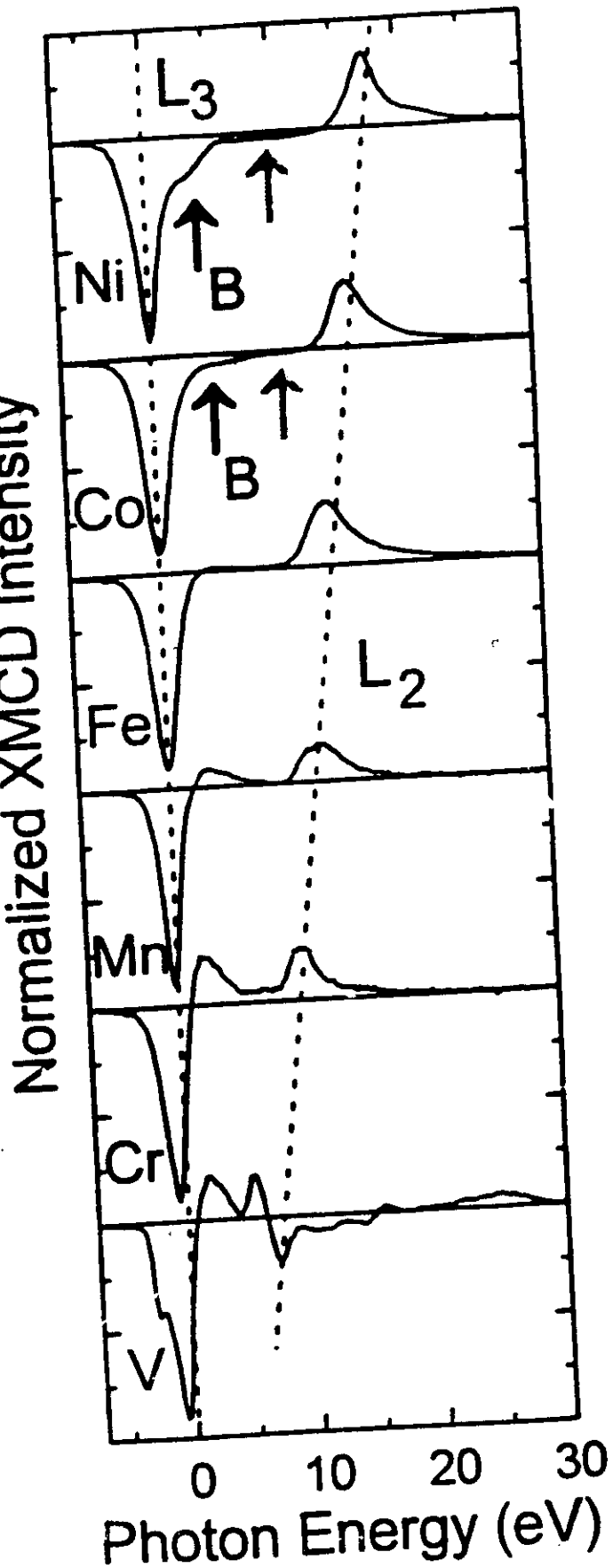
L3
Ni
B
Co
B
Fe
L2
Mn
Cr
V
Normalized XMCD Intensity
0
10
20
30
Photon Energy (eV)

Role of the spin polarization in x-ray magnetic circular dichroism spectra of itinerant magnets

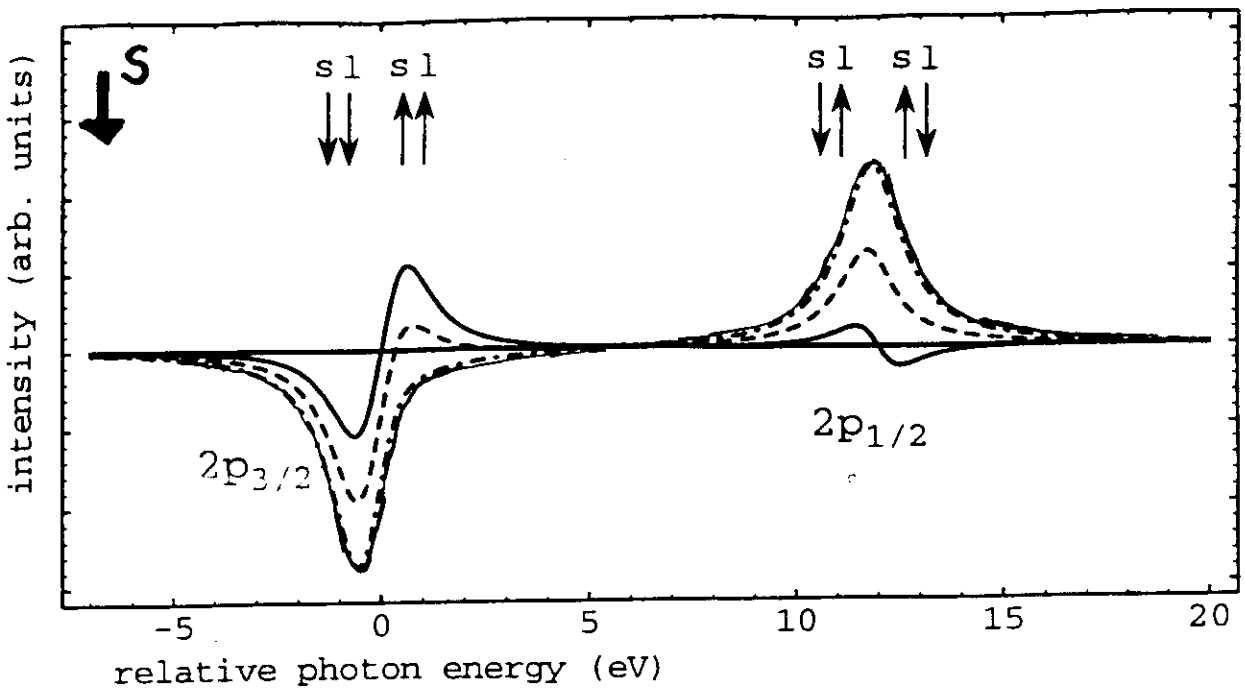

2*p* MXD in 3*d* metal

spin-orbit splitting + exchange field

Magnetic x-ray dichroism of uranium M4,5 edges in US.
Collins, Laundy, Tang, and van der Laan
J. Phys. Condens. Matter 1995

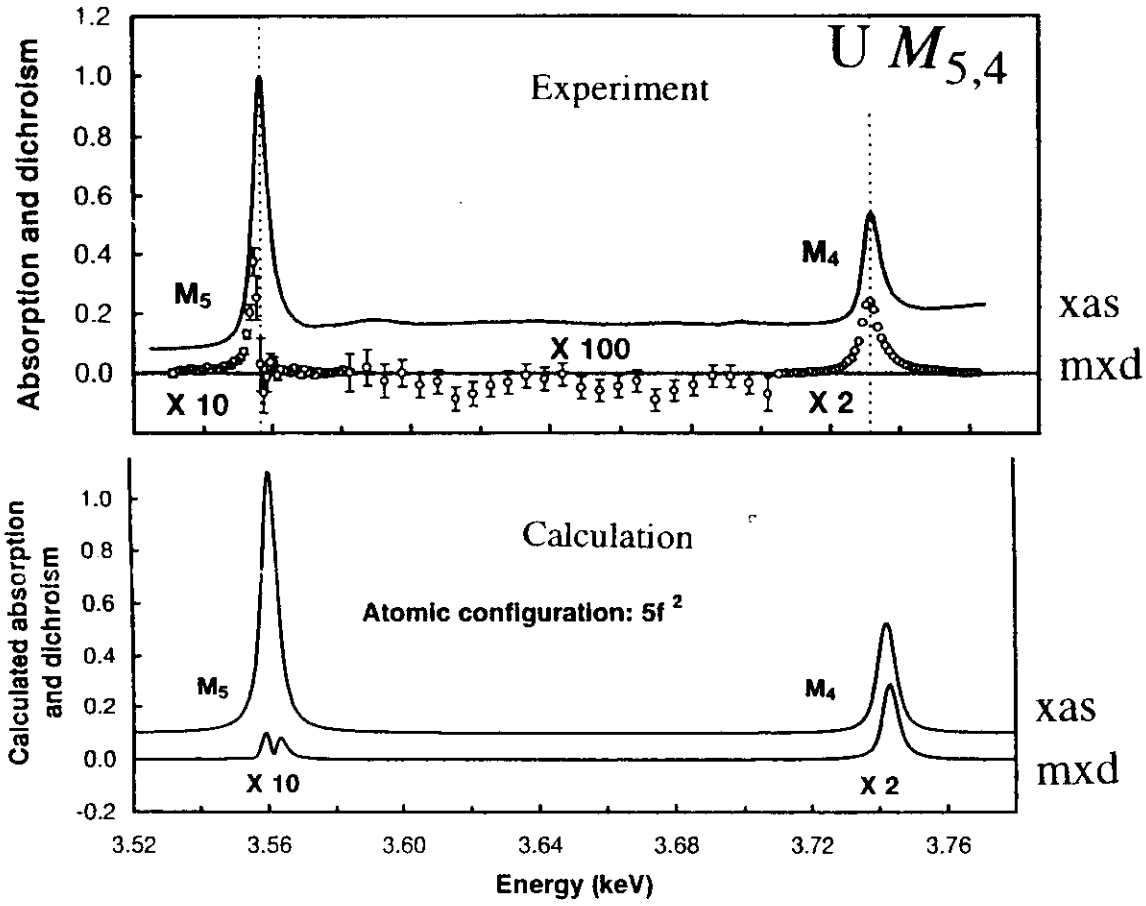

$\langle L_z \rangle = -2.6 \pm 0.2\ \mu_B$

$\langle S_z \rangle = +0.45 \pm 0.1\ \mu_B$

$\langle T_z \rangle = +0.37 \pm 0.03\ \mu_B$

$M_{\text{total}} = -1.7\ \mu_B$

L and S antiparallel

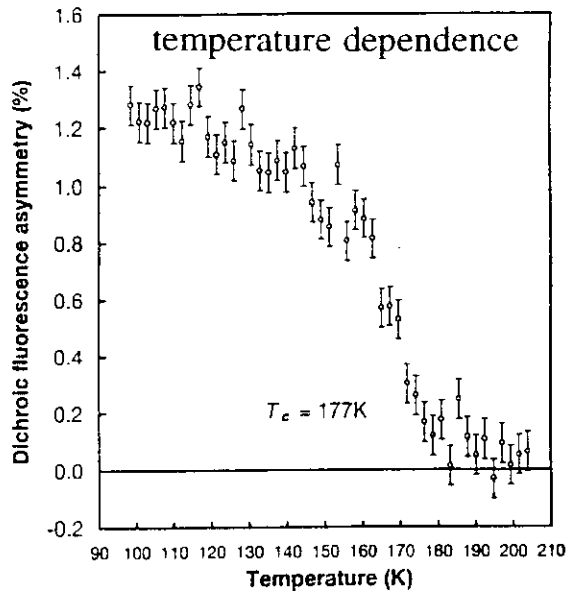

Magnetism and hybridization in ultrathin Mn films
Dürr, van der Laan, Spanke, Hillebrecht, Brookes PRB(1997)
exp. + calc.

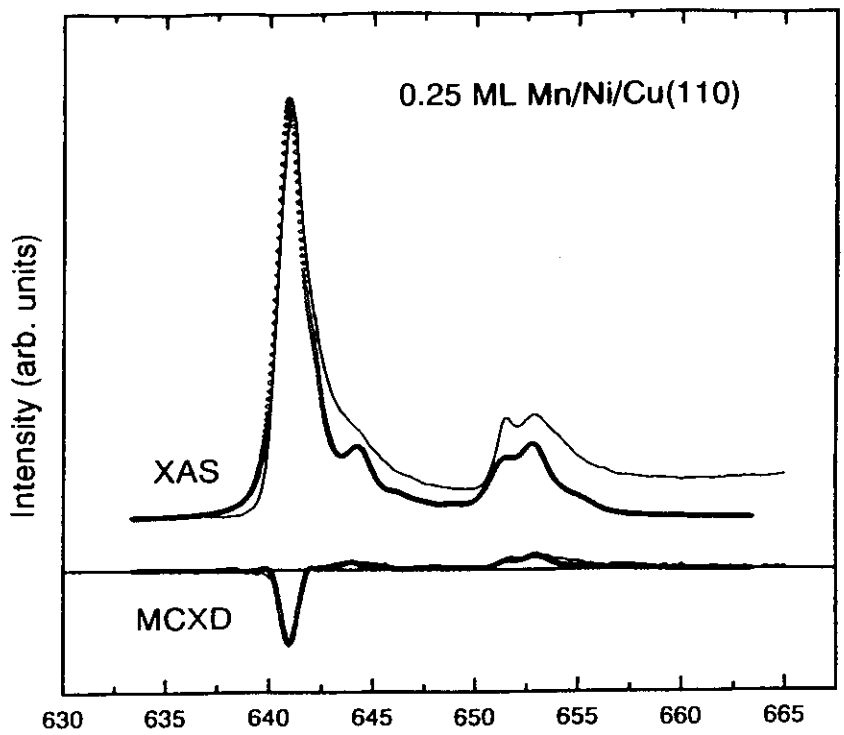

Mn/Ni

Antiferromagnetic

$5\% d^4$; $80\% d^5$; $15\% d^6$

$m_{spin} = 1.6\ \mu_B$

BR = 0.77

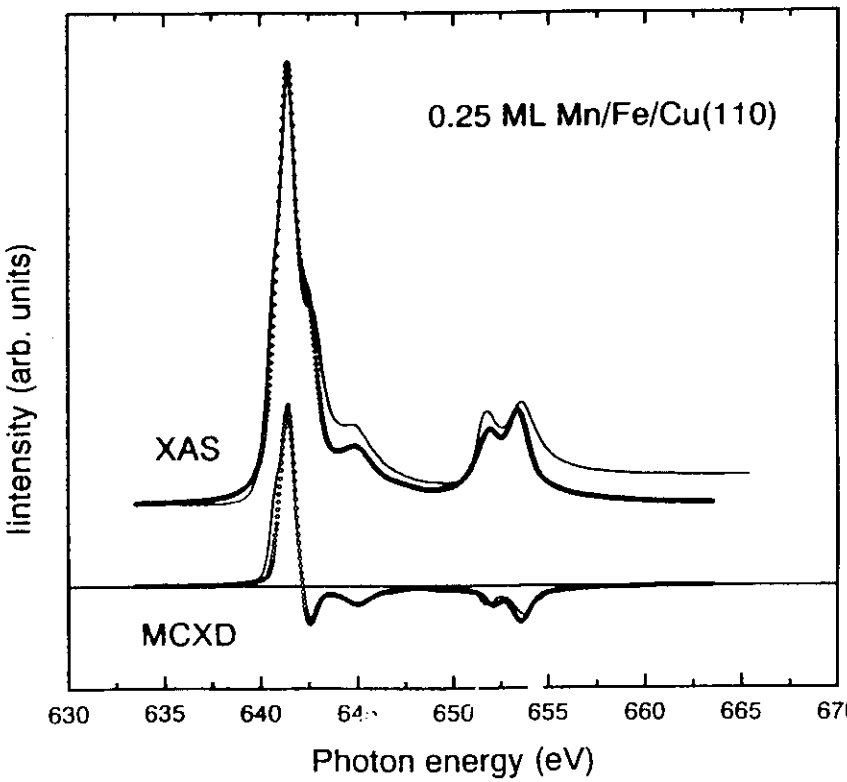

Mn/Fe

Ferromagnetic

$95\%\ d^5$; $5\%\ d^6$

$m_{spin} = 4.5\ \mu_B$

BR = 0.79

Magnetism and hybridization in ultrathin Mn films
(Dürr, van der Laan, Spanke, Hillebrecht, Brookes)
PR B 56, 8456 (1997)

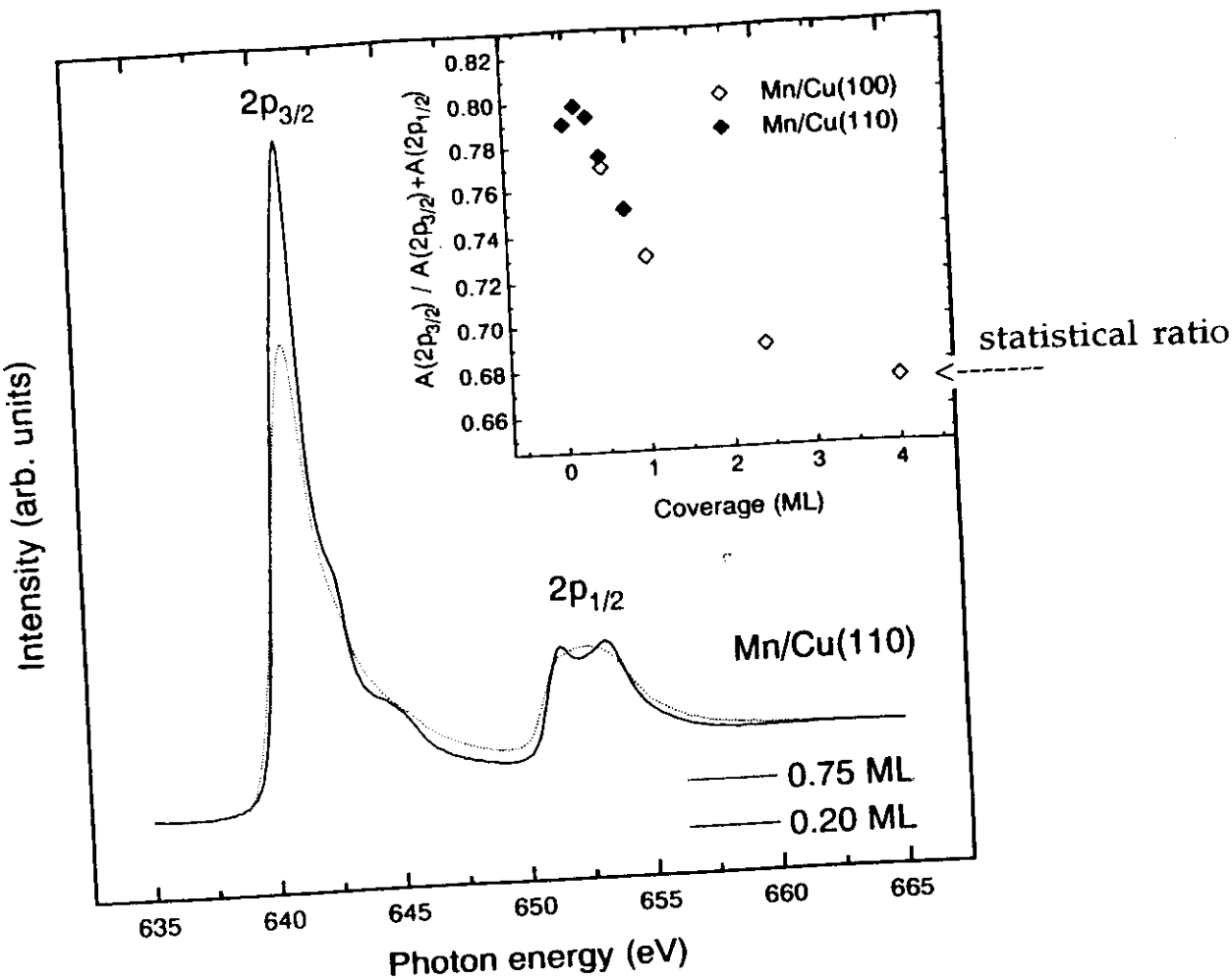

Localized 3*d* states	Itinerant 3*d* states
• 2*p* multiplet structure • large 2*p* branching ratio	smooth shape statistical ratio (without 3*d* s.o. as in Mn)

Element-specific magnetic hysteresis as a means for studying heteromagnetic multilayers

C. T. Chen Y. U. Idzerda

PHYSICAL REVIEW B JULY 1993

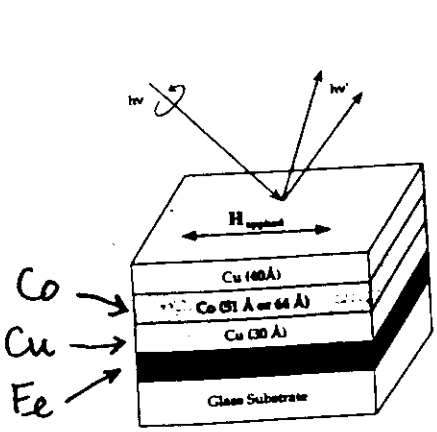

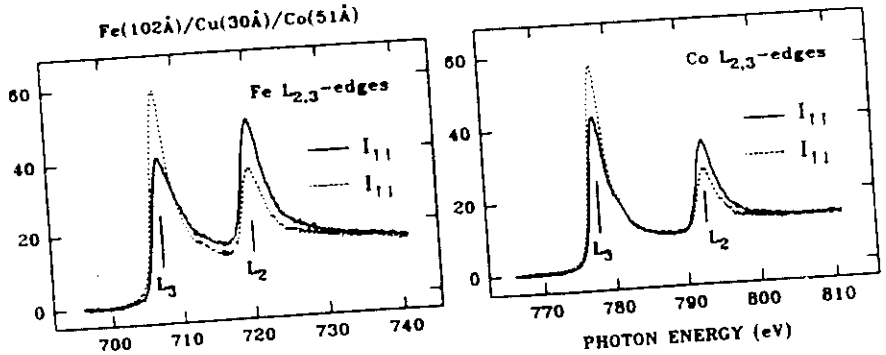

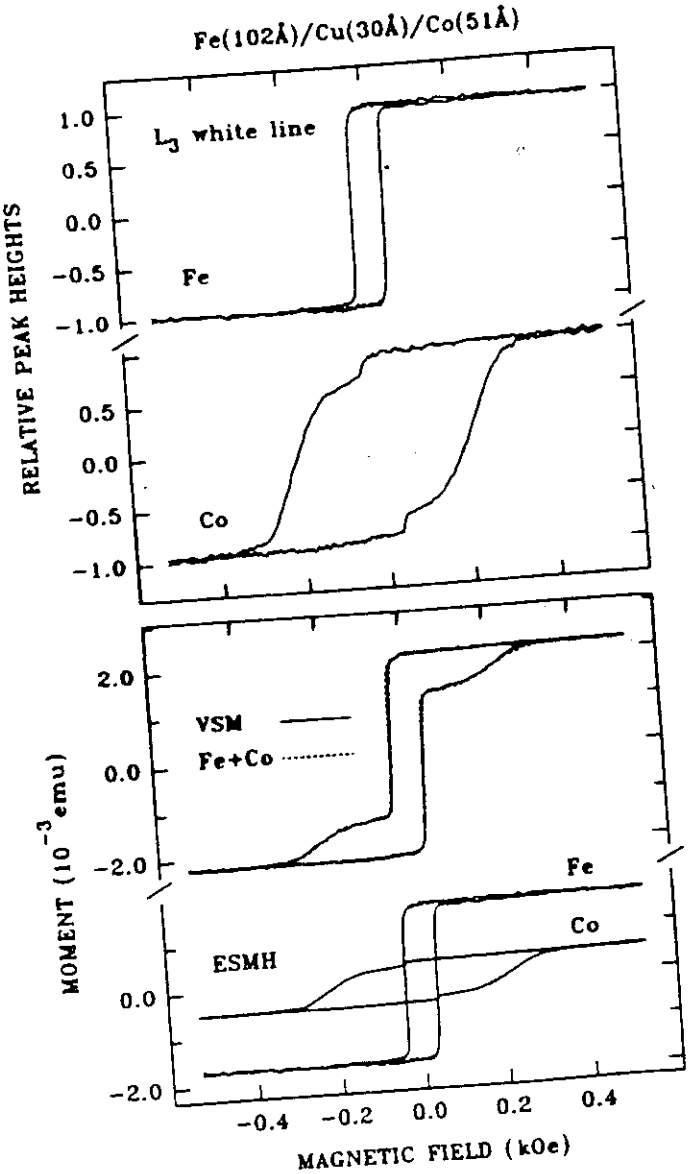

Sum rules

Orbital polarization

jj mixing

→ Higher-order moments

→ Spectral shape

→ Line shape analysis

→ Core hole polarization

→ Angular distribution

→ Angle dependence

Transverse measurements

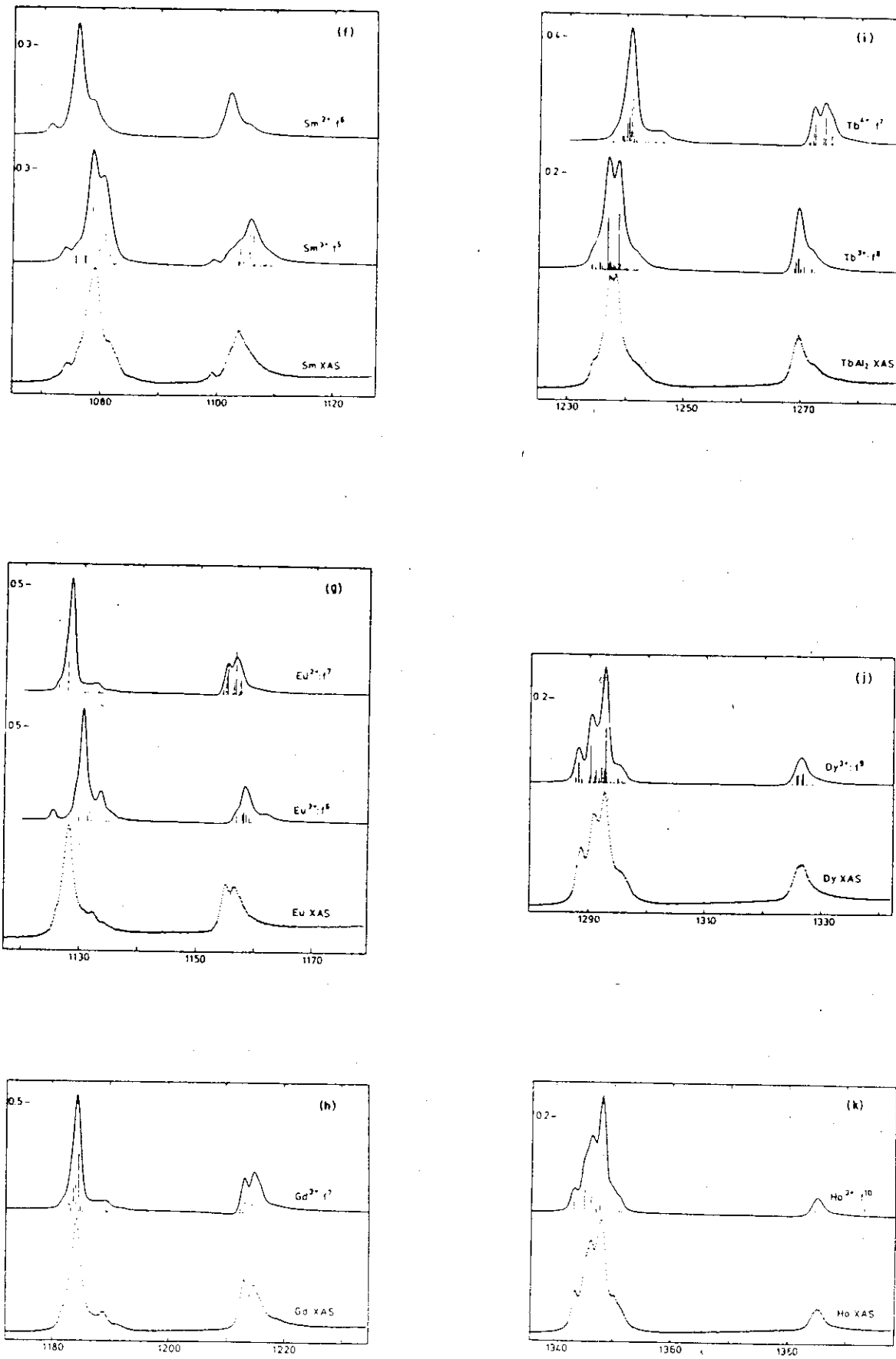

FIG. 1. (*Continued*).

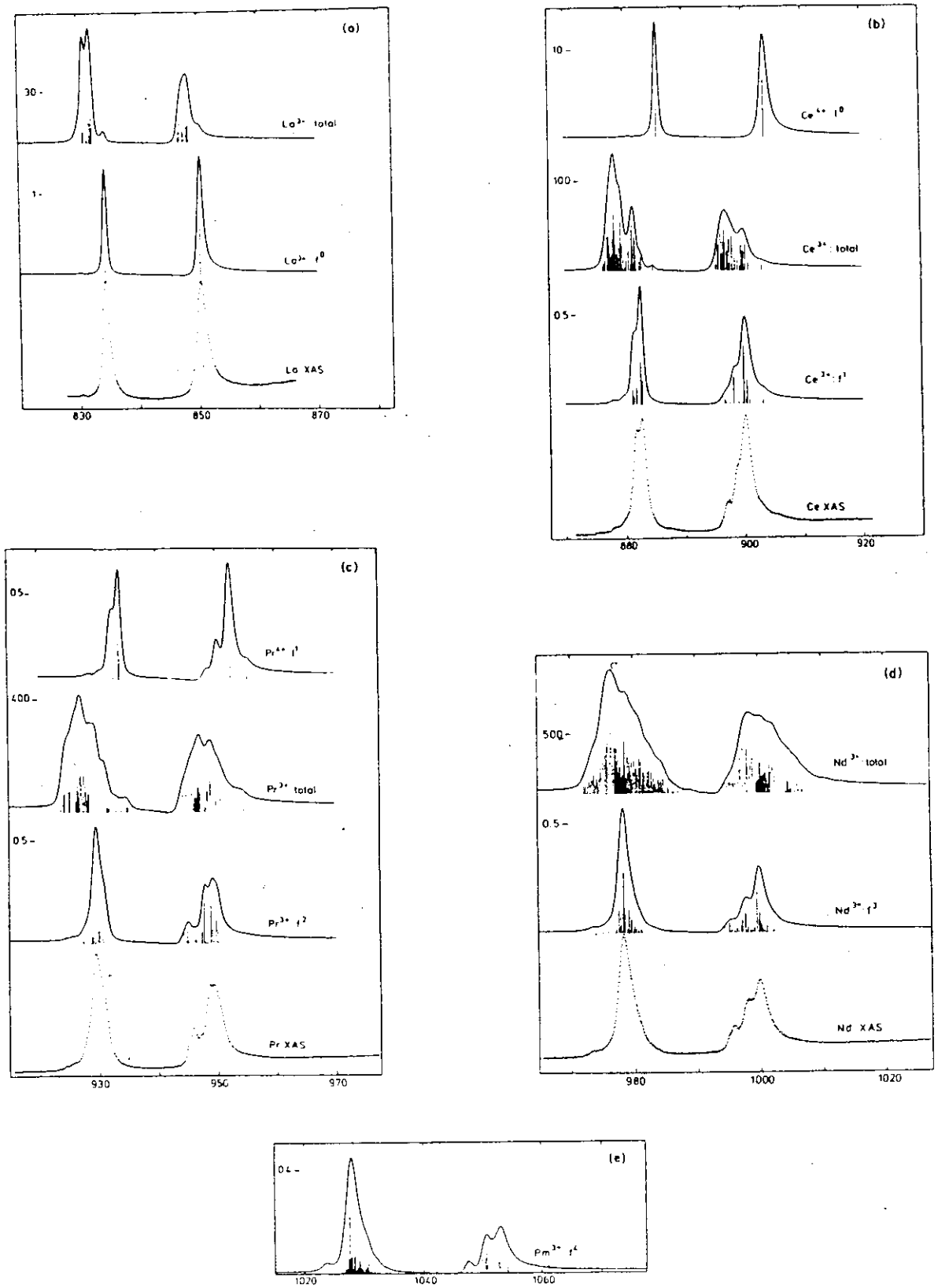

FIG. 1. Spectra of the rare-earth metals. The spectra labeled XAS are the experimental curves. The label f^n denotes the theoretical dipole excitation spectrum from the Hund's rule ground level of the configuration f^n to the levels of d^9f^{n+1}. The spectrum labeled "total" gives each level of d^9f^{n+1} with weight $2J+1$. The horizontal axes gives the excitation energy in eV. The experimental spectra have an unknown vertical scale. The scale of the theoretical spectra is indicated at the left. The dipole spectra give the absorption cross section σ in Å^2, the "total" spectra give the density of states in numbers of atomic levels per eV for the curves. The vertical lines have been normalized; close lying lines have been added.

Leapman & Grunes PRL 45, 397 (1980)

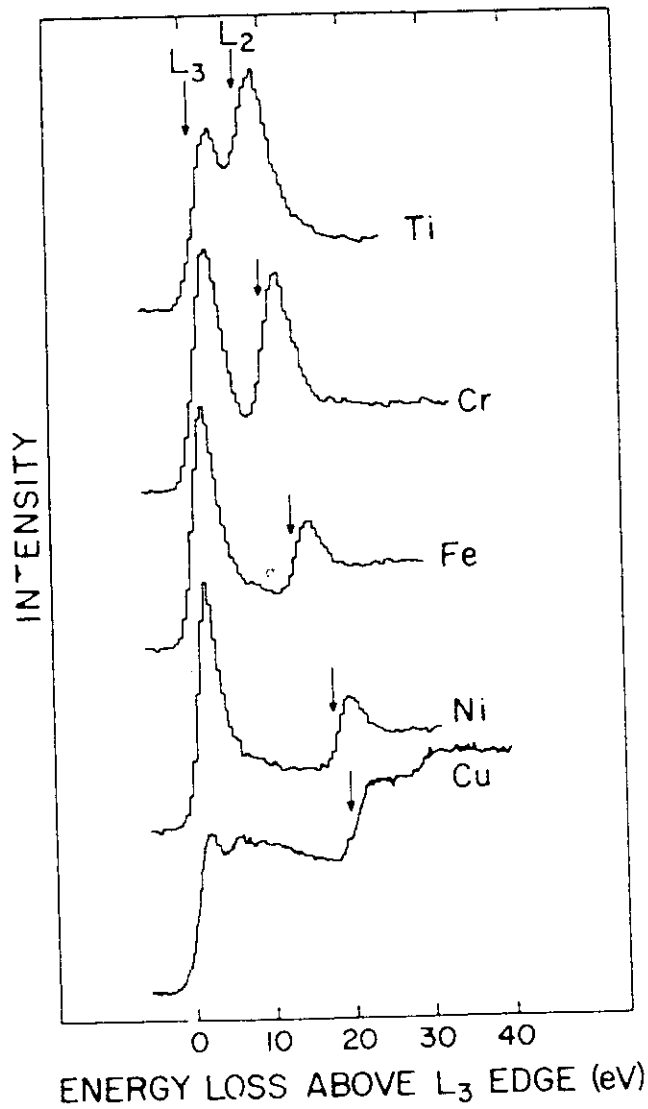

FIG. 1. L_{23}-shell excitation in the 3d transition metals and Cu.

Branching ratio in XAS

G. van der Laan
B.T. Thole

Why is the peak ratio for deep core levels non-statistical?

Why does the high energy peak decrease as the f or d shell fills up?

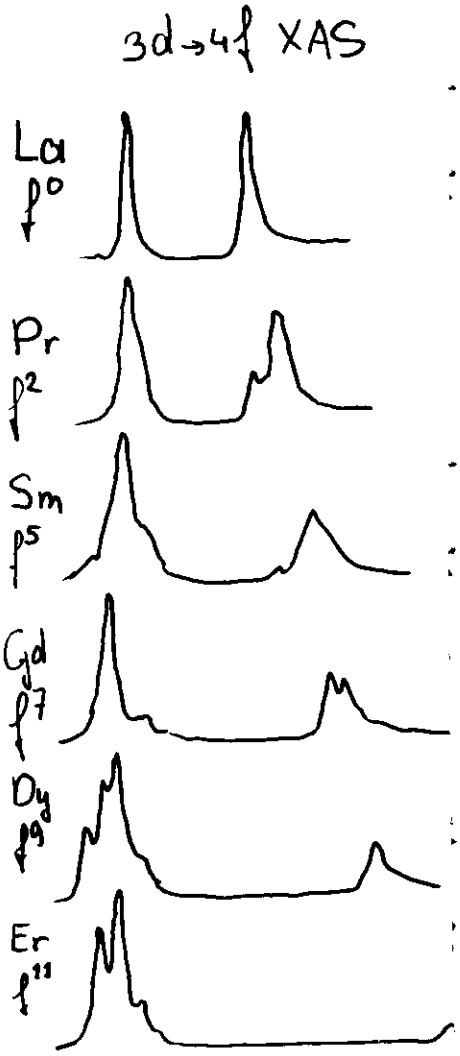

There are two effects:

— Coulomb interaction in the final state
core hole ↔ valence shell

— Spin orbit interaction in the initial state
within valence shell

Only two possible reasons for non-statistical B :

1. **Spin-orbit interaction in the valence shell.**

2. **Electrostatic interactions between core-hole and valence electrons.**

Pt $d^9 \rightarrow p^5 d^{10}$ ($\Delta J = 0, \pm 1$) *Mott*

No electrostatic interactions

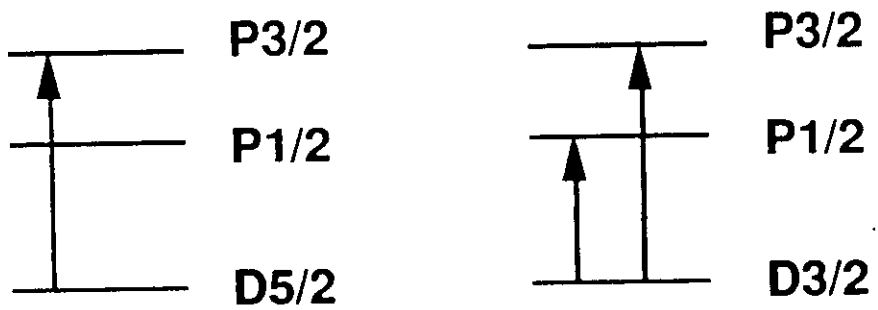

B = 1 **B = 1/6**

Average B = 2/3

$3d^8$

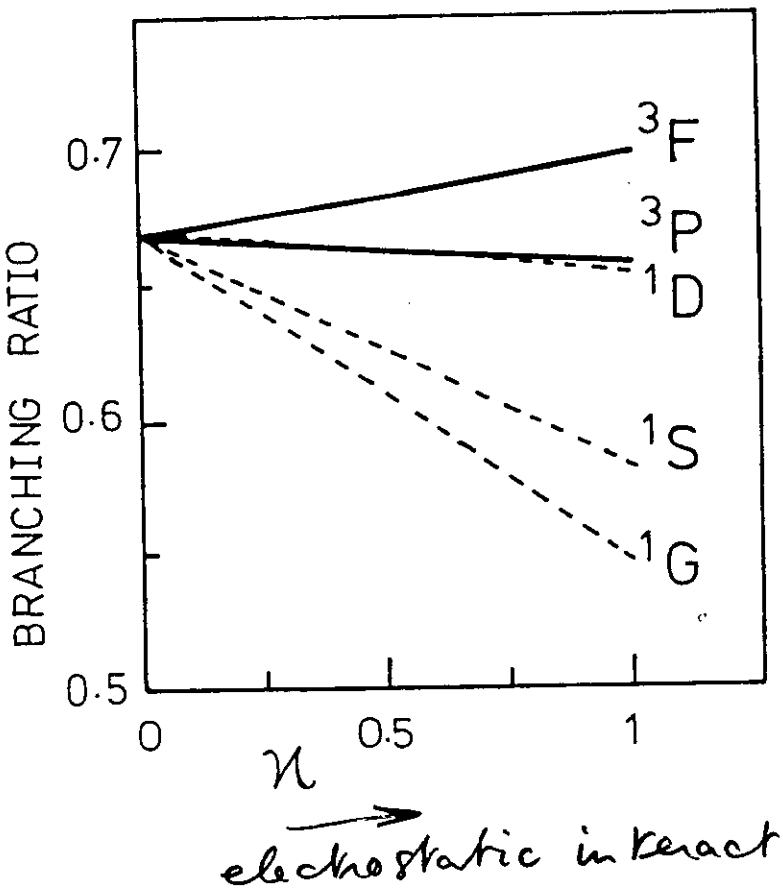

High-spin states have high BR.
Low-spin states have low BR.

This is important way to identify the spin-state.

$d^8 \longrightarrow p^5 d^9$ Coulomb effect

Consider zero core hole spin orbit

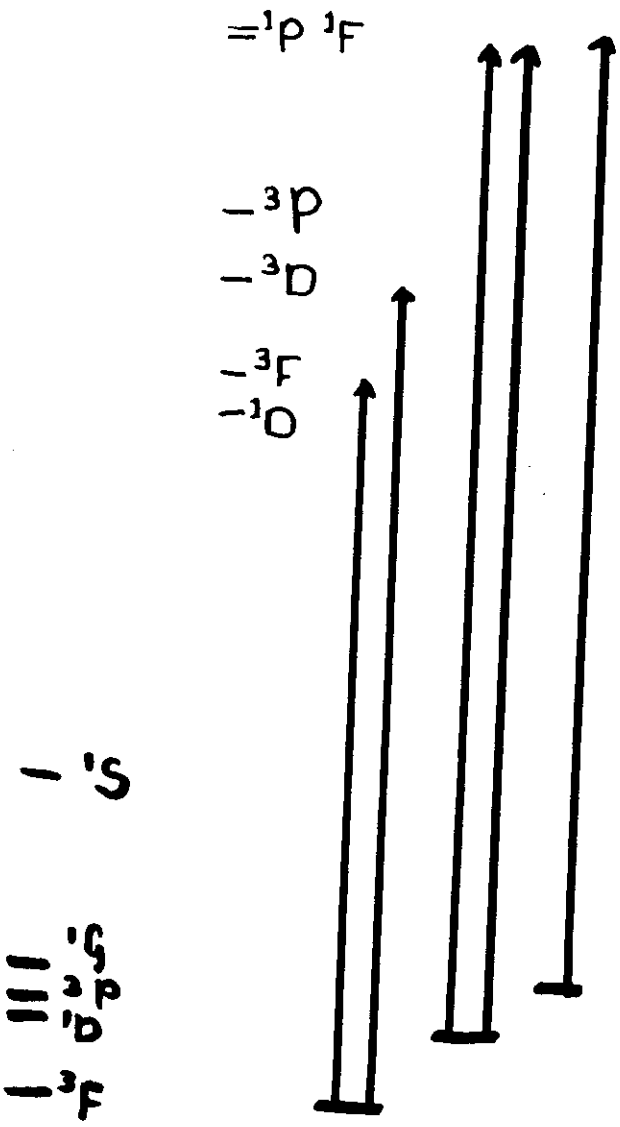

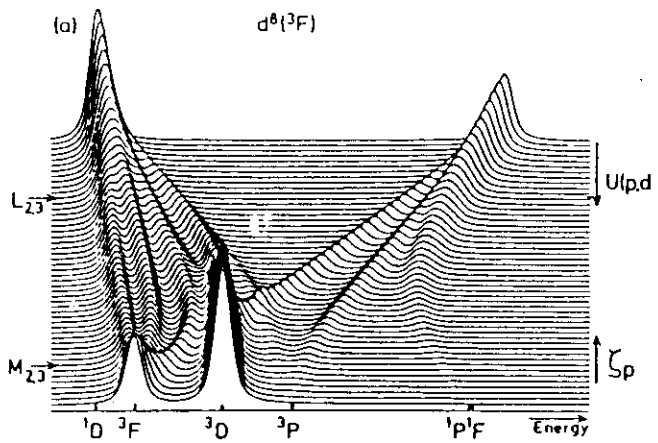

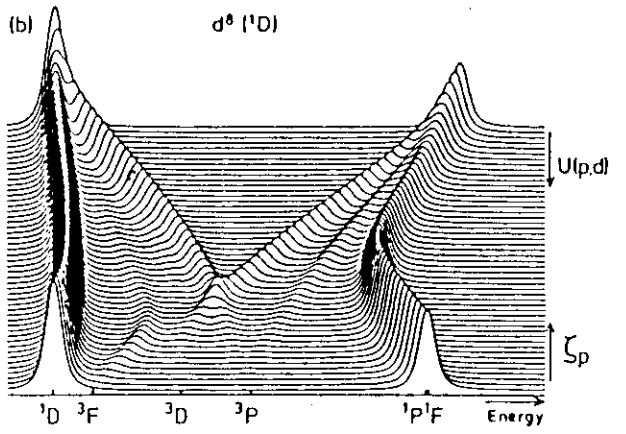

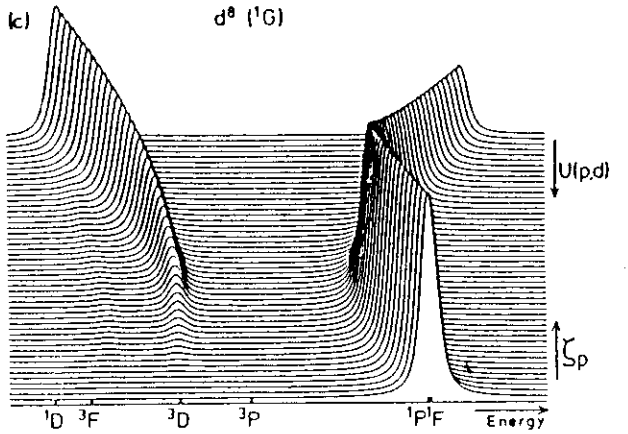

Coulomb interaction mixes $j=5/2$ and $j=3/2$ states such that the high energy side get more low spin character.

= **High spin ground state → high L_3 peak**

Linear relation between x-ray absorption branching ratio and valence-band spin-orbit expectation value

1988

B. T. Thole and G. van der Laan

$$B_j(\Psi)=\frac{2j+1}{2(2c+1)}\pm A(c,l,n)\langle\Psi\,|\,Z\,|\,\Psi\rangle\ , \tag{1}$$

$$\begin{aligned}P_j(\Psi)&=\sum_{\mu\mu'\lambda}a^*_\mu a_{\mu'}\langle\mu\,|\,C^{(1)}\,|\,\lambda j\rangle\langle\lambda j\,|\,C^{(1)}\,|\,\mu'\rangle\\&\equiv\langle\Psi\,|\,P_j\,|\,\Psi\rangle\ ,\end{aligned} \tag{2}$$

$$\begin{aligned}P_j(\mu,\mu')&\equiv\langle l^n\alpha LSJM\,|\,P_j\,|\,l^n\alpha'L'S'J'M'\rangle\\&=\delta_{JJ'}\delta_{MM'}[J]^{-1}\sum_{\alpha\underline{L}\underline{S}\underline{J}J_f}\langle l^n\alpha LSJ\|C^{(1)}\|l^{n+1}(\alpha\,\underline{L}\,\underline{S}\,\underline{J})(c\,\tfrac{1}{2}\,j)J_f\rangle\langle l^{n+1}(\alpha\,\underline{L}\,\underline{S}\,\underline{J})(c\,\tfrac{1}{2}\,j)J_f\|C^{(1)}\|l^n\alpha LSJ\rangle\ .\end{aligned} \tag{3}$$

$$\begin{aligned}D&\equiv\langle l^n\alpha LSJ\|C^{(1)}\|l^{n+1}(\alpha\,\underline{L}\,\underline{S}\,\underline{J})(c\,\tfrac{1}{2}\,j)J_f\rangle\\&=(-1)^{n+1+L+\underline{L}+S+L_f+c+J_f}\sum_{S_fL_f}[(n+1)\{\underline{L},\underline{S},\underline{J},j,J_f,J\}]^{1/2}[L_f]\\&\quad\times\langle l^{n+1}\alpha\,\underline{L}\,\underline{S}\}\,|\,l^n\alpha LS\rangle\begin{Bmatrix}\underline{L}&c&L_f\\\underline{S}&\frac{1}{2}&S_f\\\underline{J}&j&J_f\end{Bmatrix}\begin{Bmatrix}L&S&J\\J_f&1&L_f\end{Bmatrix}\begin{Bmatrix}L_f&1&L\\l&\underline{L}&c\end{Bmatrix}\delta_{SS_f}\ ,\end{aligned} \tag{4}$$

$$\begin{aligned}P_j(\mu,\mu')&=\delta_{JM,J'M'}(-1)^{K+1+S+S'+L+L'}\sum_{K\alpha\underline{L}\underline{S}}(n+1)[K,\underline{L},\underline{S},j]\langle l^{n+1}\alpha\,\underline{L}\,\underline{S}\}\,|\,l^n\alpha'L'S'\rangle\langle l^n\alpha LS\,|\,\}l^{n+1}\alpha\,\underline{L}\,\underline{S}\rangle\\&\quad\times\begin{Bmatrix}l&1&c\\c&K&l\end{Bmatrix}\begin{Bmatrix}c&j&\frac{1}{2}\\\frac{1}{2}&K&c\end{Bmatrix}\begin{Bmatrix}\frac{1}{2}&\underline{S}&S\\S'&K&\frac{1}{2}\end{Bmatrix}\begin{Bmatrix}S&J&L\\L'&K&S'\end{Bmatrix}\begin{Bmatrix}L&\underline{L}&l\\l&K&L'\end{Bmatrix}\ .\end{aligned} \tag{5}$$

$$P_j^0(\mu,\mu')=\frac{[j](4l+2-n)}{2[c,l]}\delta_{\alpha LSJM,\alpha'L'S'J'M'}\ , \tag{6}$$

$$\sum_j P_j^1(\mu,\mu')=0 \ . \tag{7}$$

$$P_{\rm tot}=\sum_j P_j=\sum_j P_j^0=\frac{(4l+2-n)}{[l]} \ , \tag{8}$$

$$B_j^0\equiv P_j^0/P_{\rm tot}=\frac{[j]}{2[c]} \tag{9}$$

$$B_j\equiv P_j/P_{\rm tot}=B_j^0+B_j^1=\frac{[j]}{2[c]}+P_j^1/P_{\rm tot} \tag{10}$$

$$Z(\mu,\mu')=(-1)^{L'+S+J}[l(l+1)(2l+1)]^{1/2}\begin{Bmatrix} S & L & J \\ L' & S' & 1 \end{Bmatrix} \times\langle l^n\alpha LS\|V^{(11)}\|l^n\alpha'L'S'\rangle\delta_{JM,J'M'} \ , \tag{11}$$

$$\langle l^n\alpha LS\|V^{(11)}\|l^n\alpha'L'S'\rangle=\sum_{\underline{\alpha}\,\underline{L}\,\underline{S}}(-1)^{l+1+\underline{L}+\underline{S}+L+S+1/2}(\tfrac{3}{2})^{1/2}(n+1)[\underline{L},\underline{S}]\begin{Bmatrix} l & l & 1 \\ L & L' & \underline{L} \end{Bmatrix} \times\begin{Bmatrix} \frac{1}{2} & \frac{1}{2} & 1 \\ S & S' & \underline{S} \end{Bmatrix}(l^{n+1}\underline{\alpha}\,\underline{L}\,\underline{S}\{\|l^n\alpha LS)(l^n\alpha'L'S'\|\}l^{n+1}\underline{\alpha}\,\underline{L}\,\underline{S}) \ . \tag{12}$$

$$Z(\mu,\mu')=[\tfrac{3}{2}l(l+1)(2l+1)]^{1/2}(-1)^{l+L+\underline{L}+S+\underline{S}+3/2+L'+S+J} \times\sum_{\underline{\alpha}\,\underline{L}\,\underline{S}}(n+1)[\underline{L},\underline{S}](l^{n+1}\underline{\alpha}\,\underline{L}\,\underline{S}\{\|l^n\alpha LS)(l^n\alpha'L'S'\|\}l^{n+1}\underline{\alpha}\,\underline{L}\,\underline{S}) \times\begin{Bmatrix} \frac{1}{2} & \underline{S} & S \\ S' & 1 & \frac{1}{2} \end{Bmatrix}\begin{Bmatrix} S & J & L \\ L' & 1 & S' \end{Bmatrix}\begin{Bmatrix} L & \underline{L} & l \\ l & 1 & L' \end{Bmatrix}\delta_{JM,J'M'} \ . \tag{13}$$

$$B_j^1(\mu,\mu')=\pm A(c,l,n)*Z(\mu,\mu') \ , \tag{14}$$

$$A(c,l,n)=\frac{2-l(l+1)-c(c+1)}{l(l+1)(2c+1)(4l+2-n)} \ . \tag{15}$$

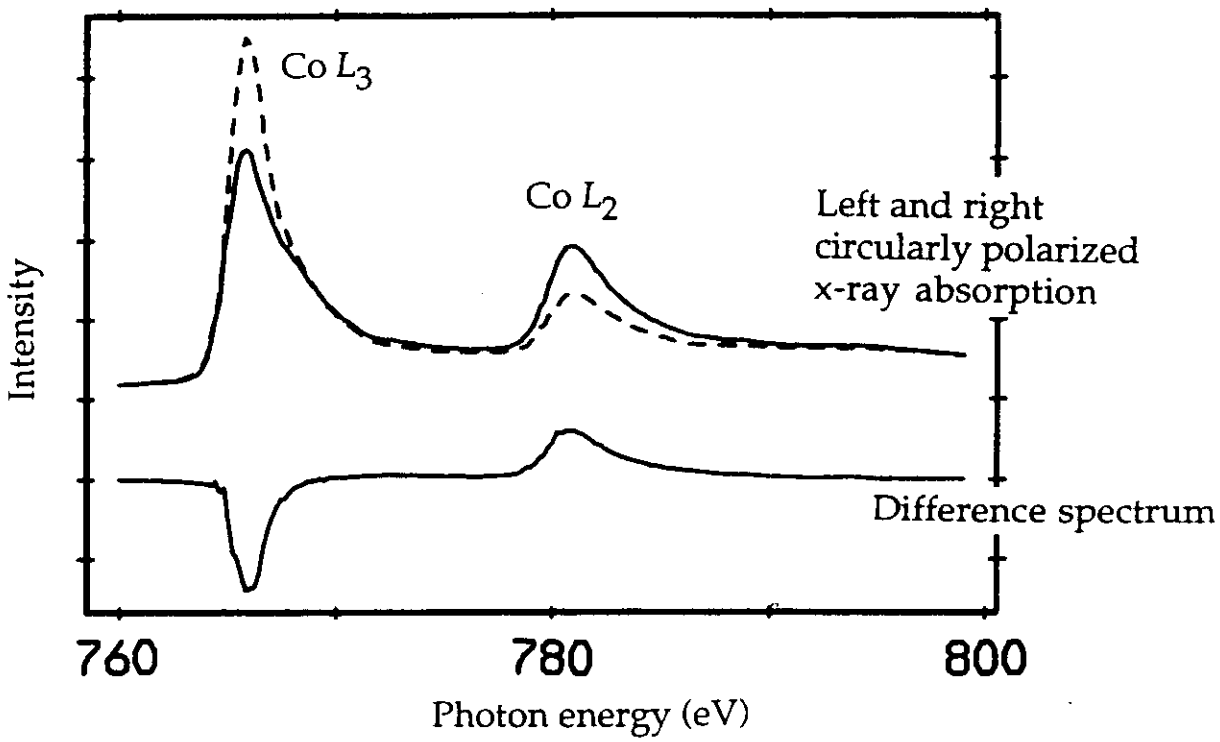
Co L_3
Co L_2
Left and right
circularly polarized
x-ray absorption
Difference spectrum
Intensity
760
780
800
Photon energy (eV)

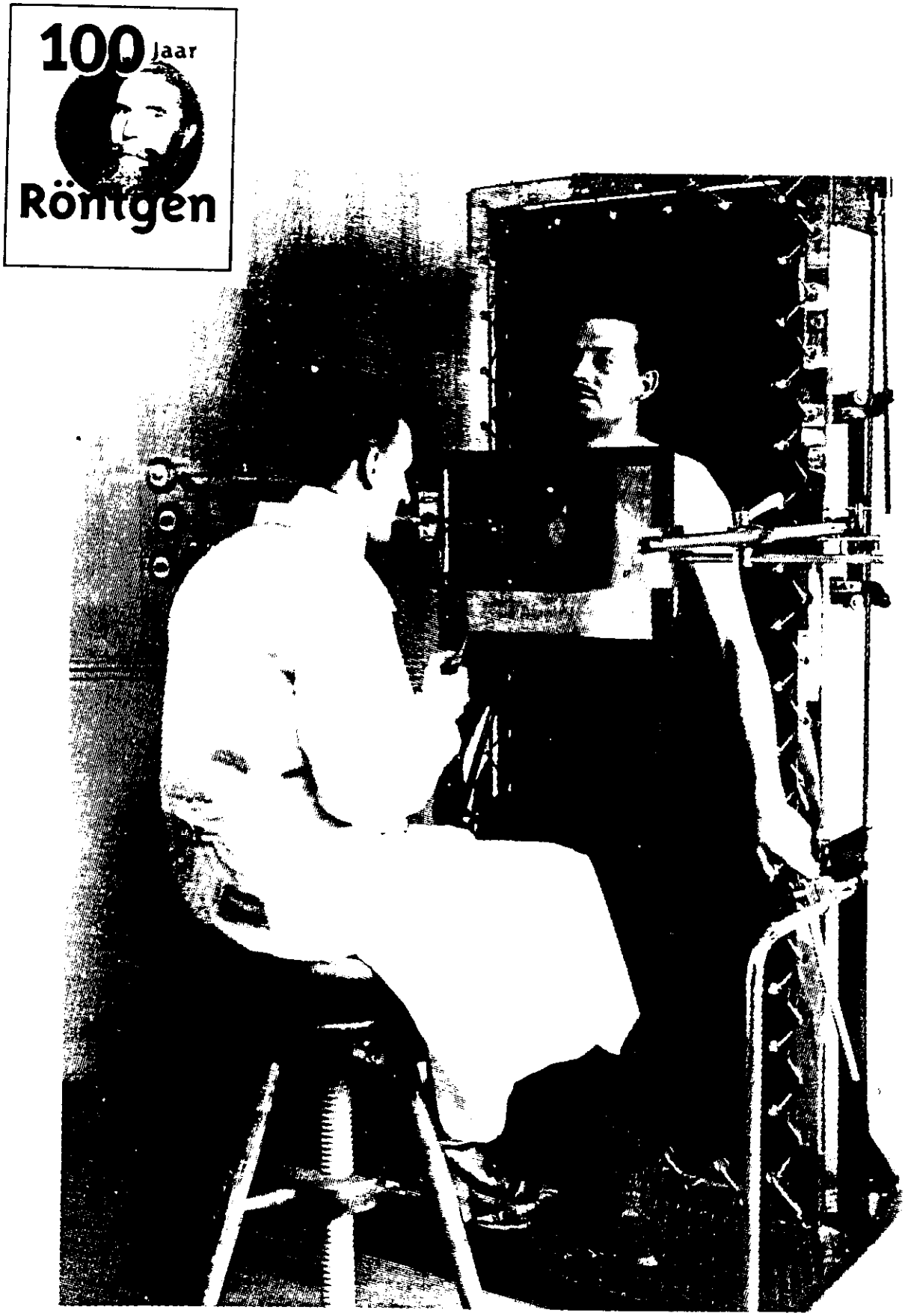
100 jaar
Röntgen

Digital Imaging

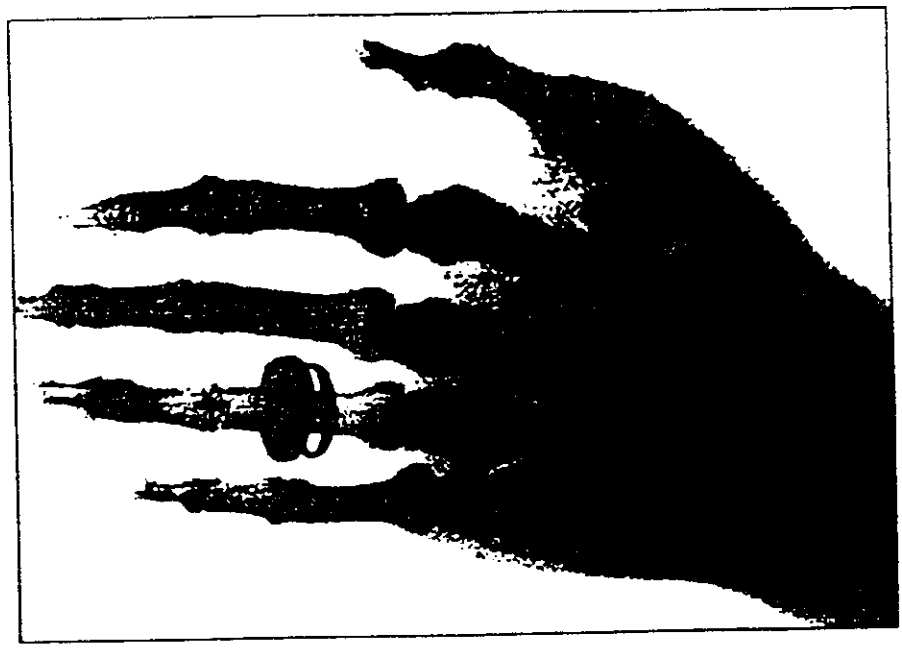

Hand, W. Röntgen (1895)

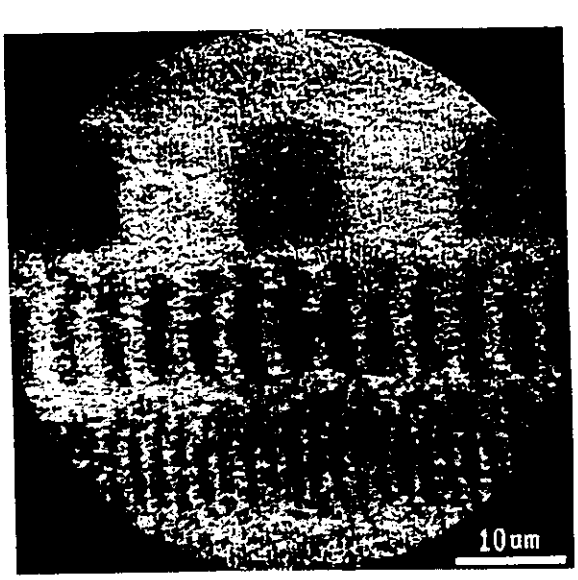

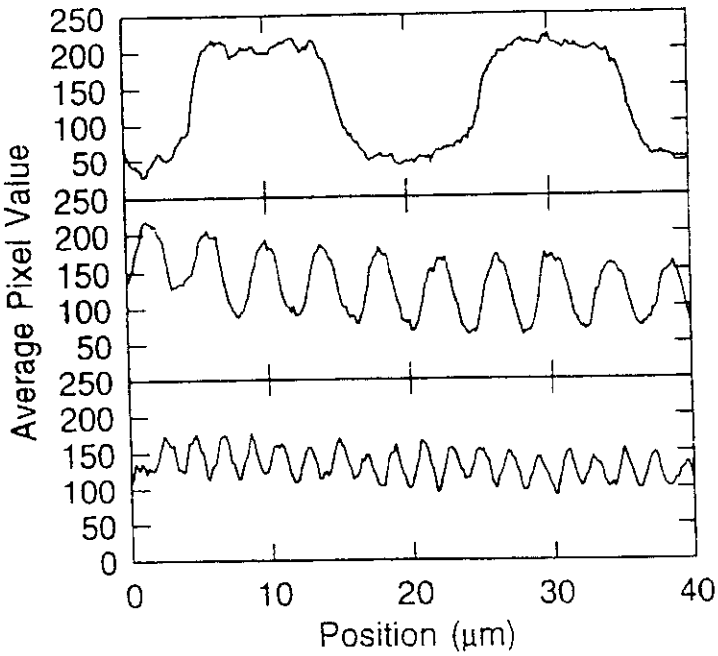

CoPtCr magnetic recording medium, IBM (1993)

magic L3L2BKGC.IAX1 (on psuc

Co L3 Edge

Background (Below Co L3 Edge)

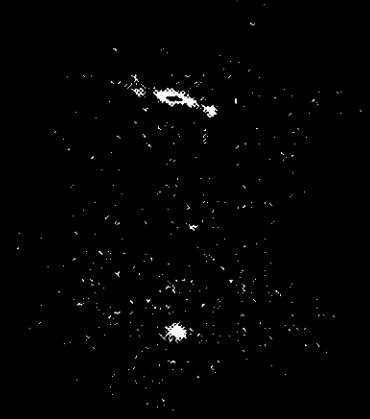

Co L2 Edge

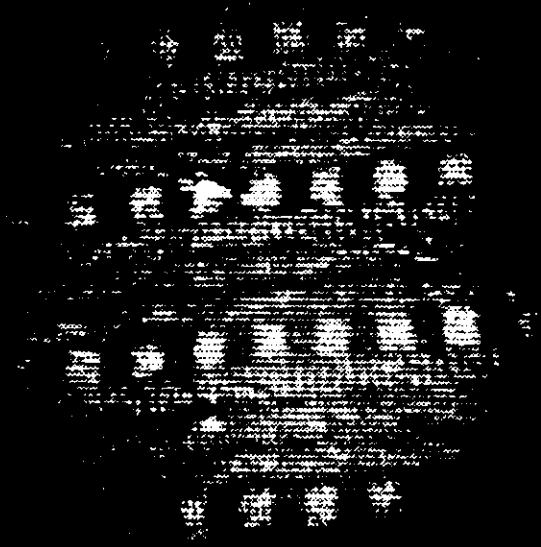

$f \rightarrow \varepsilon g$ photoemission intensities

primitive spectra

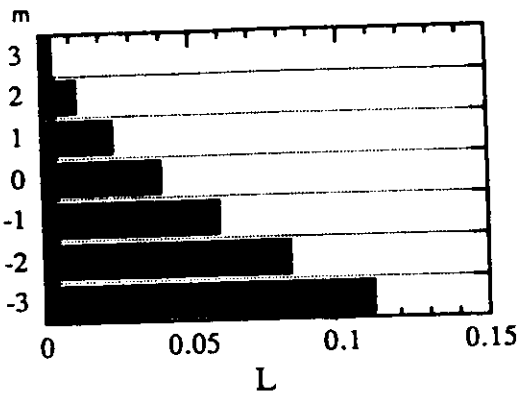

L

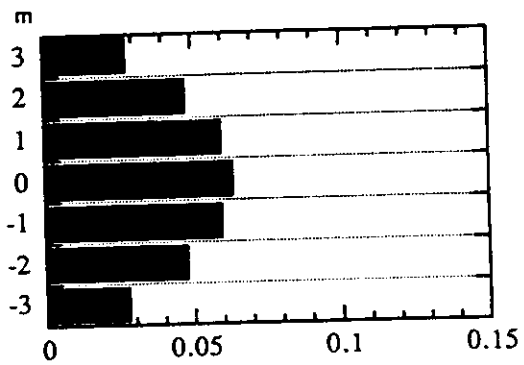

Z

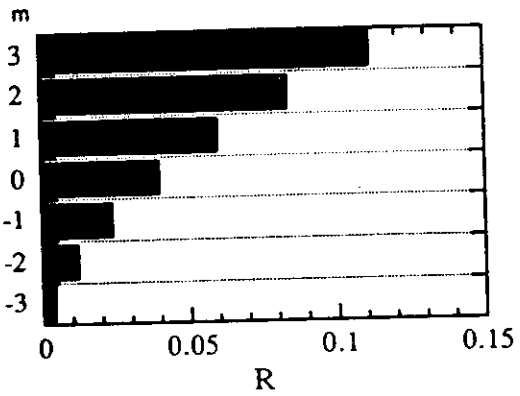

R

fundamental spectra

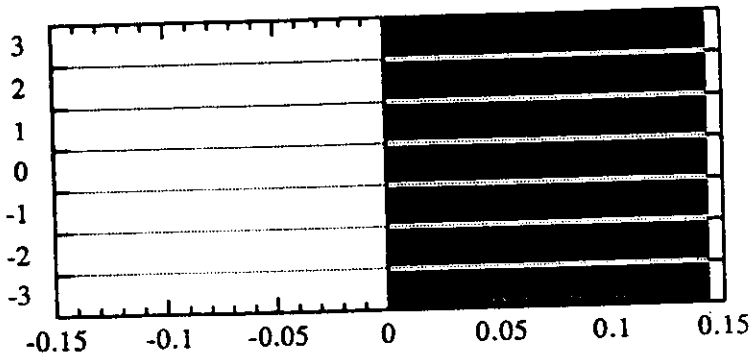

Iso

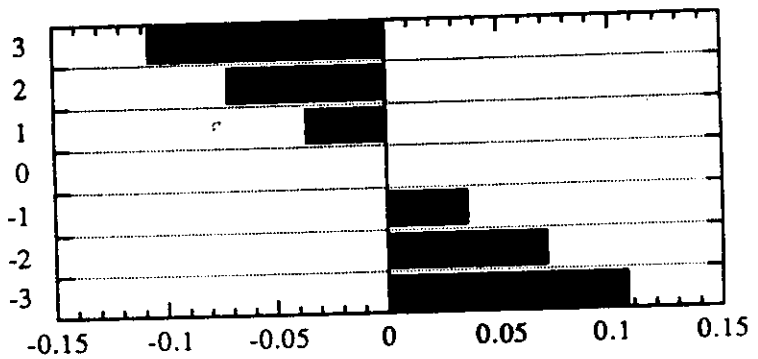

M C D

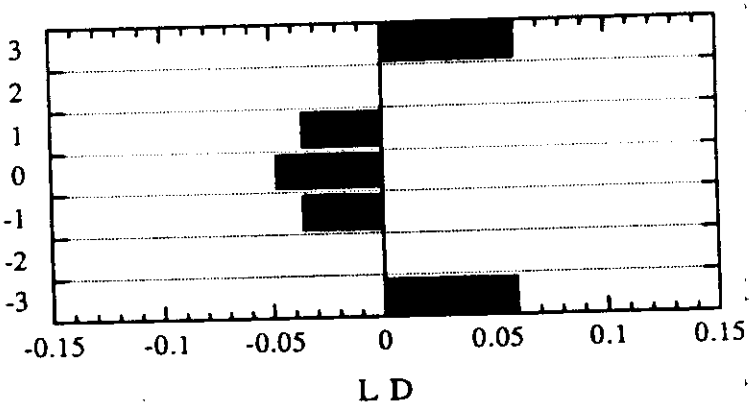

L D

$f \rightarrow \varepsilon d$ photoemission intensities

primitive spectra

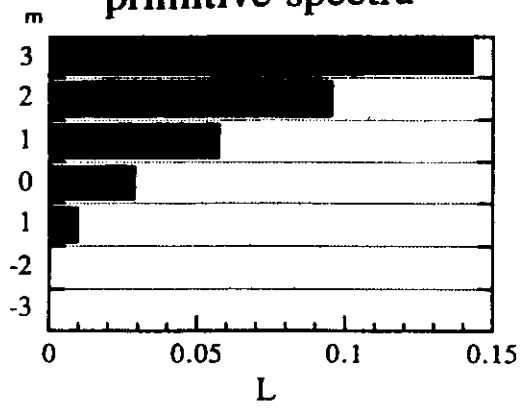

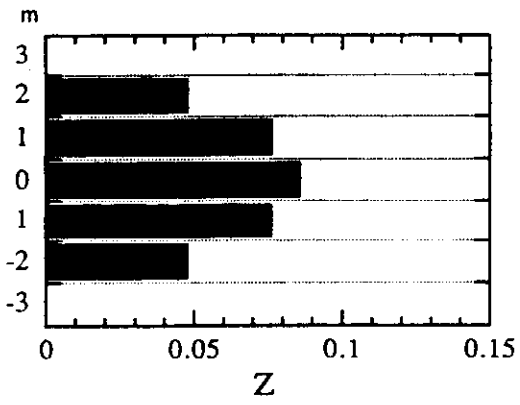

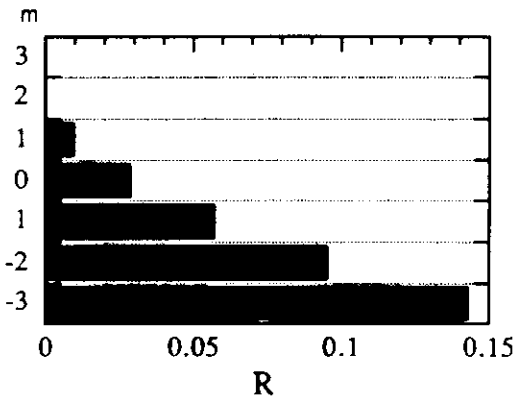

fundamental spectra

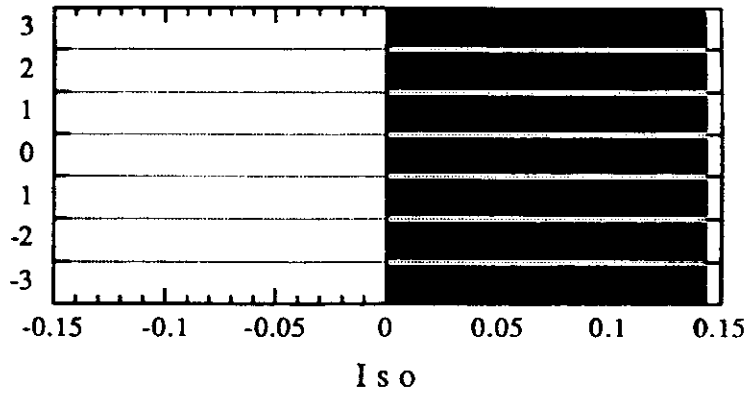

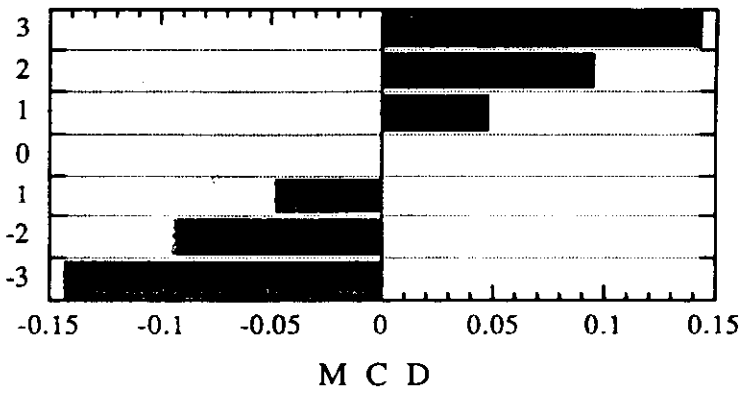

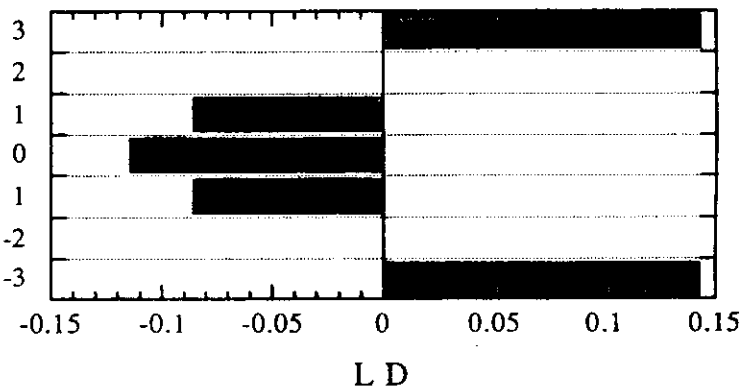

Relation between the l-1 and l+1 photoemission channels

$f \rightarrow \varepsilon d$ photoemission intensities

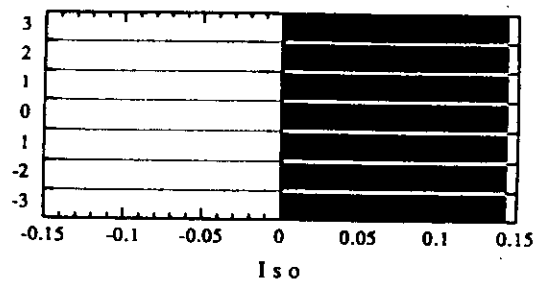

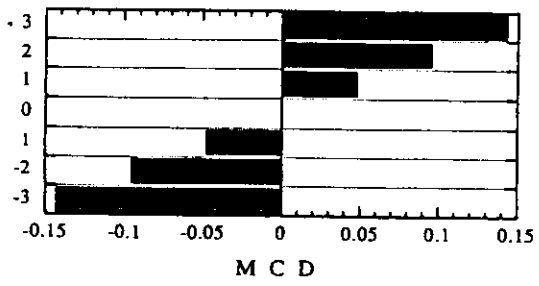

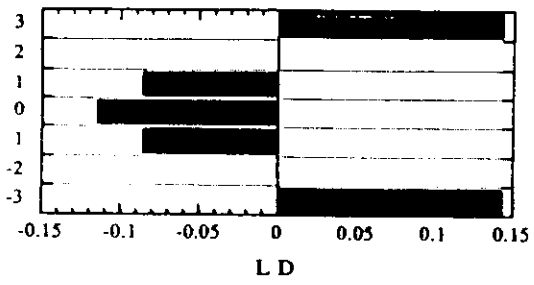

$f \rightarrow \varepsilon g$ photoemission intensities

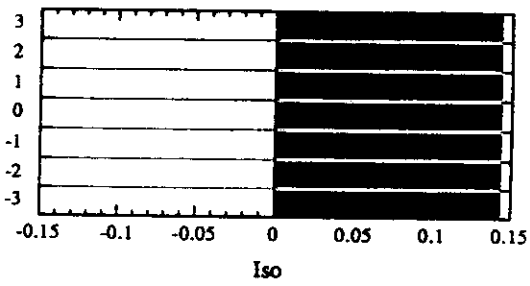

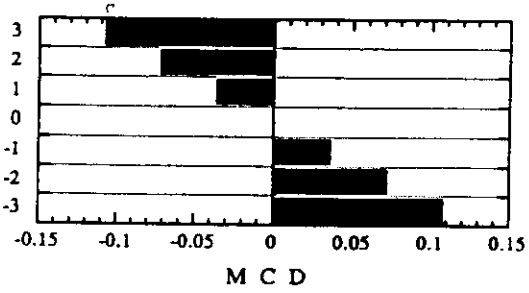

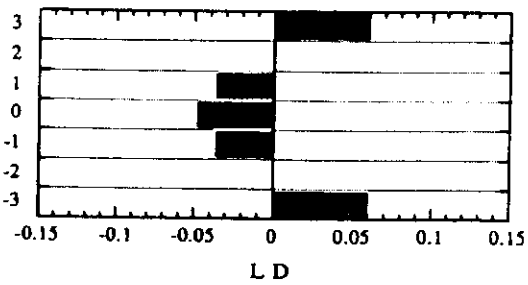

MAGNETO-CRYSTALLINE ANISOTROPY OF THIN FILMS AND MULTILAYERS FROM TRANSVERSE MAGNETIC CIRCULAR X-RAY DICHROISM

G van der Laan
H A Dürr
Daresbury Laboratory
Warrington WA4 4AD, UK

References

Dürr, van der Laan, Phys. Rev. B **54**, R760 (1996).

Dürr, Guo, van der Laan, Lee, Lauhoff, Bland, Science **277**, 213 (1997).

MAGNETOCRYSTALLINE ANISOTROPY as a function of thickness

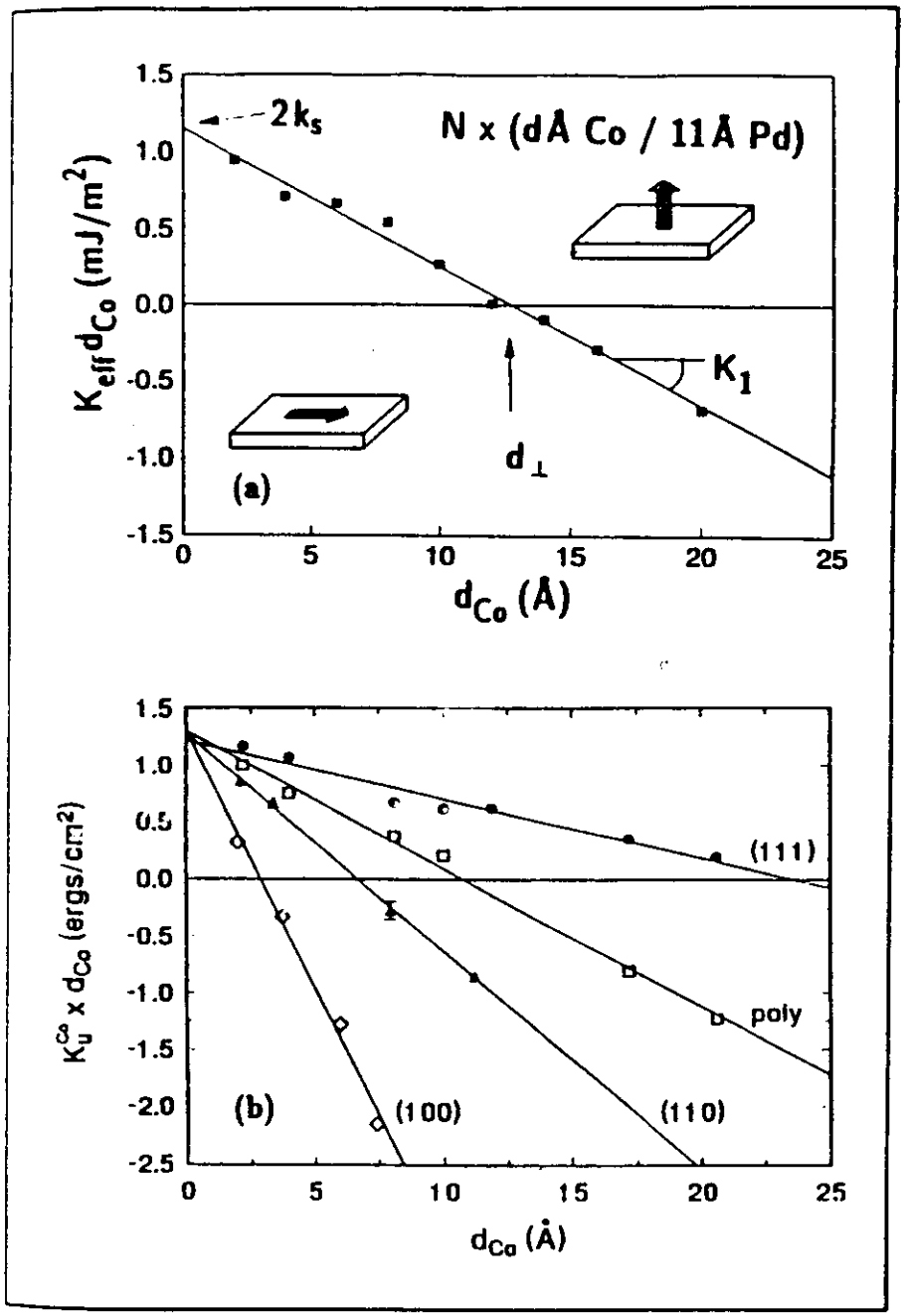

$$E = K_0 + K_1 \sin^2\theta$$

Co Pt ml in transverse geometry.

MBE {Co(4 Å)/Pt(20 Å)}$_4$ 200 Å Pt/ Si(111)

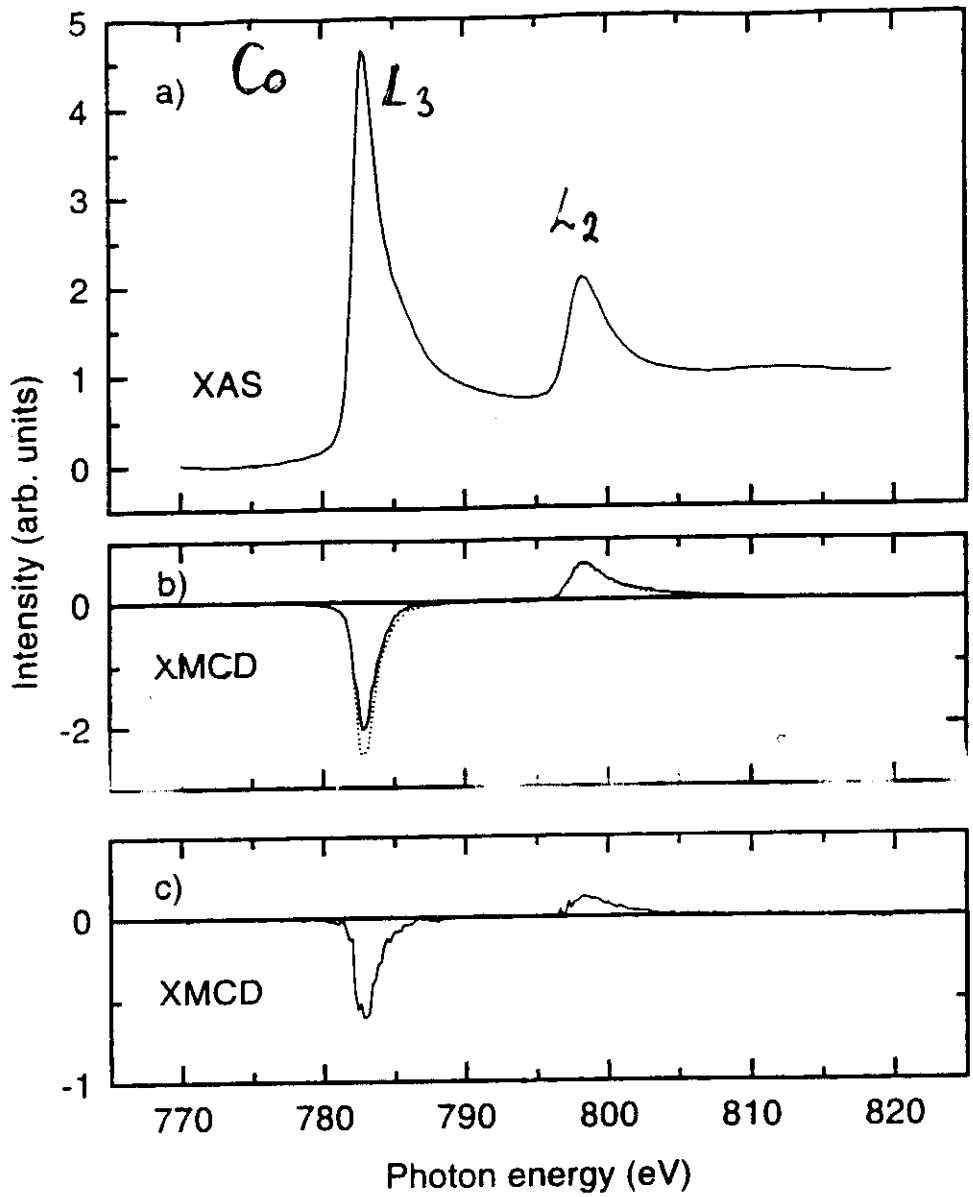

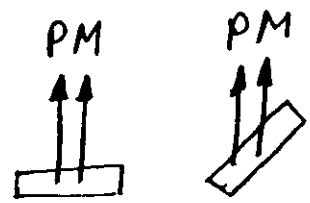

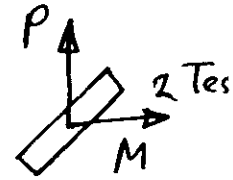

Result: $R_{zz} = 3.9$

$R_{yy} = 1.5$

* STRONG PMA !

Dürr, van der Laan, J. Appl. Phys. 81, 5355 (1997).

MOKE hysteresis loops ($H_\perp$)

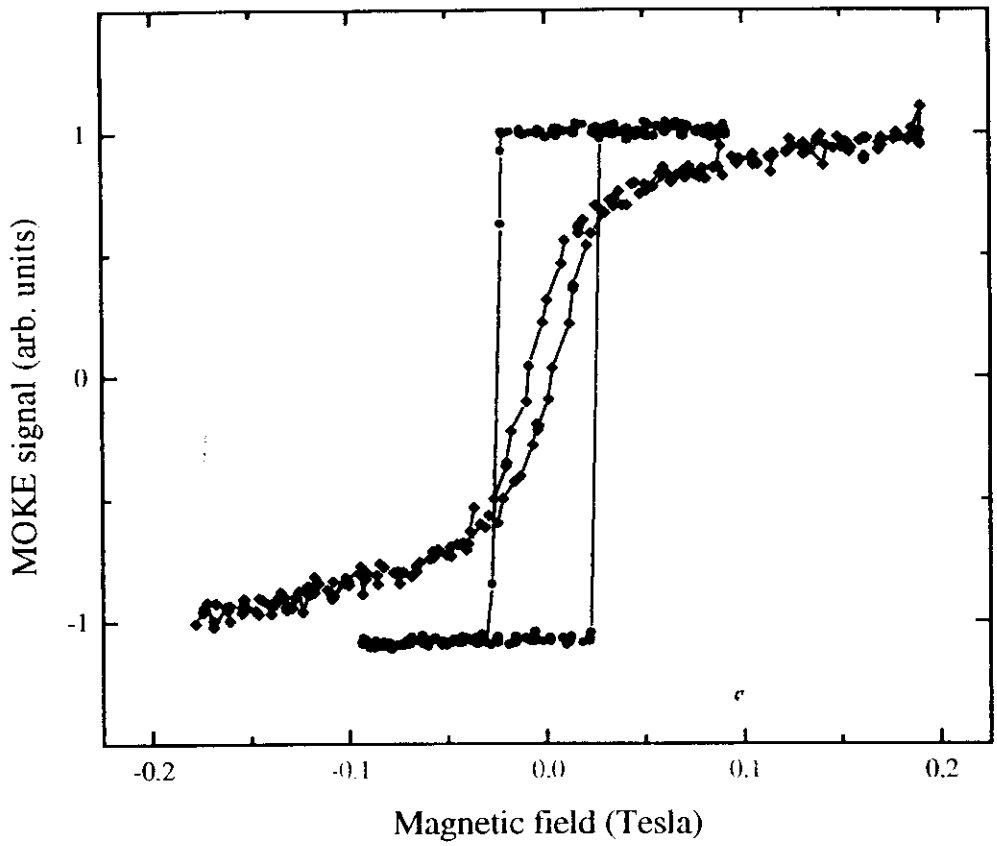

33 ml Ni / Cu / Si(100)

3 ml Co / 33 ml Ni / Cu / Si(100)

Dürr, Guo, van der Laan (SRS)
Lee, Lauhoff, Bland (Cambridge)
SCIENCE 277-213(1997)

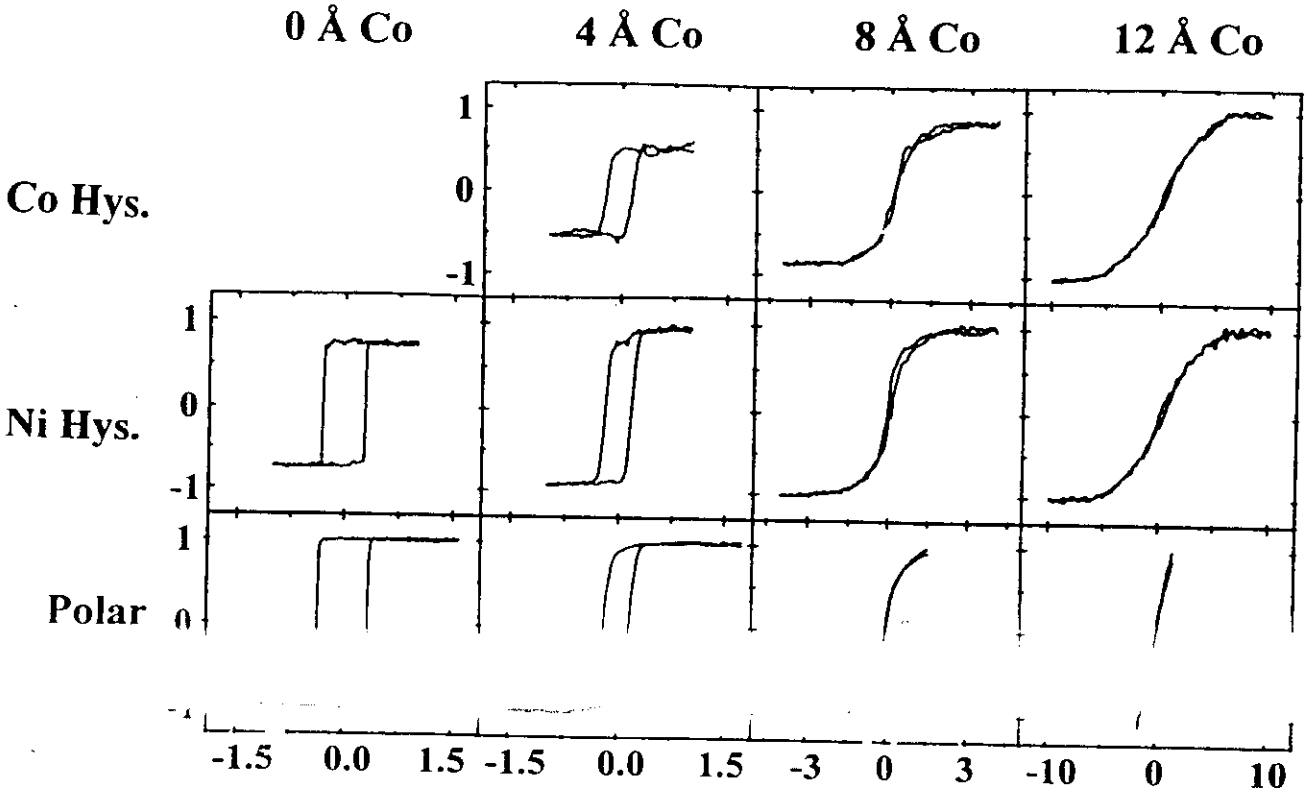

Ferromagnetic coupling and anisotropy in epitaxial Cu/Co/Ni/Cu(001)

G Lauhoff[a], Jaeyong Lee[a], J A C Bland[a], J Ph Schillé[b], G van der Laan[c]

JMMM

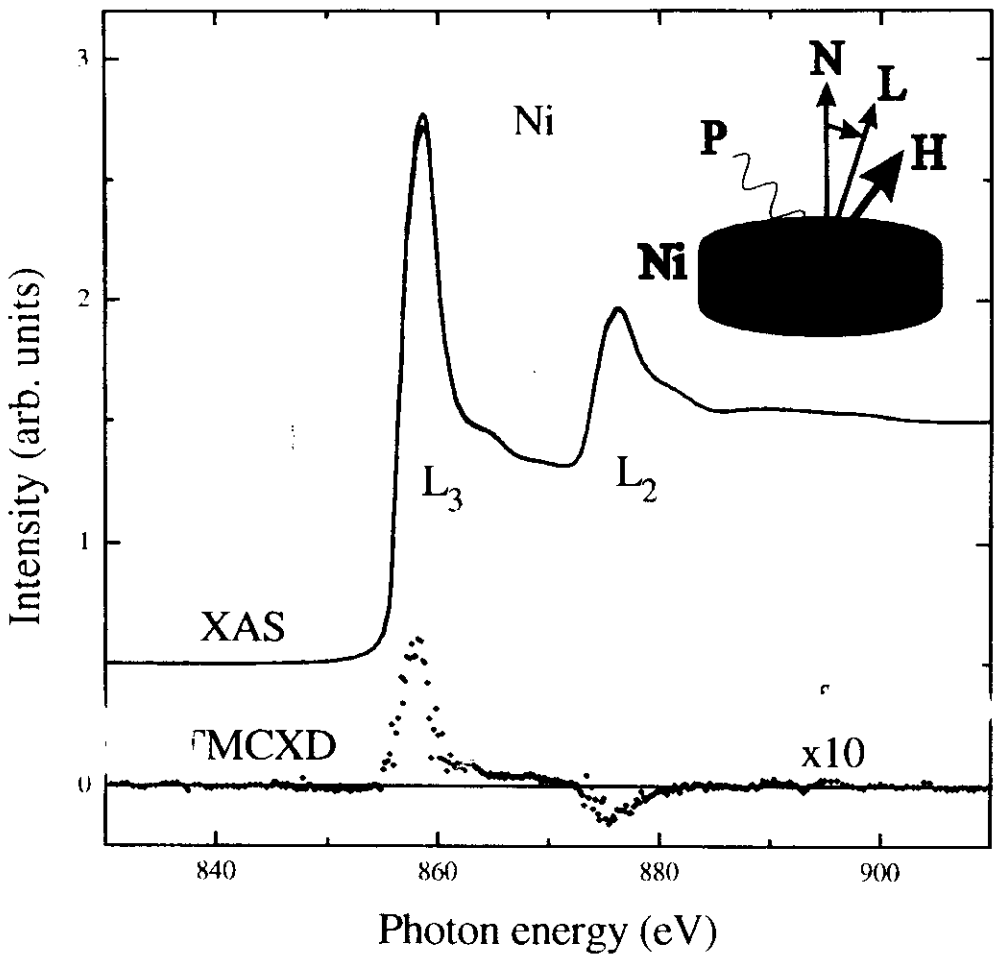

33 ml Ni: $\Delta E_{MCA} = 1.4$ meV

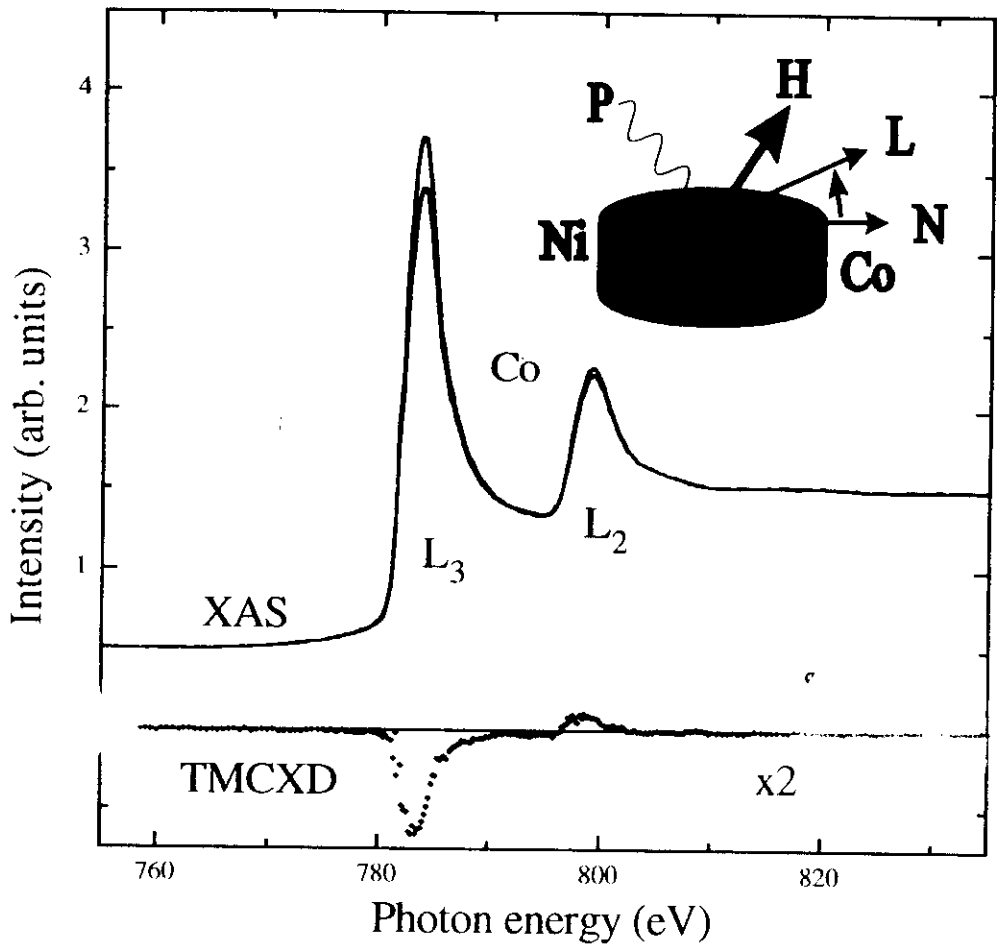

3 ml Co: $\Delta E_{MCA} = -1.1$ meV

$$E_{MCA} = -\xi\, L \cdot S$$

DL95111981/13

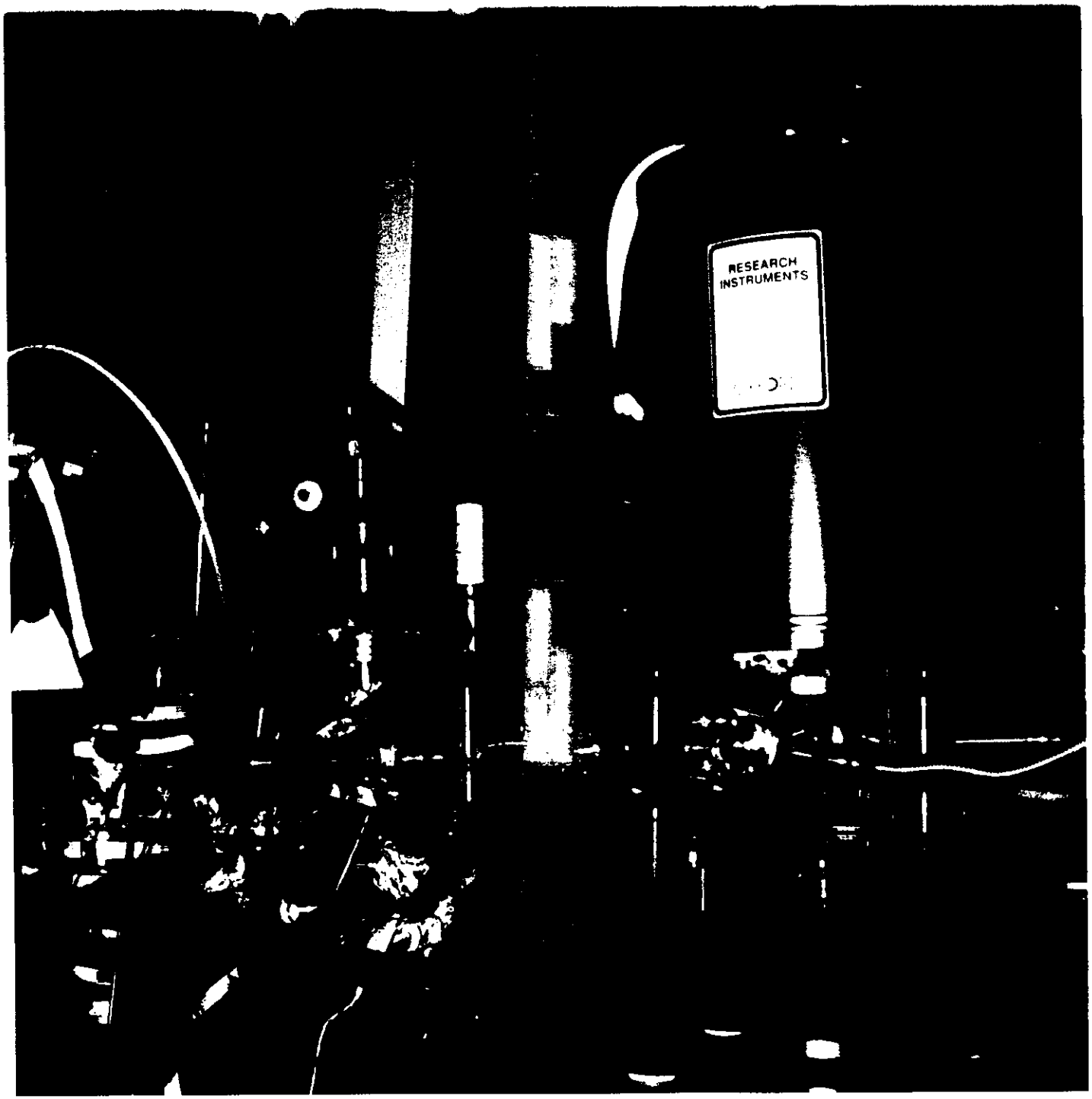

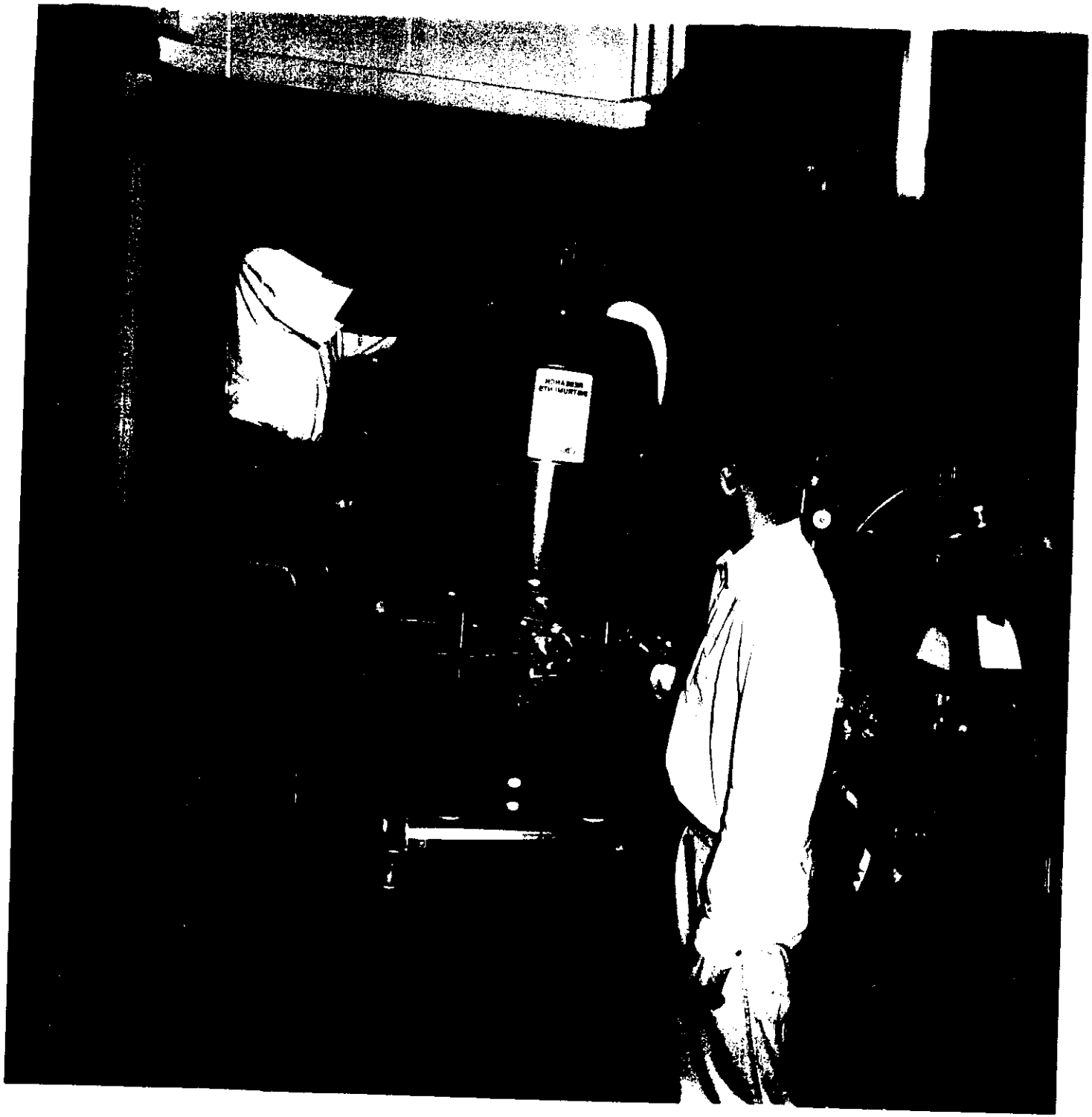

5 Tesla superconducting magnet

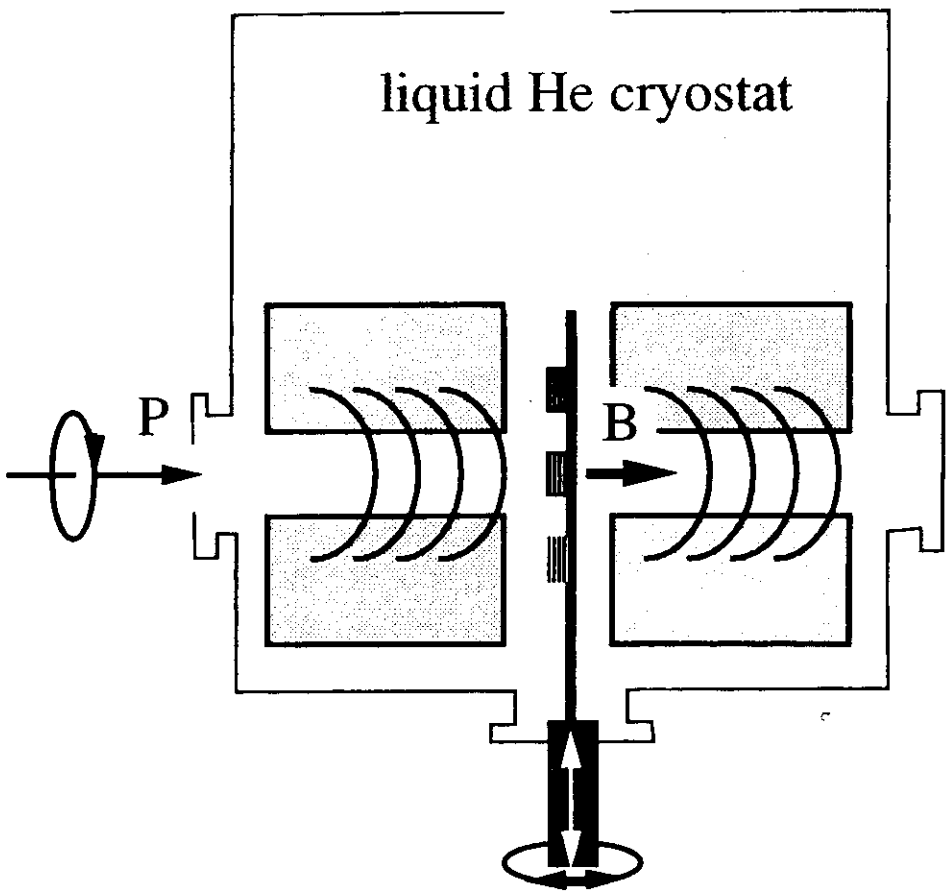

samples are capped with e.g. 20 Å Au
to enable measurements in low vacuum

Soft x-ray magnetic scattering from *striped* magnetic domain structures

G. van der Laan,
E. Dudzik, H.A. Dürr, S.S. Dhesi,
M.D. Roper, S.P. Collins
Daresbury Laboratory

J.B. Goedkoop
University of Amsterdam

M. Belakhovsky, K. Chesnel,
A. Marty, Y. Samson
CEA/Grenoble

A simple illustration of the GMR effect

Initially the magnetisations of the two magnetic layers point in opposite directions. When a current is applied electrons will pass through the multilayer. The electrons can be divided into two groups, 'spin up' (red) and 'spin down' (blue). If the spin of the electron is parallel to the layer magnetisation, the electron will pass easily through the layer. However, if the electron spin is antiparallel to the layer magnetisation, the electron will be scattered so its passage is more difficult.

When the layer magnetisations point in opposite directions neither group of electrons can pass through without being scattered at one of the layers. If all the layers are aligned the same way, half of the electrons (those spinning in the appropriate direction) will be able to pass easily through all of the material. Although only half the electrons pass through, this is better than none, as in the previous case. The net effect is that the resistance is lower. Structures like this are known as spin valves because of the valve-like effect they have on electric current.

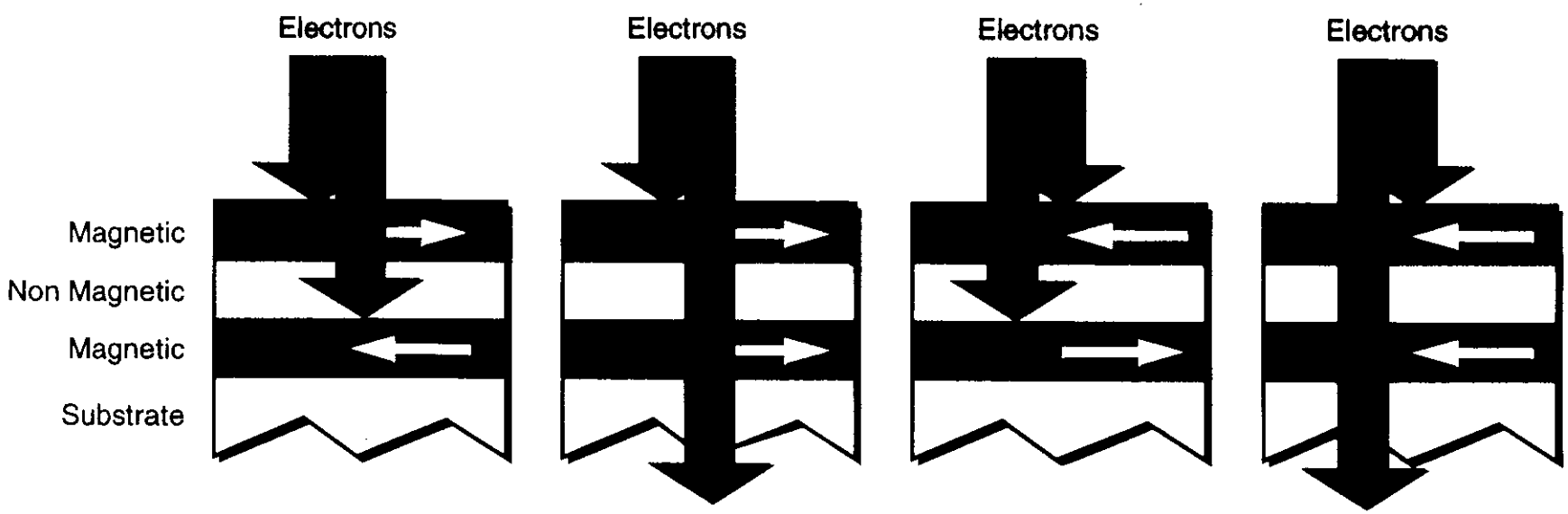

Magnetic configurations

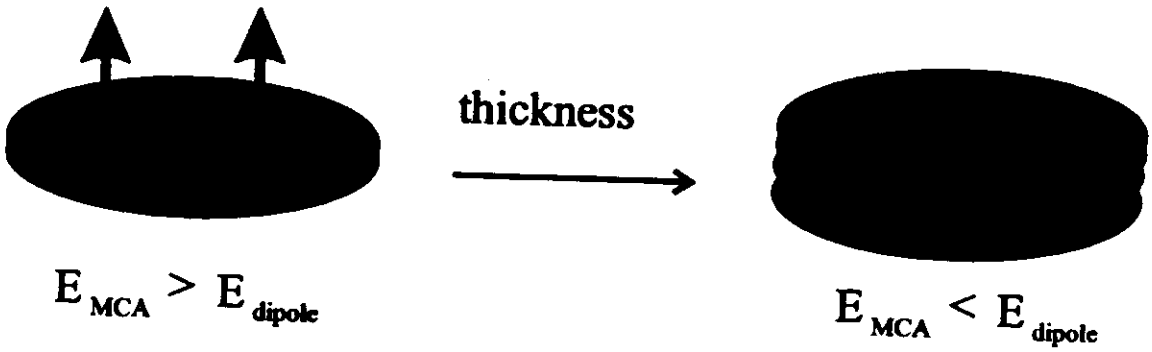

$E_{MCA} > E_{dipole}$

$E_{MCA} < E_{dipole}$

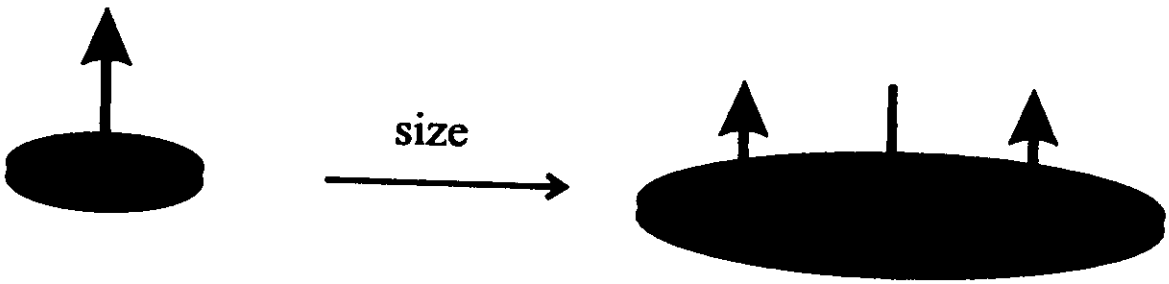

minimize $E_{MCA} + E_{dipole} + E_{wall}$

Marty et al. (1999)

FePd phase diagram

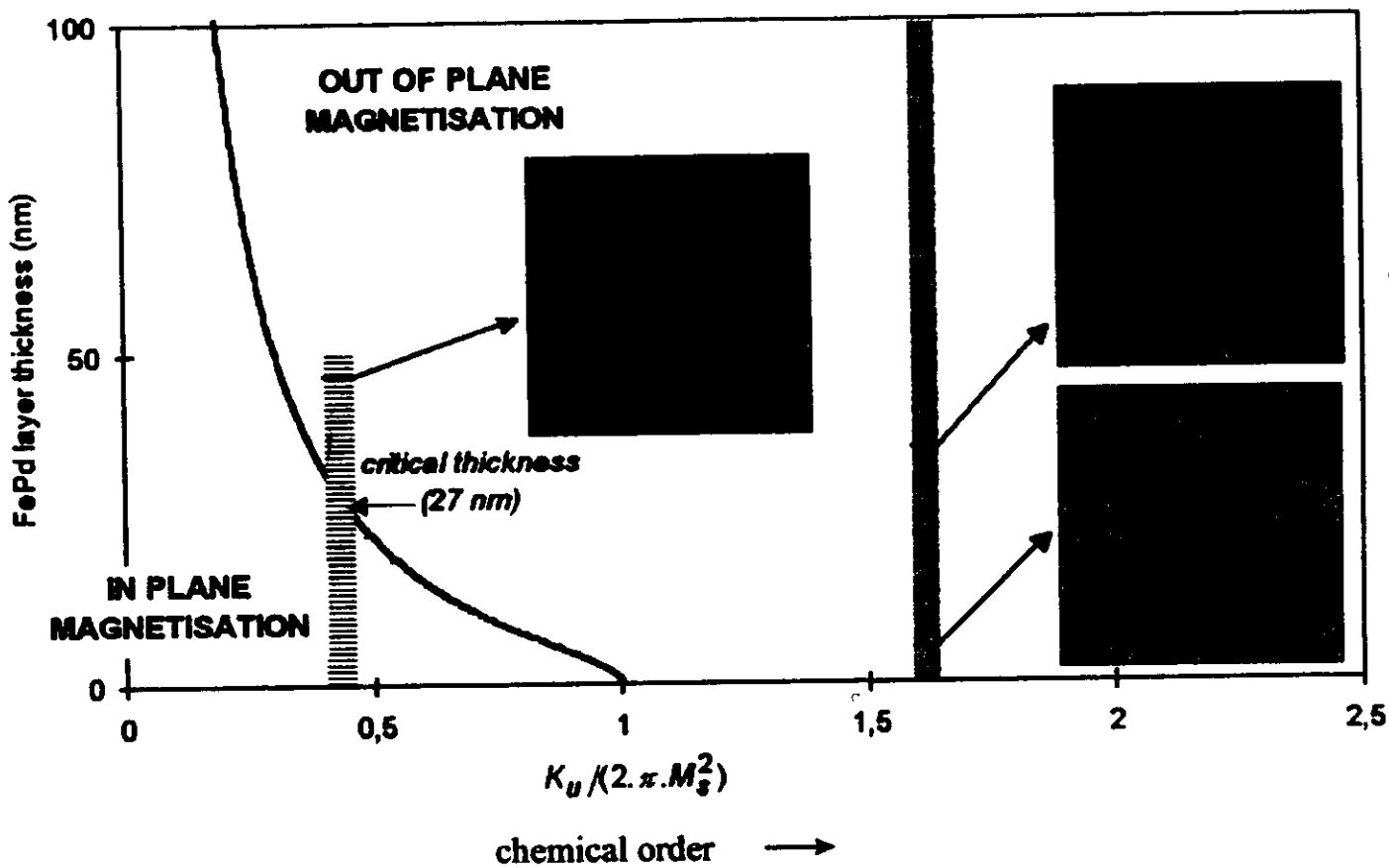

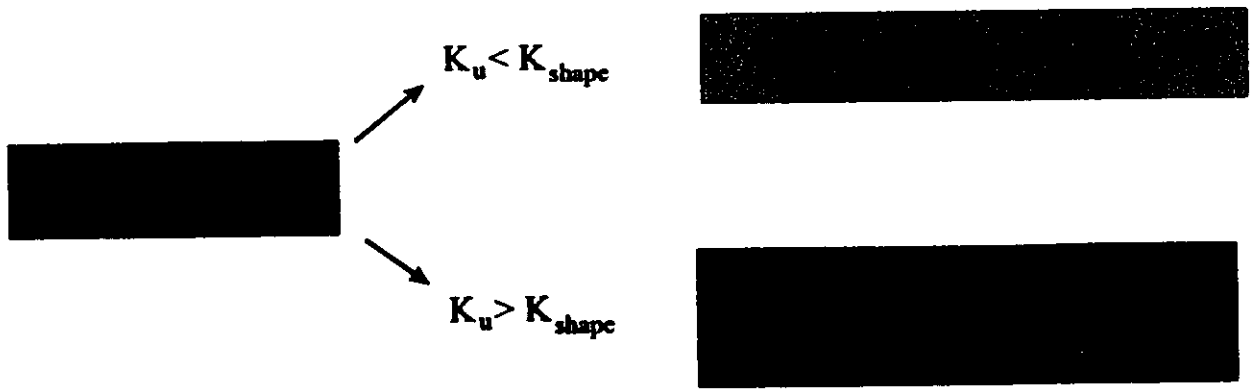

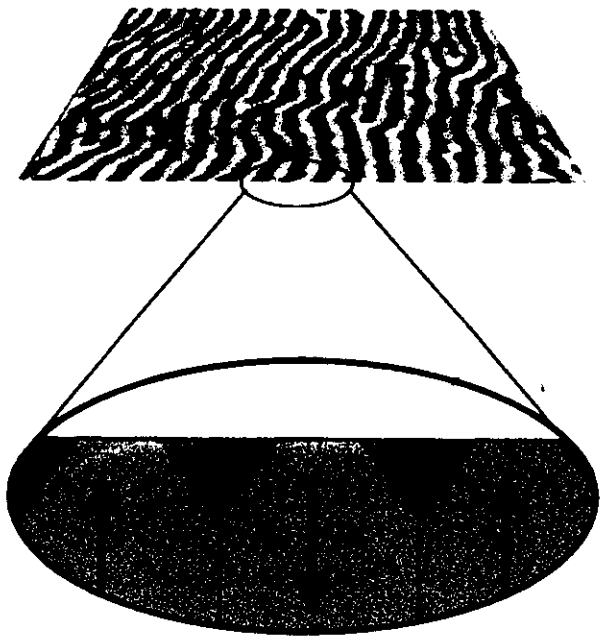

Figure 1
Dürr et al.

POLARISATION DEPENDENT SOFT X-RAY SPECTROSCOPY

ESRF
DRAGON
BEAM LINE

VERTICAL PLANE

HELIOS I

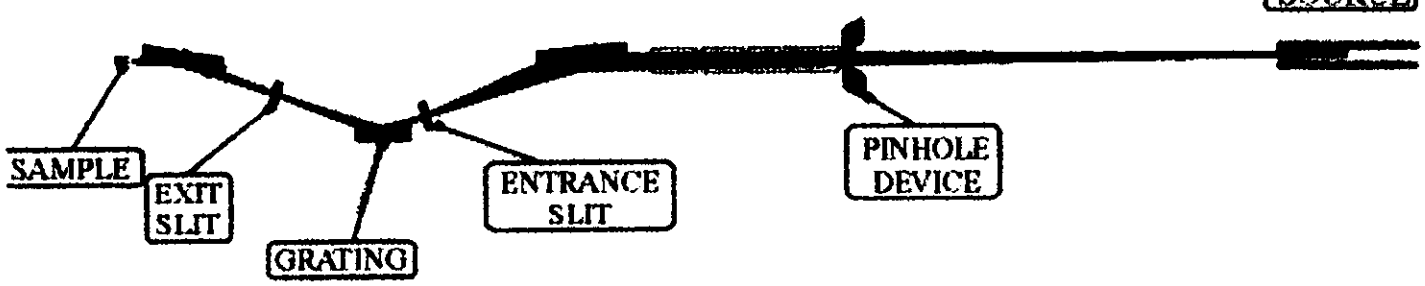

Helios 1: switchable polarisation

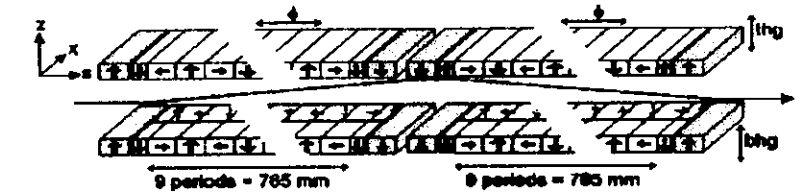

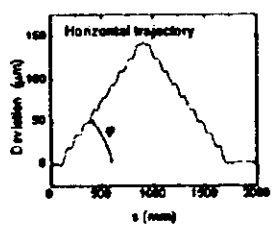

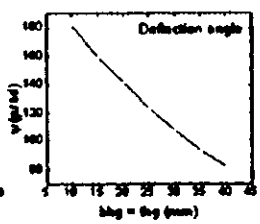

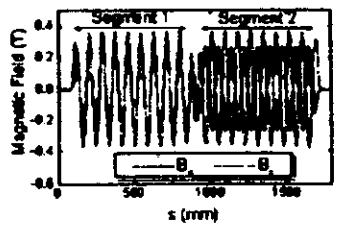

X-ray resonant magnetic scattering

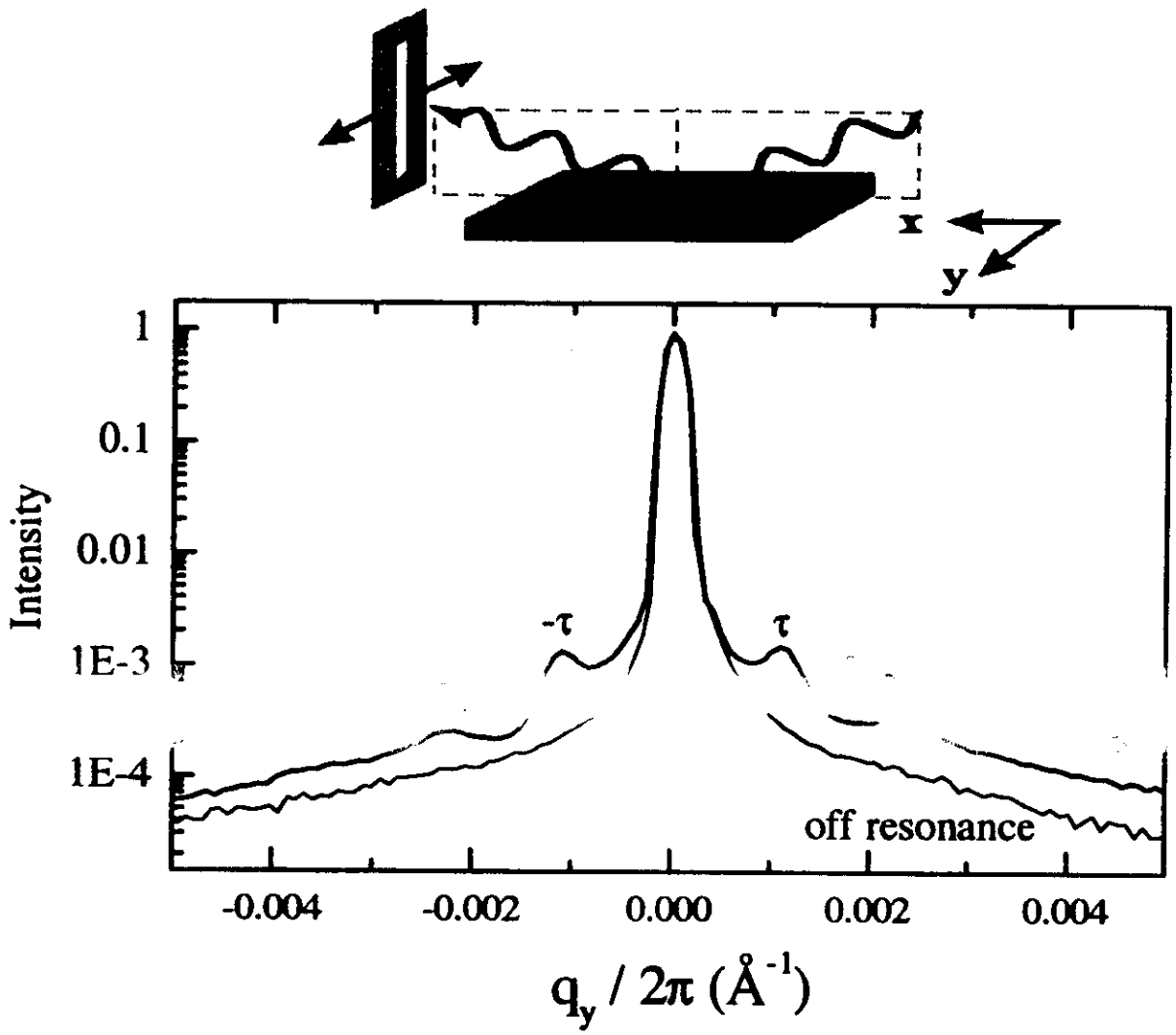

periodicity: $1/\tau = 900$ Å

resonant scattering amplitude:

$$f = \hat{e}'\cdot\hat{e}\, F^{(0)} - i(\hat{e}' \times \hat{e})\cdot\hat{M}\, F^{(1)} + (\hat{e}'\cdot\hat{M})(\hat{e}\cdot\hat{M})\, F^{(2)}$$

specular peak — $q_y = \pm\tau$ — $q_y = \pm 2\tau$

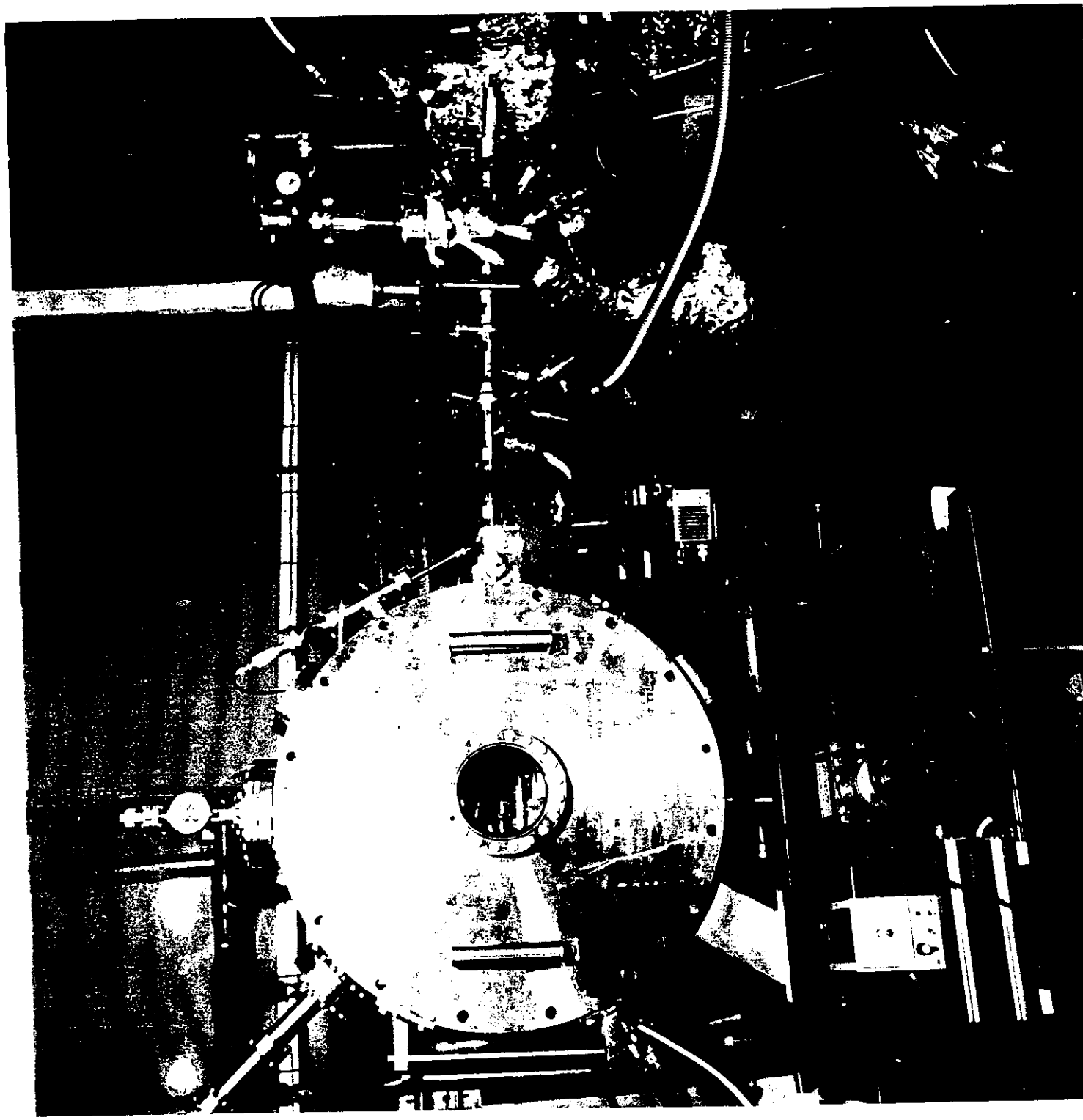

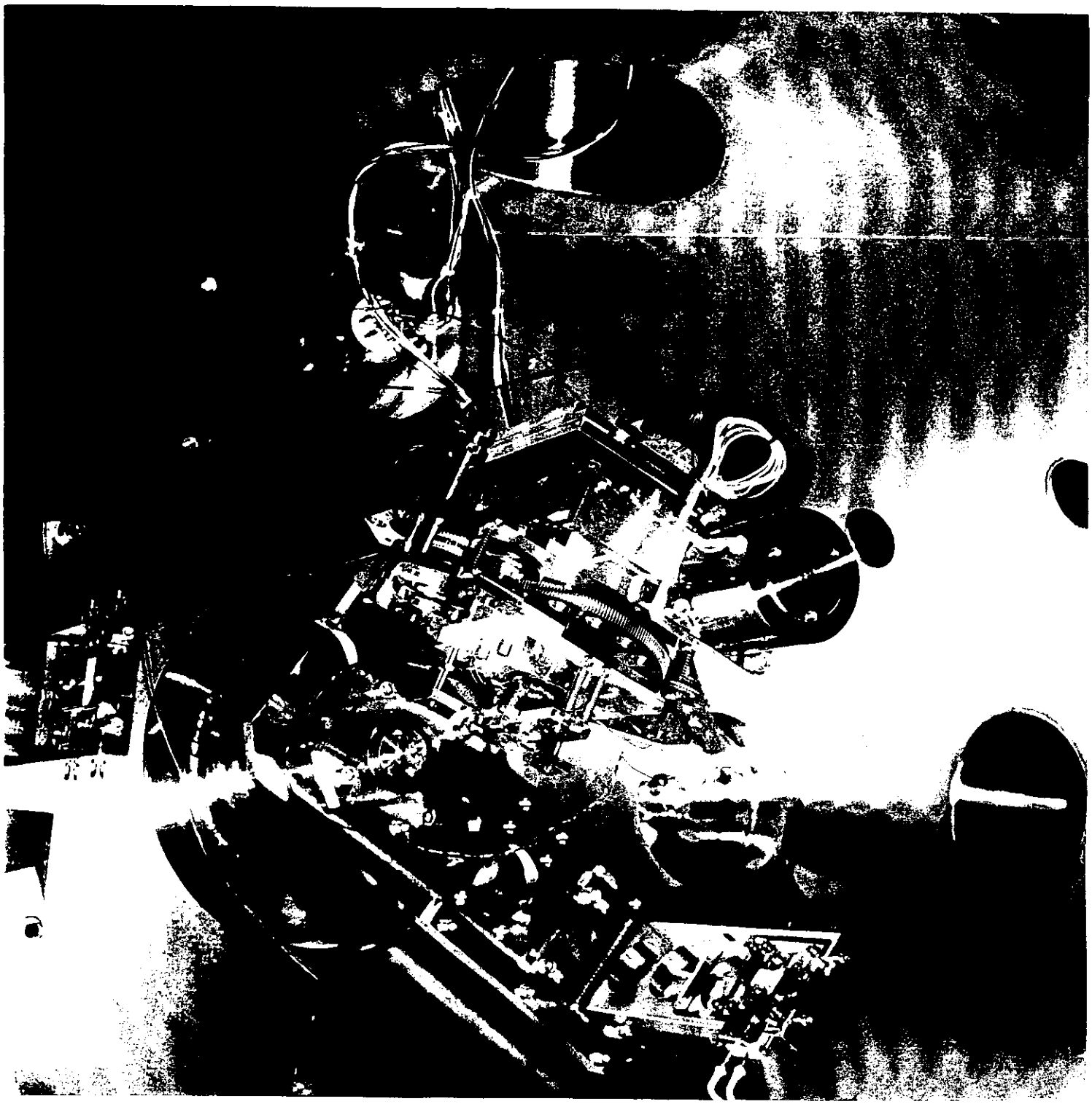

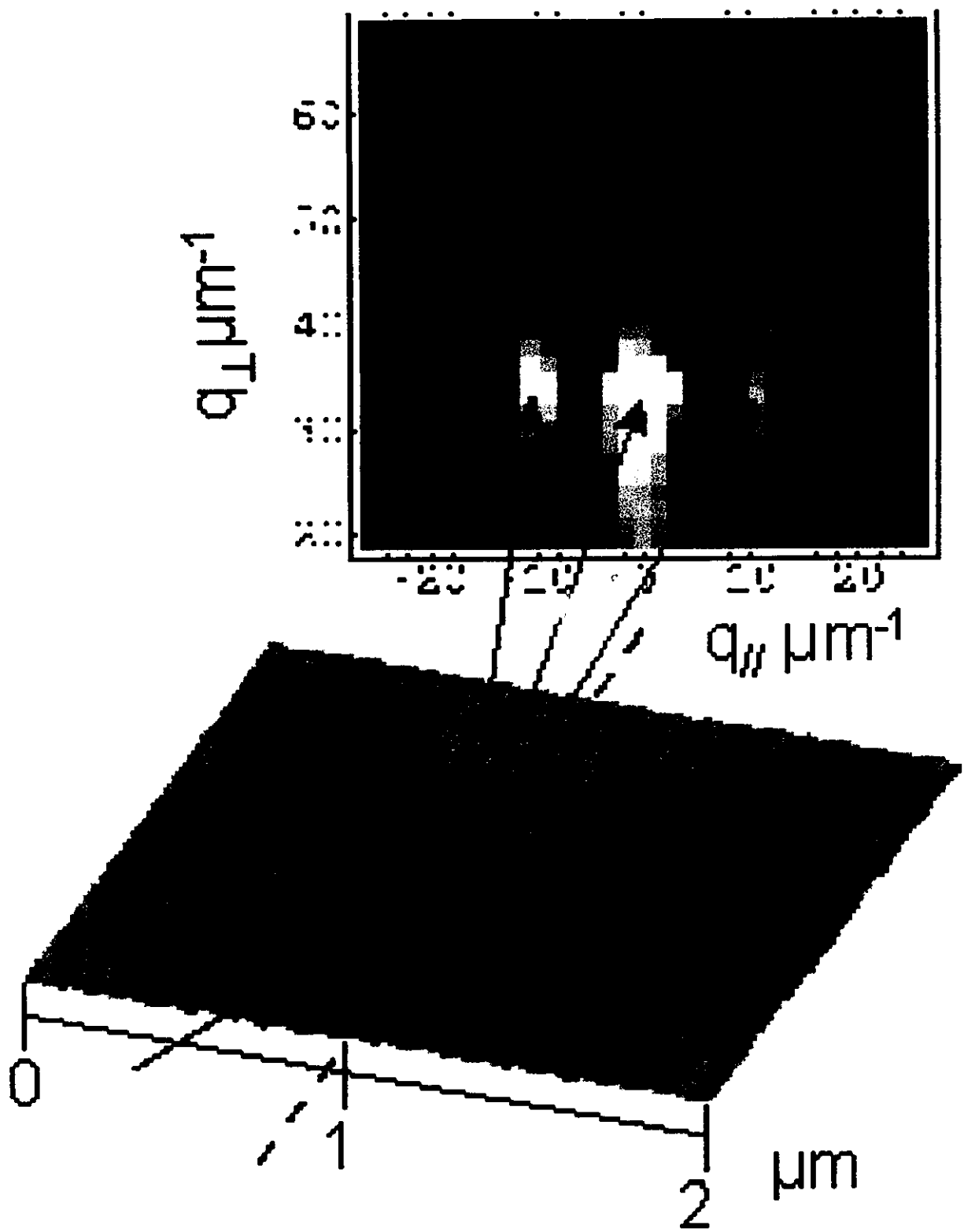
$q_\perp \mu m^{-1}$
$q_{//}\ \mu m^{-1}$
0
1
2
μm

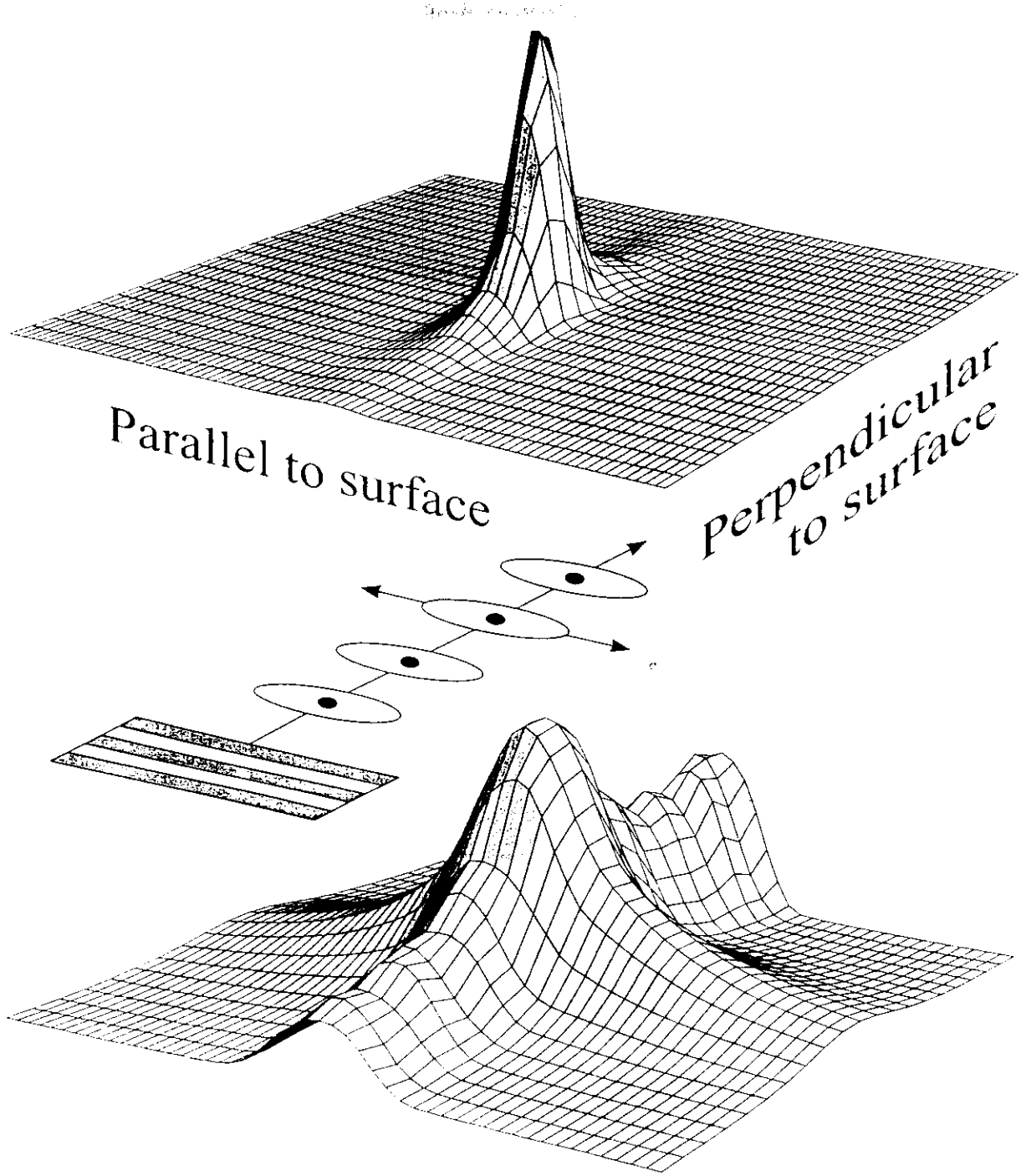
Parallel to surface
Perpendicular to surface

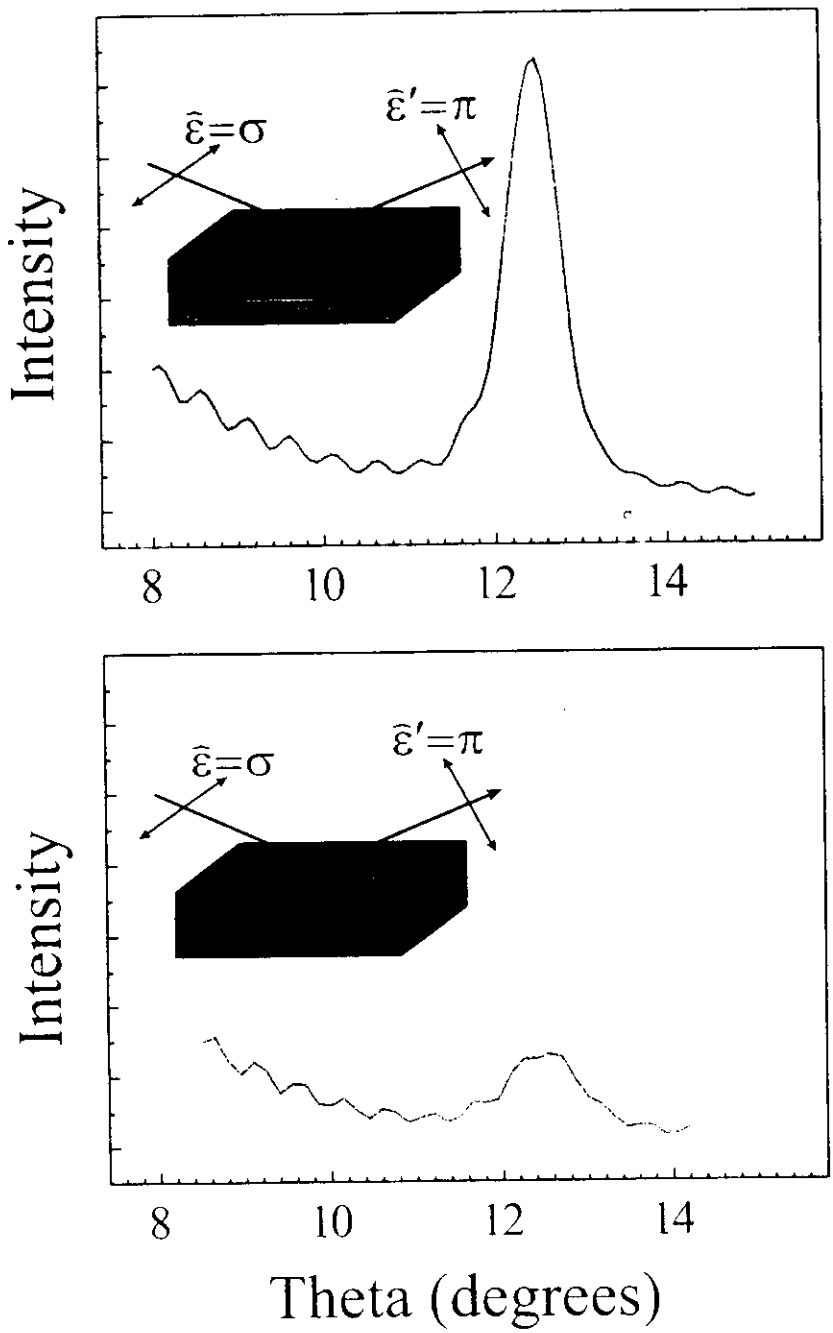

60% GMR at RT ml [Co (10 Å) / Cu (10 Å)] × 50

linear polarization

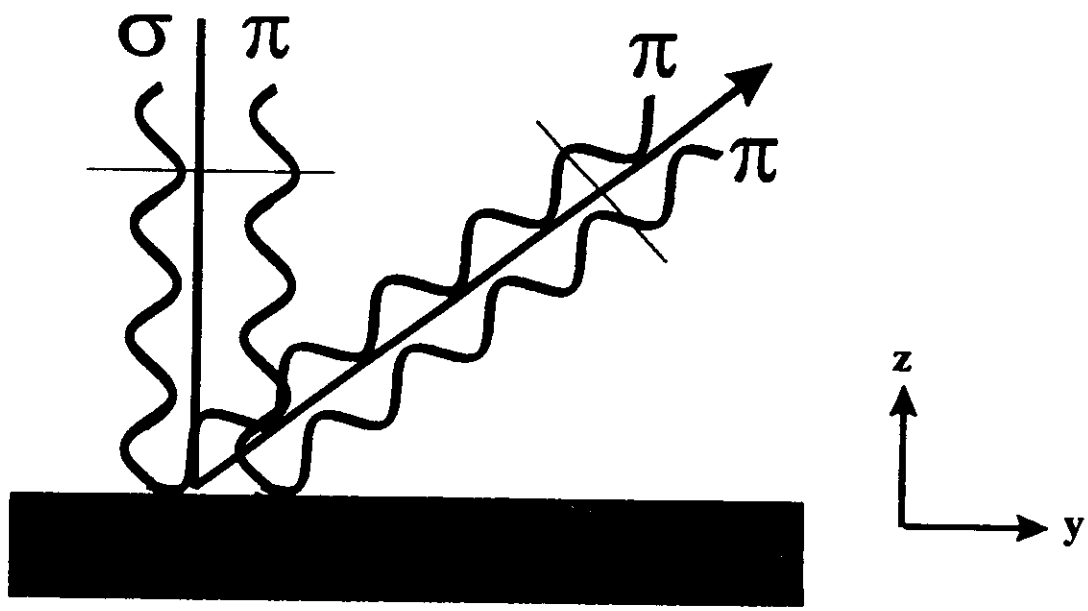

circular polarization

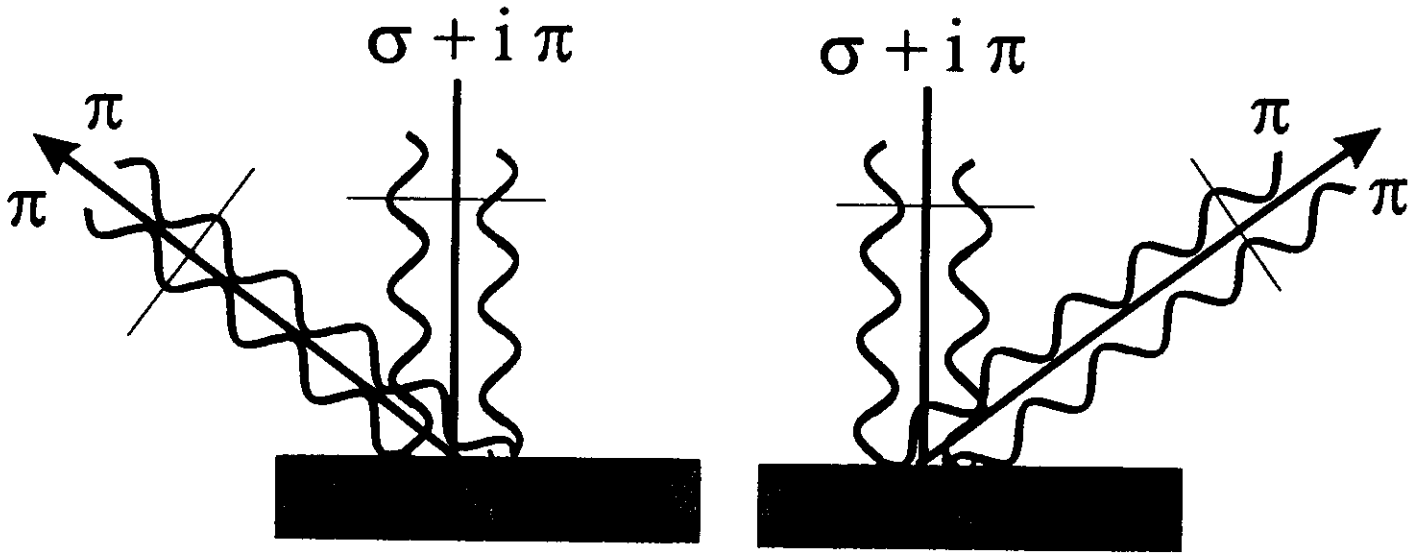

$q_y = -\tau$ $\quad$ $q_y = \tau$

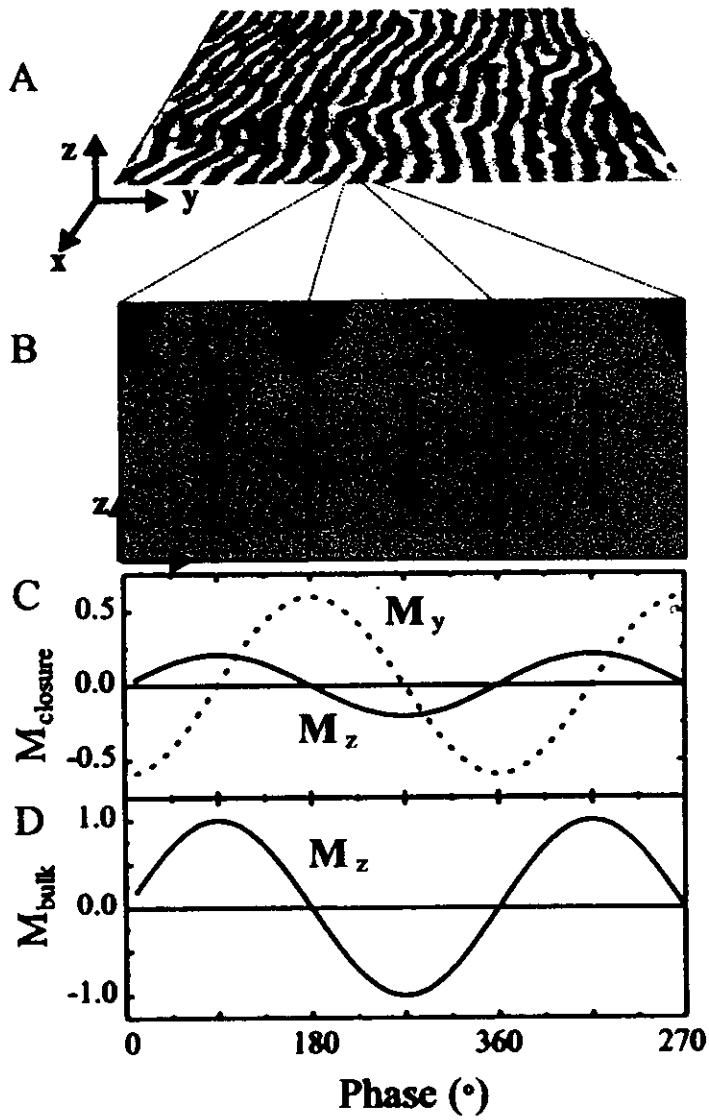

Figure 1
Dürr et al.

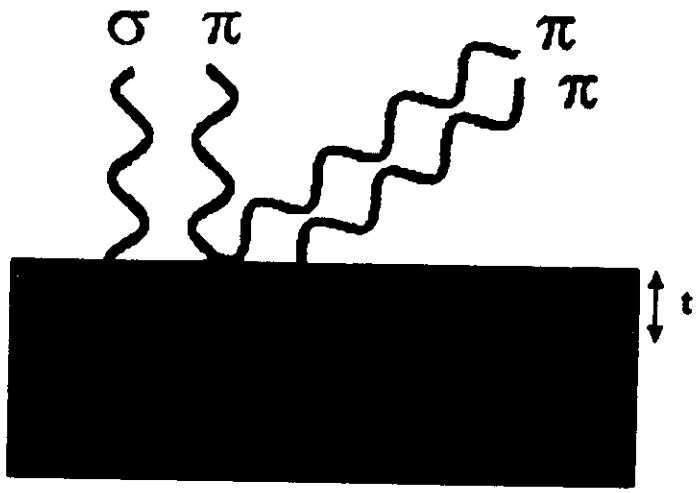
σ
π
π
π
t

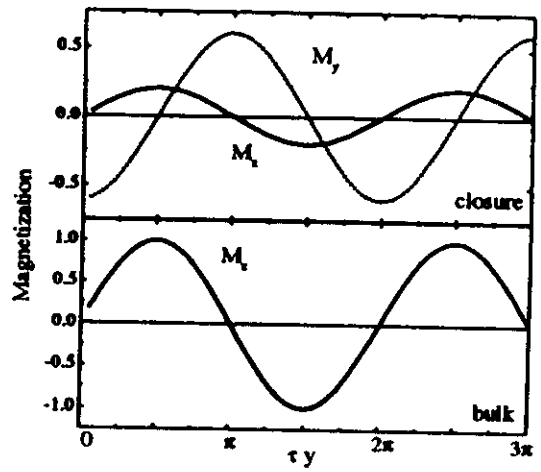
Magnetization
0.5
0.0
-0.5
M_y
M_x
closure
1.0
0.5
0.0
-0.5
-1.0
M_x
bulk
0
π
τ y
2π
3π

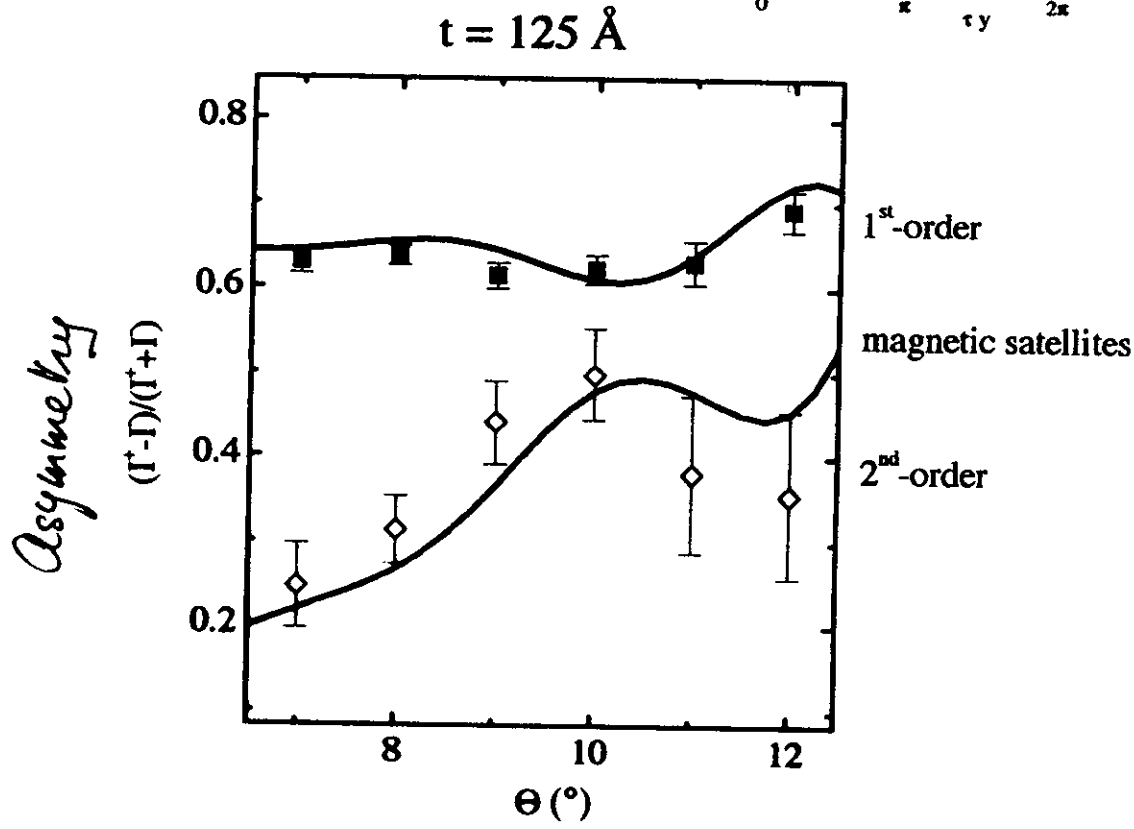
t = 125 Å
Asymmetry
(I⁺-I)/(I⁺+I)
0.8
0.6
0.4
0.2
8
10
12
Θ (°)
1st-order
magnetic satellites
2nd-order

Photoelectron Diffraction in Magnetic Linear Dichroism

Rose, Hillebrecht, Kinoshita, Idzerda, van der Laan,

Denecke and Ley, Phys. Rev Lett. (1995)

PRL 75, 2883 (1995)

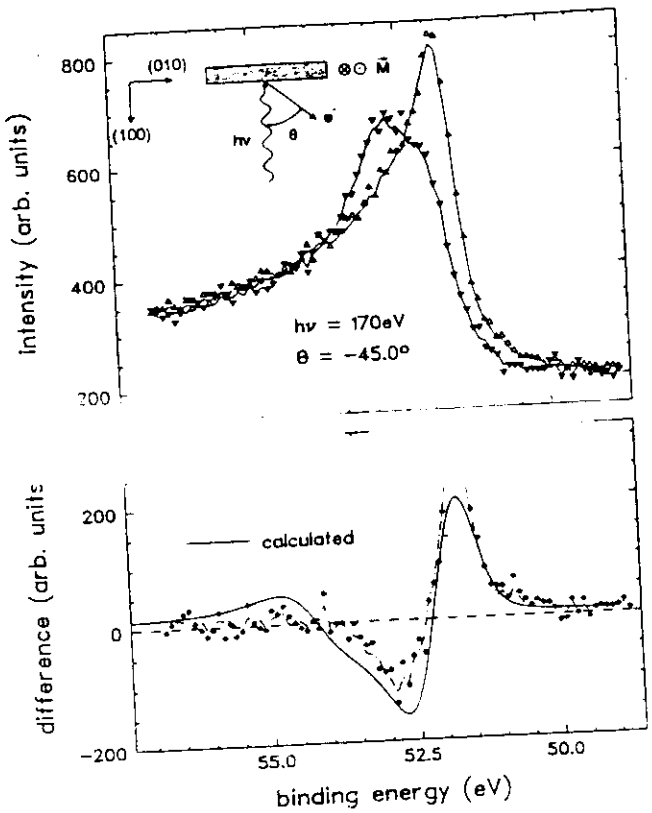

Fe 3*p* MLDAD

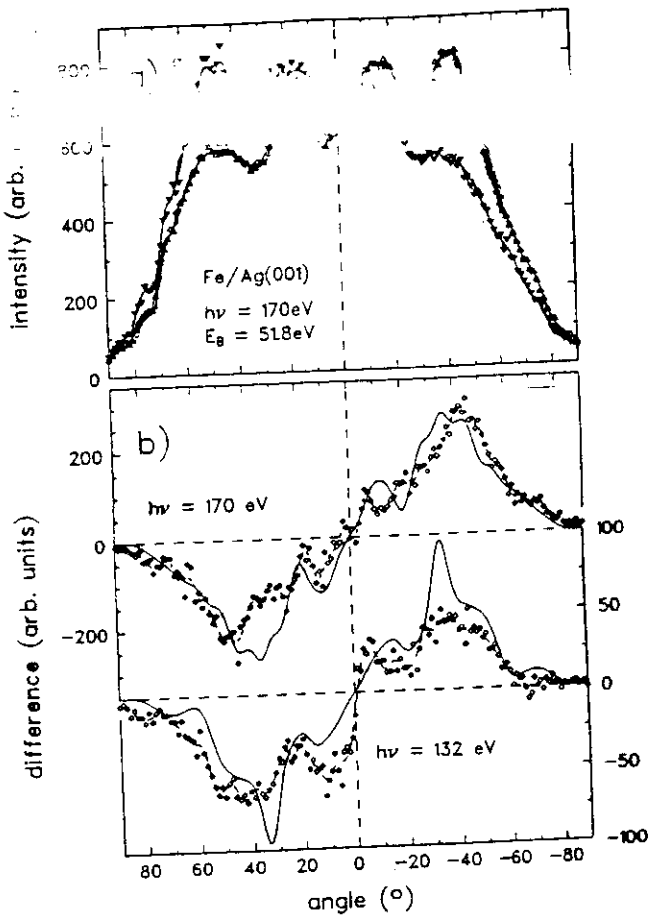

angular dependence
at different photon energies

Gd 4d ResPes + Absaption

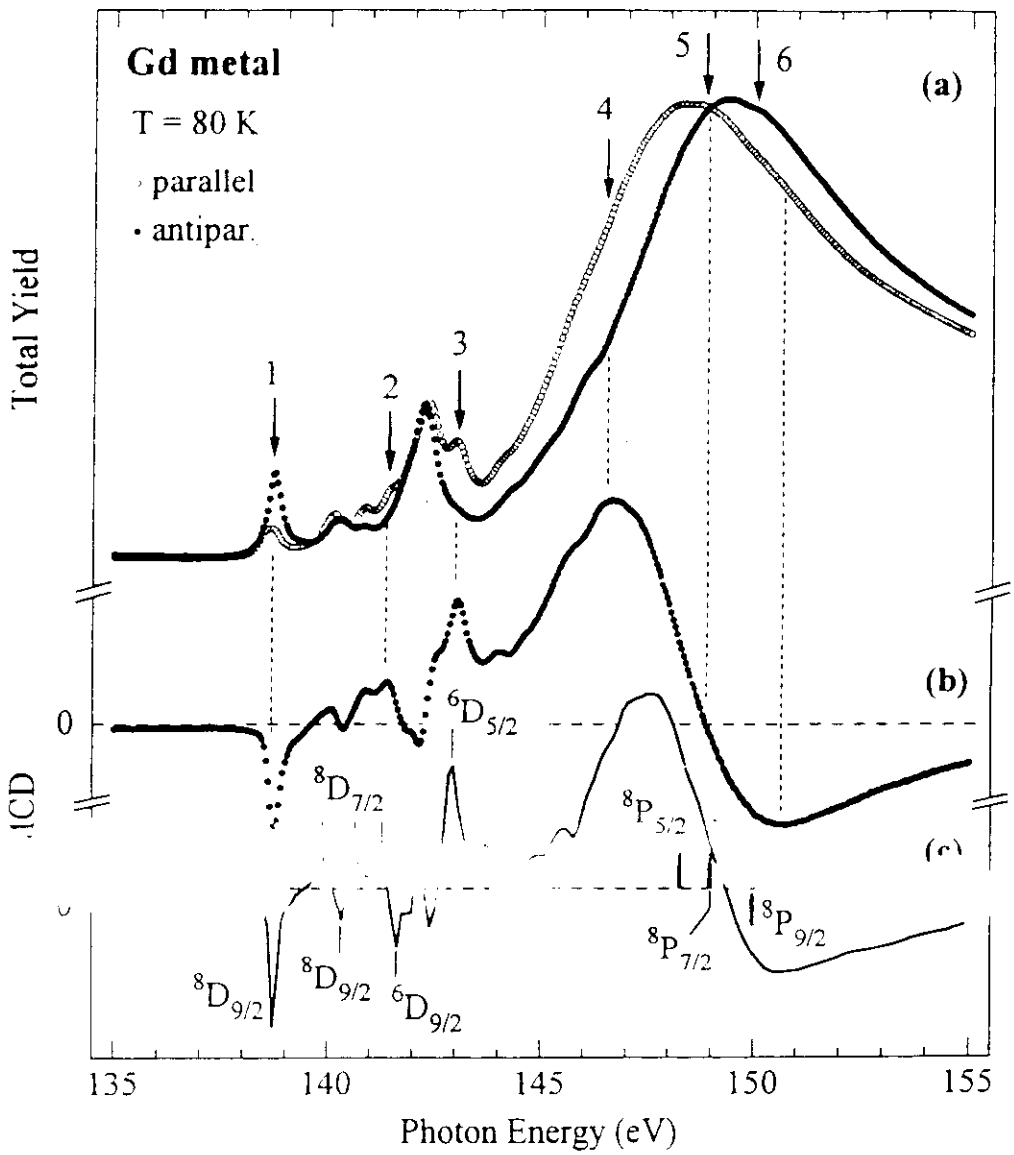

Starke, Navas, Arenholz, Hu, Baumgarten,
van der Laan, Chen, and Kaindl
Magnetic circular dichroism in 4d -> 4f resonant photoemission and photoabsorption of Gd metal
Phys. Rev. B ~~submitted~~ 15 Jan '97
PRB 55, 5672 (1997)

Magnetic circular dichroism in Tb $3d \rightarrow 4f$ resonant photoemission

G. van der Laan
Daresbury Laboratory, Warrington WA4 4AD, United Kingdom

E. Arenholz, Z. Hu, A. Bauer, E. Weschke, Ch. Schüssler-Langeheine, E. Navas, A. Mühlig, and G. Kaindl
Institut für Experimentalphysik, Freie Universität Berlin, D-14195 Berlin-Dahlem, Germany

J. B. Goedkoop and N. B. Brookes
European Synchrotron Radiation Facility, Boîte Postale 220, F-38043 Grenoble, France

$4f^8 \xrightarrow{h\nu} 3d^9 4f^9 \longleftrightarrow 4f^7 + \varepsilon l$

← Absaption spectra

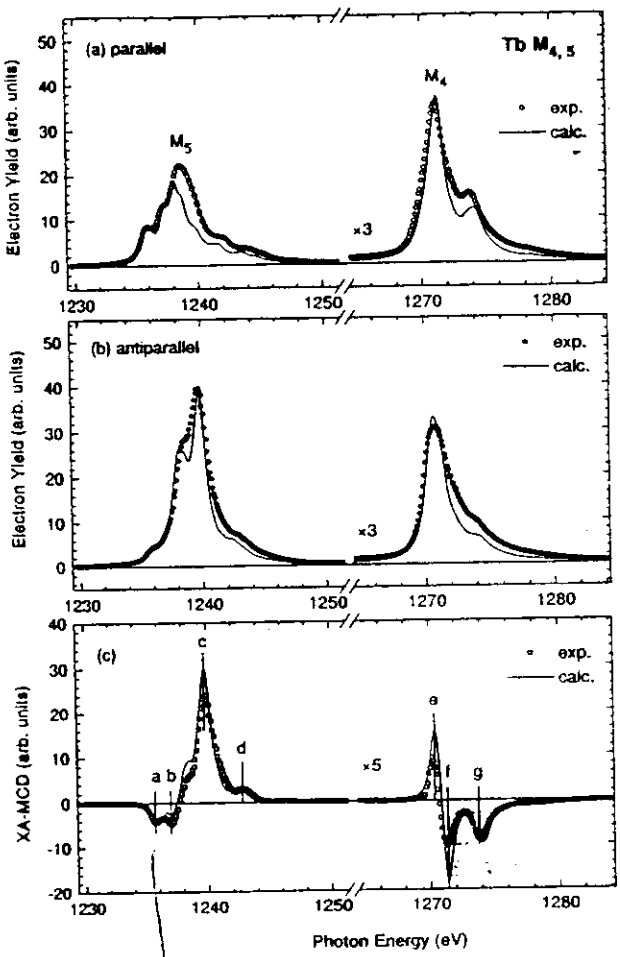

absorption peak ⓐ

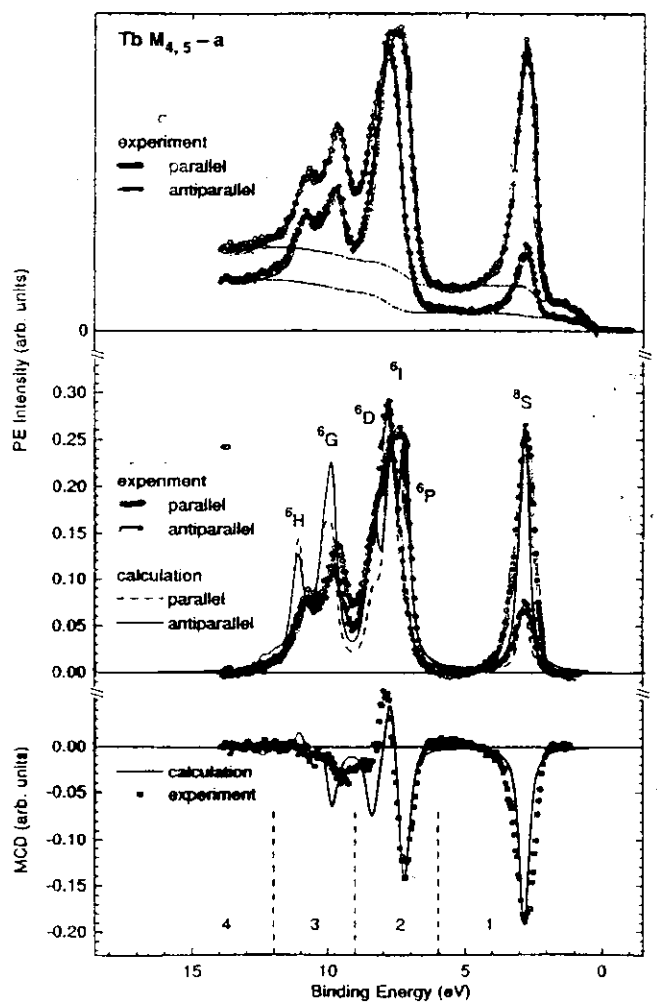

Photoemission Spectra →

PRB 59, 8835 (1999)

Mn/Cu(110)
Localization <----> Delocalization

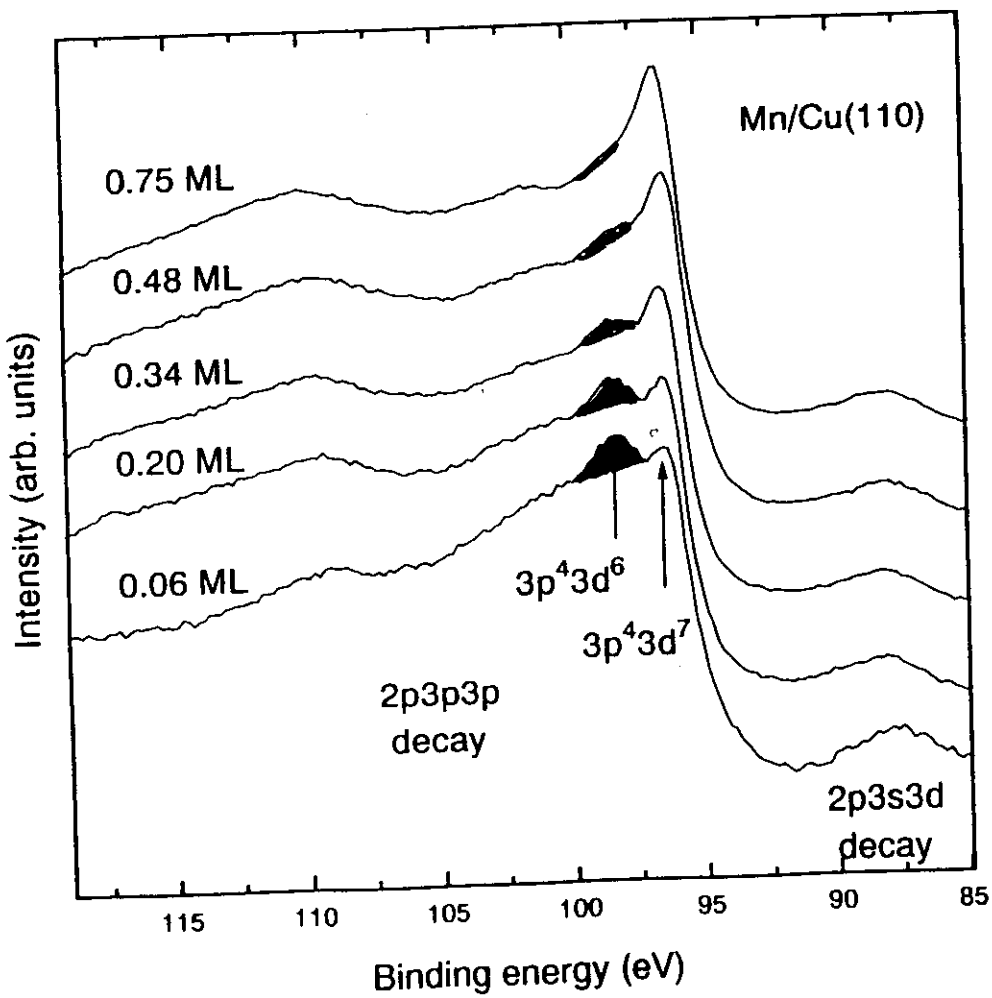

$2p3p3p$ resonant photoemission decay
(Dürr, van der Laan, Spanke, Hillebrecht, Brookes)
PRB 56, 8156 (1997)

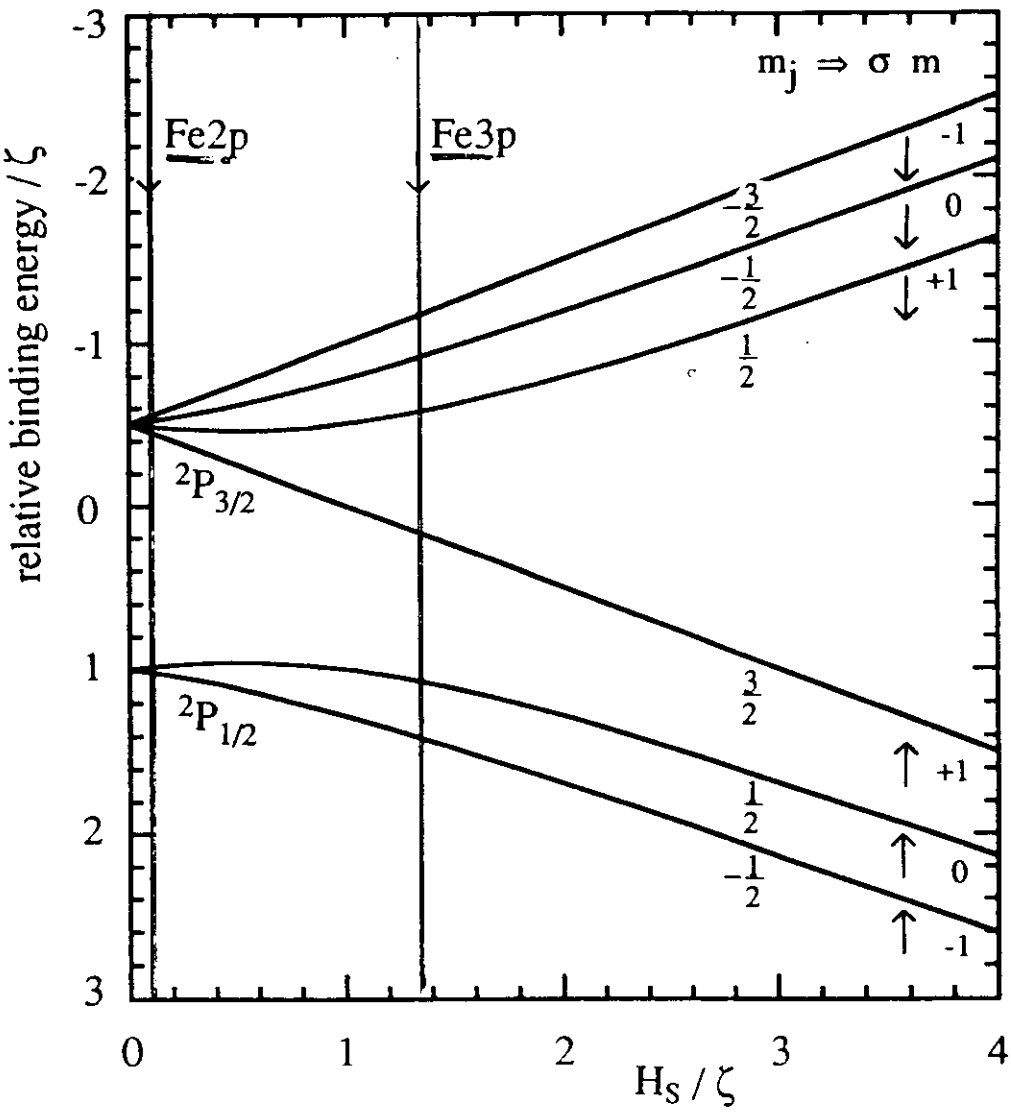

G. van der Laan PRB 51, 240 (1995)

Cu $d^9(J=5/2)$ + hv -> $2p^5d^9$ + εd

G. van der Laan, J.P.C.M. 3, 1051 (1991)

Multiplet structure depends on polarization of the light.
Spin-orbit coupling & 2p-3d electrostatic interactions

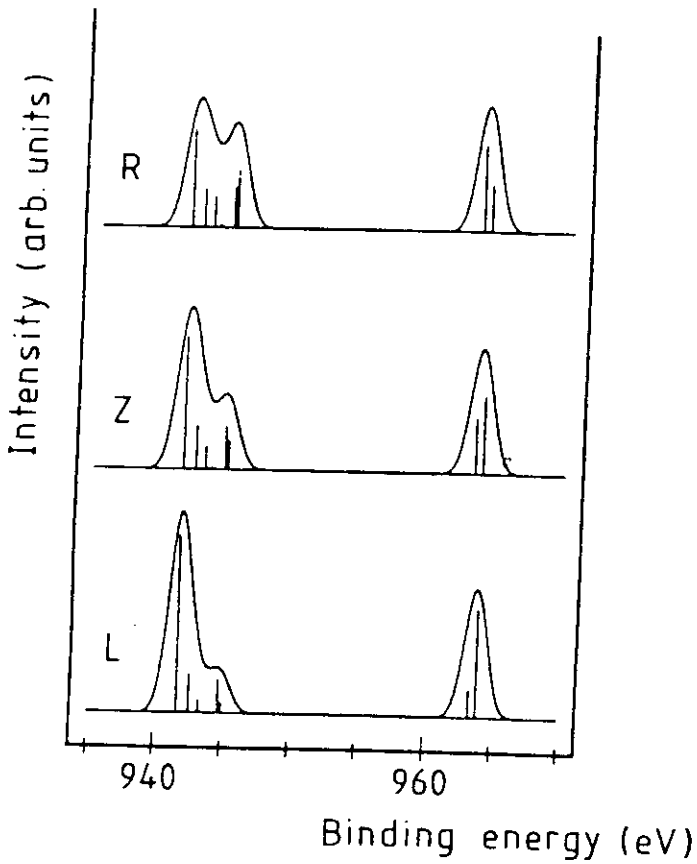

Polarization dependence of each final state term due to the alignment of the angular momenta of the core hole and the valence shell

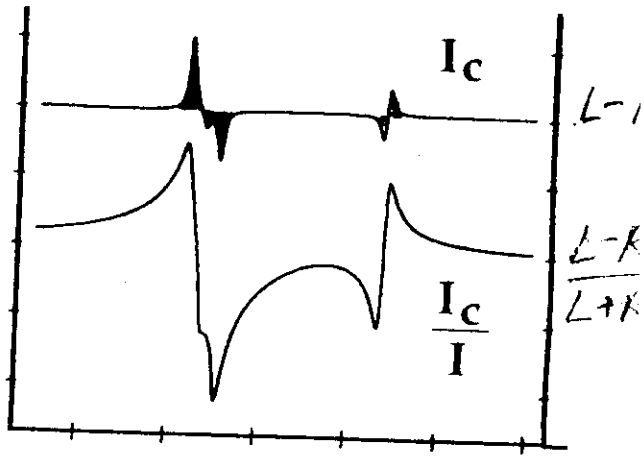

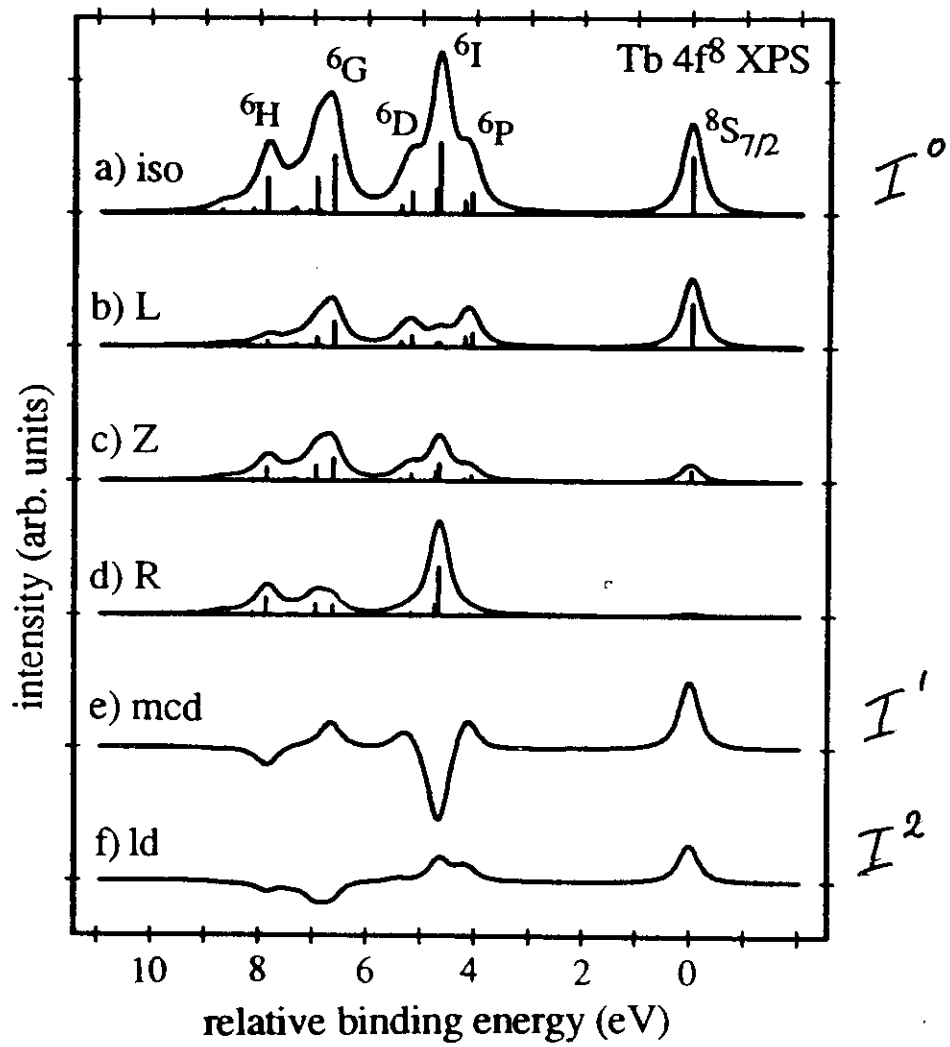

van der Laa / Thole, PRB 48, 210 (1993)

MCD in 4f-PE from Tb(0001)/W(110)

$T_c = 220\,K$

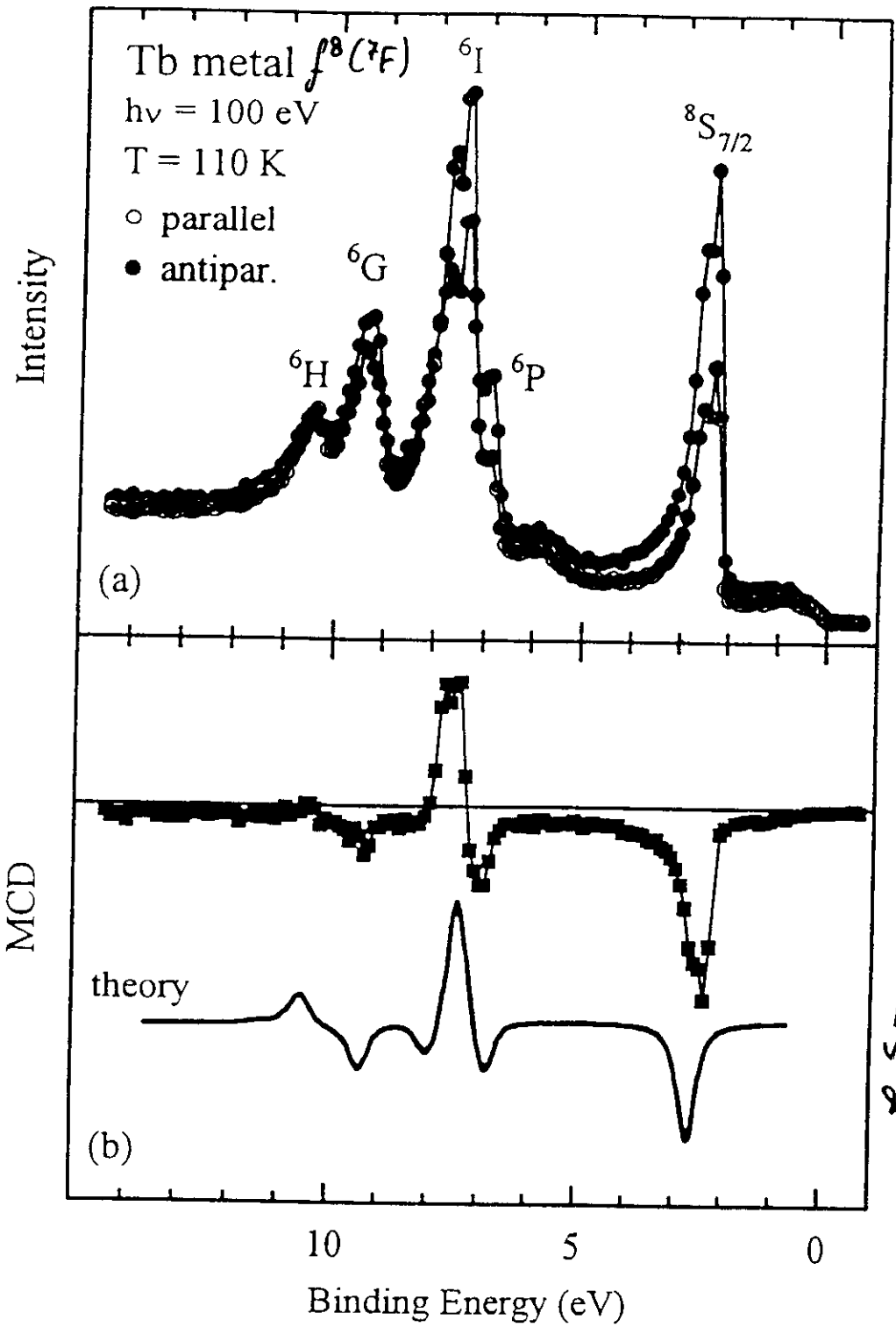

$t = T/T_c = 0.5$

exp.
Kaindl group

prediction
van der Laan
& Thole ('93

$T = 0$

MCD in Gd 4d photoemission

van der Laan, Arenholz, Navas, Bauer, and Kaindl (1996)

PRB 53, R5998 (1996)

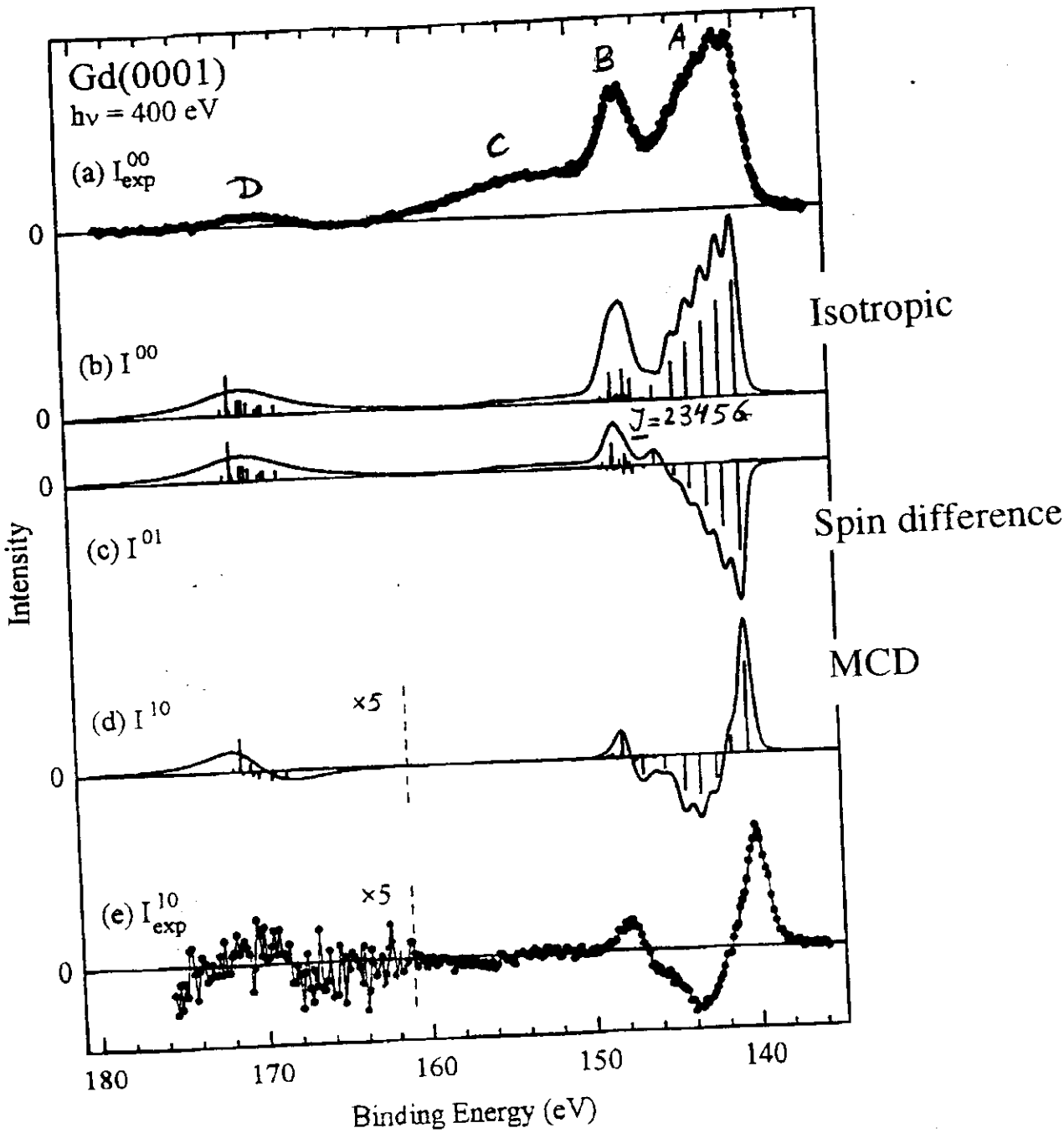

5*p* core level photoemission from Gd(0001)

Arenholz, Kaindl, van der Laan

PRB 56, 3244 (1997)

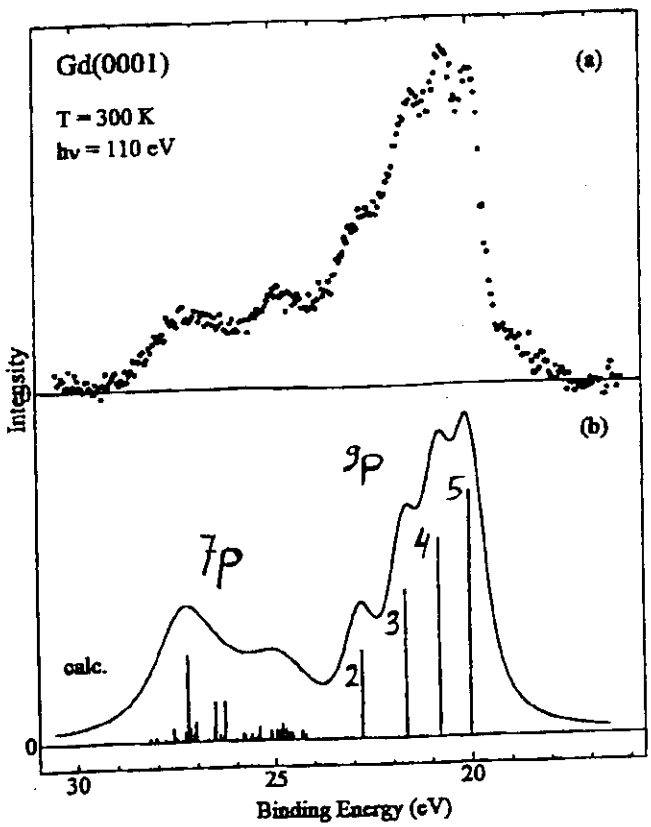

Isotropic spectrum

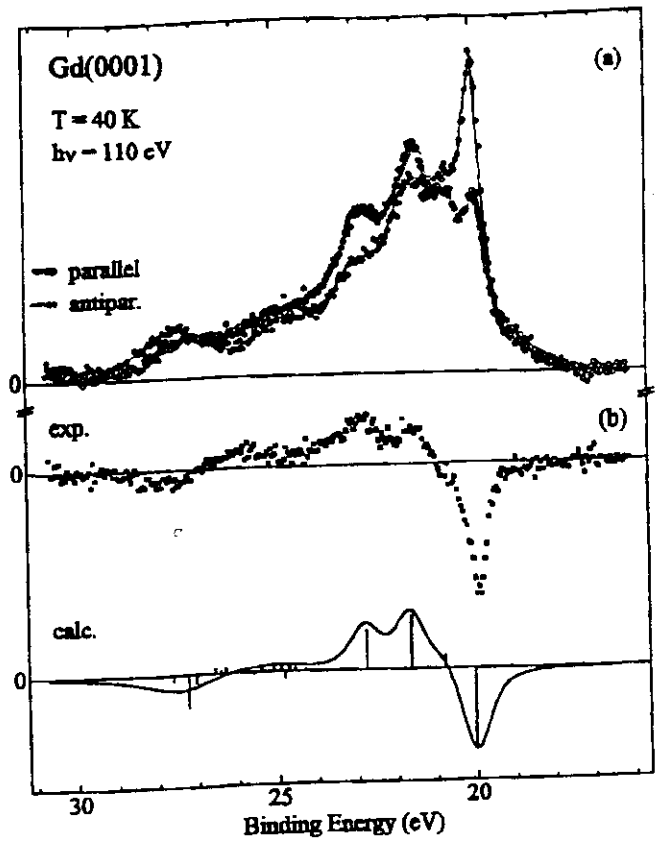

Magnetic circular dichroism

MCD in 5*p* photoemission from Gd(0001)
Schematic explanation

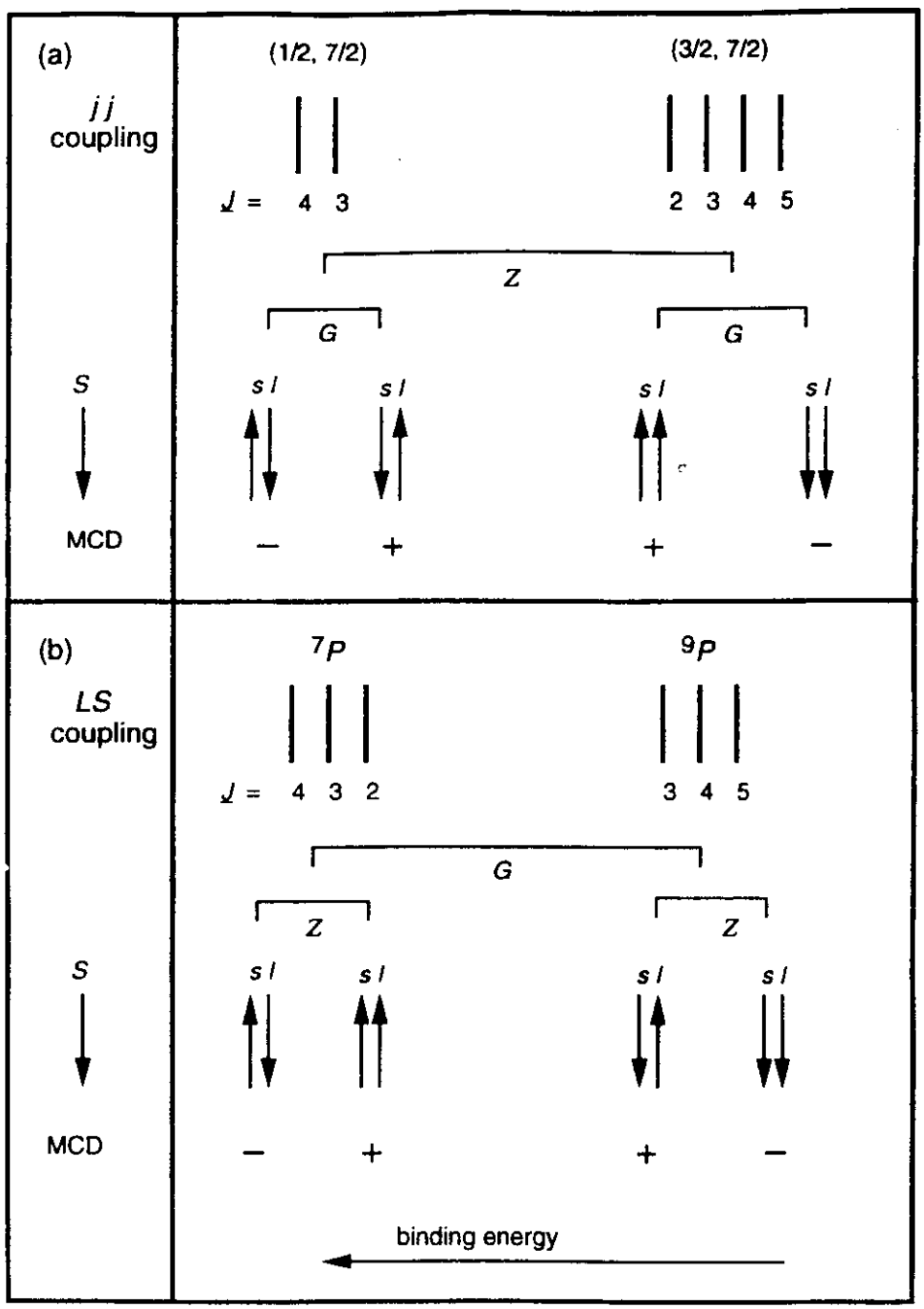

GvdL, PRB 56, 3244 (1997)